AD-A185 643 TURBULENCE TURBULENCE CONTROL AND DRAG REDUCTION(U) 1/2
YALE UNIV NEW HAVEN CT MASON LAB K R SREENIVASAN
01 AUG 87 AFOSR-TR-87-0984 $AFOSR-82-0299

UNCLASSIFIED F/G 20/4 NL

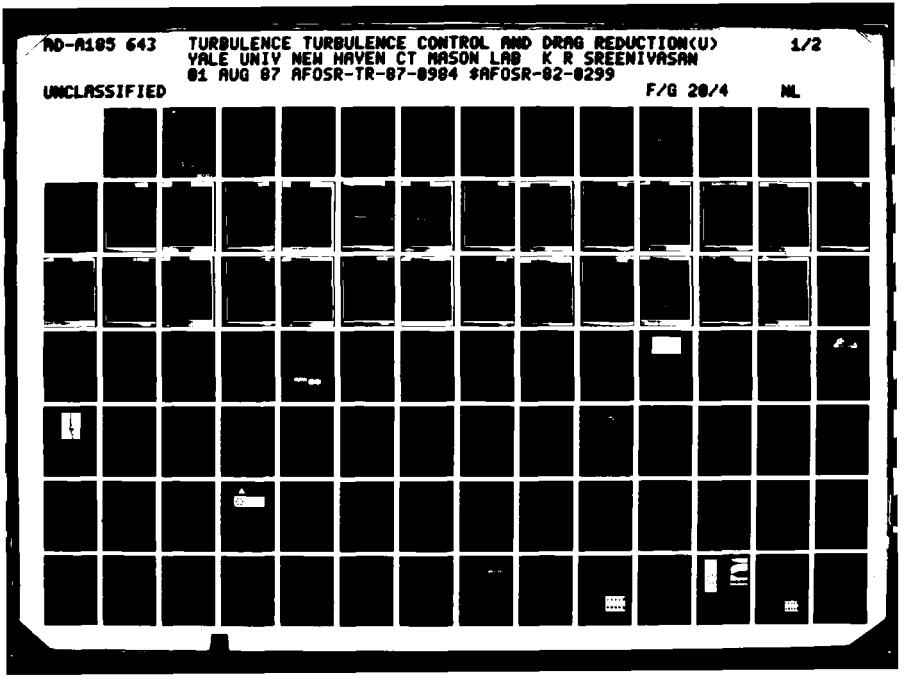

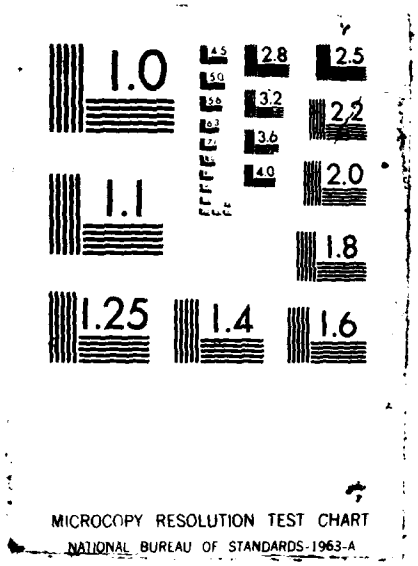
1.0
1.1
1.25
1.4
1.6
2.8
3.2
3.6
4.0
2.5
2.2
2.0
1.8
MICROCOPY RESOLUTION TEST CHART
NATIONAL BUREAU OF STANDARDS-1963-A

UNCLASSIFIED

SECURITY CLASSIFICATION OF THIS PAGE

DTIC FILE COPY

(2)

REPORT DOCUMENTATION PAGE

AD-A185 643

1b RESTRICTIVE MARKINGS	
2a DECLASSIFICATION/DOWNGRADING SCHEDULE	3 DISTRIBUTION/AVAILABILITY OF REPORT: APPROVED FOR PUBLIC RELEASE DISTRIBUTION IS UNLIMITED
4. PERFORMING ORGANIZATION REPORT NUMBER(S)	5. MONITORING ORGANIZATION REPORT NUMBER(S): AFOSR-TR- 87-0984
6a. NAME OF PERFORMING ORGANIZATION: YALE UNIVERSITY; 6b. OFFICE SYMBOL (If applicable)	7a. NAME OF MONITORING ORGANIZATION: AFOSR/NA
6c. ADDRESS (City, State and ZIP Code): DEPT. OF MECHANICAL ENGINEERING, PO BOX 2159, MASON LAB, NEW HAVEN CT 06520	7b. ADDRESS (City, State and ZIP Code): BUILDING 410, BOLLING AFB, DC 20332-6448
8a. NAME OF FUNDING/SPONSORING ORGANIZATION: AFOSR/NA; 8b. OFFICE SYMBOL (If applicable): NA	9 PROCUREMENT INSTRUMENT IDENTIFICATION NUMBER: AFOSR-82-0299
8c. ADDRESS (City, State and ZIP Code): BUILDING 410, BOLLING AFB, DC 20332-6448	10 SOURCE OF FUNDING NOS: PROGRAM ELEMENT NO 61102F; PROJECT NO. 2307; TASK NO. A2; WORK UNIT NO.

11. TITLE (Include Security Classification): (U) TURBULENCE, TURBULENCE CONTROL, AND DRAG REDUCTION

12. PERSONAL AUTHOR(S): K. R. SREENIVASAN

13a. TYPE OF REPORT: FINAL TECHNICAL	13b. TIME COVERED: FROM AUG 1982 TO AUG 1985	14. DATE OF REPORT (Yr, Mo, Day): 1 AUGUST 1987	15. PAGE COUNT: 107

16. SUPPLEMENTARY NOTATION

17. COSATI CODES: FIELD	GROUP	SUB GR	18 SUBJECT TERMS (Continue on reverse if necessary and identify by block number): TURBULENCE, FLOW CONTROL, DRAG REDUCTION

19. ABSTRACT (Continue on reverse if necessary and identify by block number)

Progress is reported on fundamental studies in turbulence dynamics, flow control, and drag reduction. Publications, theses and reports arising from these studies are listed and discussed briefly. The publications are enclosed as a part of this report, but not the theses and unpublished reports.

DTIC ELECTE S D OCT 0 1 1987 D

20. DISTRIBUTION/AVAILABILITY OF ABSTRACT: UNCLASSIFIED/UNLIMITED ☒ XXX SAME AS RPT ☐ DTIC USERS ☐	21 ABSTRACT SECURITY CLASSIFICATION: UNCLASSIFIED
22a NAME OF RESPONSIBLE INDIVIDUAL: JAMES M MCMICHAEL	22b TELEPHONE NUMBER (Include Area Code): 202-767-4935; 22c OFFICE SYMBOL: AFOSR/NA

DD FORM 1473, 83 APR 87 EDITION OF 1 JAN 73 IS OBSOLETE

UNCLASSIFIED

Report AFOSR-82-0299

AFOSR-TR- 87-0984

TURBULENCE, TURBULENCE CONTROL AND DRAG REDUCTION

K.R. Sreenivasan
Department of Mechanical Engineering, P.O. Box 2159
Mason Lab., Yale University, New Haven, CT 06520

1 August 1987

Final Report for Period 29 August 1982-29 August 1985

AIR FORCE OFFICE OF SCIENTIFIC RESEARCH
BOLLING AIR FORCE BASE
WASHINGTON, D.C. 20332

DTIC COPY INSPECTED

Accesion For
NTIS CRA&I
DTIC TAB
Unannounced
Justification
By
Distribution /
Availability Codes
Dist Special
A-1

Progress Report: Summary of work done under AFOSR sponsorship during 82-85

Preamble

This report, documenting the progress made under AFOSR sponsorship (AFOSR-82-0299), is a summary of the three yearly progress reports submitted to AFOSR, and also includes material described verbally to the Program Manager, Dr. James McMichael, during our periodical meetings. The research falls within the general area of 'Turbulence, Turbulence Control and Drag Reduction'. The progress made during the three year period 1982-85 can be classified under the following four categories:

(1) Fundamental studies on turbulence dynamics
(2) Flow control studies
(3) Viscous drag reduction
(4) Miscellaneous.

Each of these areas will now be described briefly in the following sections; each section also contains some general qualitative remarks.

1. Fundamental studies on turbulence dynamics

The emphasis in this part work has been the examination of whether, and if so how, the modern notions of dynamical systems, chaos and nonlinear systems can enhance our understanding of turbulent flows in a way that we can use this improved understanding to predict better quantities of direct interest in practical circumstances, such as mixing and drag. The strides made so far may not be remarkable in an absolute sense, but we have definitely made some non-trivial progress. When this work was begun, it was not fashionable within the fluid mechanics community (in fact, some workers looked upon it rather unkindly), but many more groups are now engaged in similar work. We think that turbulence is not chaos, and is more complex than the complex behavior associated with simple maps (for instance), but that many tools employed for analyzing chaos can be used profitably to gain a better understanding of turbulence. Furthermore, in spite of the protests of some, we also believe that the canonical routes to chaos have some relevance to the manner in which transition to turbulence occurs at least in some special circumstances.

Some idea of the work done can be had by the list of publications (including reports and theses) that arose from it. We list them below, and discuss them briefly. Most publications are enclosed, but not the theses and the interim reports (partly because they have already been mailed to AFOSR at different times, and partly because they duplicate some of the published material).

The significance of this work is that it brings together the recent mathematical concepts from nonlinear dynamics and some classical concerns in fluid mechanics. It is believed that this cross fertilization will have significant impact on our understanding of turbulence in the next ten years (or so). The publications are:

a. K.R. Sreenivasan & P.J. Strykowski (1984) 'On anologies between turbulence in unconfined flows and chaotic dynamical systems'; In '**Turbulent and chaotic phenomena in fluids**', pp. 191-196, North-Holland (ed. T.Tatsumi)

It was in this paper that the dimension of the attractor was first calculated from experimental signals (more or less concurrently with others in the physics community who did similar calculations in the Taylor-Couette flow). We indicated that the Ruelle-Takens scenario may hold during transition to turbulence in coiled pipes. We have not pursued this flow much because of the difficulty in obtaining purely periodic phenomena, but have pursued this line of enquiry in other flows (see below).

b. K.R. Sreenivasan (1985) 'Transition and turbulence in fluid flows, and low-dimensional chaos'; In '**Frontiers of fluid mechanics**', pp.41-67, Springer-Verlag (ed. S.H. Davis & J.L. Lumley)

We showed that the points of view now developing from the understanding of chaotic dynamical systems can be useful for interpreting the phenomena associated with transition to

turbulence in wakes behind cylinders. This manuscript created some interest, and there are claims that the windows of chaos and order observed in this paper were due to the aeroelastic coupling between the flow and the cylinder. It is quite clear that aeroelastic coupling is a sufficient condition for producing these windows of order and chaos, but that is not a necessary condition. Our present view, based on a number of unpublished measurements including those on cylinder vibrations, is that small three dimensionalities (invariably present) in the wake of a rigid cylinder will be enough to produce the results obtained in this manuscript. Further work is in progress.

c. K.R. Sreenivasan (1986) 'Chaos in open flow systems', In '**Dimensions and entropies**', pp 222-230, Springer-Verlag (ed. G. Mayer-Kress)

In this paper, we discussed the general difficulties associated with measurement of dimensions and Lyapunov exponents in open flows, and presented trends with Reynolds number. Flows examined were wakes, jets, mixing layers and flow through coiled pipes.

d. K.R. Sreenivasan & C. Meneveau (1986) 'The fractal facets of turbulence' **J. Fluid Mech.** 173, 357-386.

In this paper, we showed that there are various facets of turbulent flows that are fractal-like, and measured by experiment the fractal dimensions of turbulent/non-turbulent interfaces, iso-velocity surfaces, iso-dissipation surfaces, etc. Part of our contribution in this paper (and in reference (c) above) is believed to be the rendering of some mathematical properties of strange sets amenable to measurement, and the interpretation of these measured measurements in contexts of fluid flows. In particular, we examined the following questions: (a) Is the turbulent/non-turbulent interface a self-similar fractal, and (if so) what is its fractal dimension? Does this quantity differ from one class of flows to another? Are constant-property surfaces (such as the iso-velocity and iso-concentration surfaces) in fully developed flows fractals? What are their fractal dimensions? (c) Do dissipative structures in fully developed turbulence form a fractal set? What is the fractal dimension of this set? Answers to these questions shed some light also on some long standing questions in turbulence – for example, the growth of material lines in a turbulent environment. The overwhelming conclusion turned out to be that several facets of turbulence can be described by fractals, and that their fractal dimension can be measured. Currently, we are trying the explain our findings in terms of the dynamics of turbulence, and examine the implications of these findings to turbulent mixing.

e. K.R. Sreenivasan & R. Ramshankar (1986) 'Transition intermittency in open flows, and intermittency routes to chaos', **Physica 23D**, 241-258.

The intermittent transition to turbulence in open flows (mainly pipe flows) was examined in this paper in the context of intermittency routes to chaos. Preliminary conclusions were that some quantitative connections could be discerned, but that they were incomplete. In a similar manner, connections with phase transition and other critical phenomena were also found to be imperfect. Some measurements which we hope will be useful in developing alternative models describing the essentials of the phenomena were described.

f. K.R. Sreenivasan, P.J. Strykowski & D.J. Olinger (1987) 'Hopf bifurcation, Landau equation, and vortex shedding behind circular cylinders', In '**Forum on unsteady flow separation' of the ASME Transactions**, pp. 1-13 (ed. K.N. Ghia).

In this paper, we have shown by measurement that the bifurcation accompanying the vortex shedding behind circular cylinders is of the Hopf type, and that the Landau equation (with constants possibly depending on the spatial position) describes the post-critical behavior quite accurately. We determine typical Landau constants. Finally, we have examined the sense in which absolute instability is relevant to the vortex shedding problem.

2. Flow control research

This has been a central issue of our research, but a number of things resulting from it have remained unpublished to-date, although they are at various stages of publication now. The bulk of the work can be found in two Ph.D.theses, whose titles and abstracts are given below.

a) P.J. Strykowski (1986): 'The Control of Absolutely and Convectively Unstable Shear Flows'

The control of the absolutely unstable wake flow and the convectively unstable boundary layer is investigated. The control (i.e., suppression) of disturbances in the wake and the boundary layer is achieved through different means, because the flows are governed by different types of instabilities. For instance, vortex shedding behind circular cylinders can be suppressed (over a limited range of Reynolds number) by the proper placement of a second smaller cylinder in the near-wake of the main shedding cylinder. The control is new and quite dramatic, and is a consequence of the wake being absolutely unstable. Control in the boundary layer is achieved by acting on the disturbances directly because the flow is dominated by the convective instablity. In the boundary layer, control is successfully applied to Tollmien-Schlichting waves and narrow band-passed random waves using the wave superposition principle. The control is achieved by using a novel technique, namely suction and blowing, by which disturbances are produced and subsequently controlled.

A publication that has resulted from this work is:

P.J. Strykowski & K.R. Sreenivasan (1985) 'The control of transitional flows' **AIAA Paper -85-0559**, Presented at the AIAA conference on Shear Flow Control, Boulder.

Two other papers are expected to be prepared on the basis of this thesis.

b)S.Raghu (1987): 'Control of Combustion and Acoustically Coupled Fluid Dynamic Instabilities'

The purpose of the present research is to demonstrate experimentally a set of methods for the active control of combustion and acoustically coupled fluid dynamic instabilities. These methods are based on the theoretical understanding of the interaction of mass, momentum or energy sources with a disturbance in the system. The disturbance could be linear or nonlinear and either vortical, acoustic or in the entropy mode. It has been shown that periodic addition of mass, momentum or energy can result in either the amplification or the decay of the energy in a periodic disturbance depending on the phase in which this addition occurs. Successful control has been achieved in several cases of fluid dynamic and combustion instability ranging from laboratory scale experiments to an operational, large combustion tunnel.

The method of heat addition was used to succesfully control oscillations in a Rijke tube, a whistler nozzle, resonance in a pipe set up by loud speaker, and a turbulent pipe flow with superposed acoustic resonance. It was found that more control heat is necessary to suppress oscillations in a large background of turbulent noise. Drag forces generated by fine screens was used to suppress the oscillations in a whistler nozzle. A feedback mechanism was designed to oscillate the screens in the proper phase to achieve the desired control action. The resonance in a pipe set up by a loud speaker was suppressed by periodic mass addition using a feedback control system. Finally, a combination of screens and heating coils was used to control oscillations in a large combustion tunnel. The methods of control explored in this work are independent of the source of instability, and hence have a broad range of applications in real systems.

One publication that has resulted from this work is:

K.R. Sreenivasan, B.T. Chu & S. Raghu (1987) 'The control of pressure oscillations in combustion and fluid dynamic systems', **AIAA Paper-85-0540**, Presented at the AIAA meeting on Shear Flow Control, Boulder.

Three more publications that will follow are:

B.T. Chu, K.R. Sreenivasan & S. Raghu (1987) 'On the control of combustion instability', to appear in **Progress in Aerospace Sciences**.

S. Raghu & K.R. Sreenivasan (1987) 'Control of acoustically coupled combustion and fluid dynamic instabilities', **AIAA Paper -87-2690** to be presented in the **11th Aeroacoustic Conference** in Sunnyvale, CA, Oct. 19-21.

S. Raghu, R.P. Bradley & W.M. Roquemore (1987) 'Control of combustion oscillations', to be presented at the NATO Advanced Study Institute in a **Conference on Instrumentation for Combustion and Flow**, September 14-25, 1987, Portugal.

3. Viscous Drag Reduction

Again, the bulk of this work has remained unpublished, but a majority of the work has been summarized in the following Ph.D. thesis.

a) T. B. Lynn (1987): 'Manipulation of the Structure of a Turbulent Boundary Layer'

The manipulation of a turbulent boundary layer for the purpose of net drag reduction is an attractive topic for research, because even modest success will result in large energy savings. The focus of this work is passive manipulation, one of the simplest manipulation techniques. The most promising manipulator to-date is the so-called BLADE device, consisting of two thin ribbons or foils suspended in the outer portion of the boundary layer. BLADE devices were devised and researched first at the Illinois Institute of Technology (IIT) and NASA Langely. When we began this research, there was significant controversy over the magnitude of net drag reduction possible (20% reported by the IIT group) and the maximum skin friction reduction obtainable (50% reported by the IIT group).

Accurate local skin-friction have been made using sublayer fences in a perturbed boundary layer. By comparing our direct measurements with those obtained by indirect methods, we have determined that the degree of drag reduction depends on the method used to calculate the combined devise drag and skin friction drag.

Using auto and two-point correlation measurements as well as space-time correlations, we investigated the effects of BLADE devices on the turbulent structures in the boundary layer, comparing them with wire devices which are known not to produce a net reduction in drag. The sustained effects of the BLADE devices were, in all length scale measurements, stronger and longer lasting than those of the wire devices. The space-time correlation revealed that the most significant effect of the BLADE device was on the large structure (the dominant structure in the outer region of the boundary layer). In contrast, the wire manipulator had no effect on the large structures. The BLADE's alteration of the large structure was evident in the marked difference in the development of the wakes downstream of the two devices.

We have also investigated inner layer devices consisting of sublayer wires. The results from both the inner and outer layer manipulations suggest the effective alteration of a turbulent boundary layer depends on the scaling of the device. The dominant turbulent structure in the region of interest dictates the proper scaling of the device.

b) In addition, a Master's degree work by Mr. Mark Lee partly on the effect of a rotating cylinder immersed in the turbulent boundary layer should be mentioned. This work showed the importance for drag reduction of lifting objects immersed in the turbulent boundary layer. This is a matter of ongoing research, and will be reported elsewhere.

c) Some of our work on the so-called BLADE manipulators was summarized also in an invited talk (with R. Narasimha) at the **AIAA Conference on Shear Flow Control,** Boulder. The talk was prepared in the form of the following report:

R. Narasimha & K.R. Sreenivasan (1987); 'Flat plate drag reduction by turbulence manipulation', Report Number 86FM4, Department of Aerospace Engineering, Indian Institute of Science, Bangalore.

4. Miscellaneous items

In the course of work we did several years ago, it became evident that the zero normal velocity boundary condition, imposed in the interior of a turbulent flow, will have a srong effect on the flow evolution. To test these ideas, we set up several experiments in grid turbulence, but have pursued them only sporadically, the reason being that our resources were limited, and we had to make a choice on priorities.

For the same reason, we have also not written up on our pipe flow work, related to the effects of initial conditions on the evolution of the flow.

However, two pieces of research in this category have been written up. These are enclosed, and a brief description is included below.

a) K.R. Sreenivasan (1983): 'Some studies in non-simple pipe flows', Invited paper in **Trans. Inst. Engineers Australia**, vol. ME8, pp.200-208.

A variety of phenomena occurs in pipe flows, especially if we stray away from straight circular pipes of uniform crosssection. This paper illustrates a few of the complexities arising from the relatively simple changes in geometry, namely, the sudden expansion and the coiling of the circular pipe. In particular, the phenomena examined are relaminarization, large amplitude self-excited oscillations in sudden expansions, transition to turbulene, and retransition from the relaminarized state to a turbulent one.

b) K.R. Sreenivasan (1984): 'On the scaling of the turbulence energy dissipation rate', **Phys. Fluids**, 27, 1048-1051.

From an examination of all data to-date on the dissipation of turbulent energy in grid turbulence, it was concluded that, for square-mesh configuration, the ratio of the time scale characteristic of dissipation rate to that characteristic of energy-containing eddies is a constant independent of Reynolds number, for microscale Reynolds numbers in excess of about 50. Insufficient data available for other grid configurations suggest a possibility that the ratio could assume different numerical values for different configurations. The persistent effect of initial conditions on the time scale ratio is further illustrated by reference to the jet-grid data of Gad-el-Hak and Corrsin.

Concluding remarks

A part of progress achieved during this period has been of qualitative nature, that is, of the type that has helped us to pose the right questions for further inquiry. In fact, some of the work now being done by us, which seems to hold more promise, has had its roots in the exploratory work done under AFOSR sponsorship during the period under consideration. In this sense, the significance of the work to be described below lies beyond the specifics. We are happy to acknowledge this indebtedness to AFOSR.

It may not be out of place to note that, as a secondary outcome of the AFOSR support, three Ph.D.'s and two M.S.'s were produced at Yale. One of the Ph.D.'s (Paul Strykowski) has accepted a professorial position at Brown, the second (Ted Lynn) a post-doctoral position at DFVLR in Berlin, while the third is a post-doctoral fellow at Yale. One of the two Master's degree recepients (Mark Lee) is currently employed at the Wright Patterson Air Force Base, while the second (David Kyle) has taken a break from studies to pursue a different career.

TURBULENCE AND CHAOTIC PHENOMENA IN FLUIDS
T. Tatsumi (editor)
Elsevier Science Publishers B.V. (North-Holland)
© IUTAM, 1984

ON ANALOGIES BETWEEN TURBULENCE IN OPEN FLOWS AND CHAOTIC DYNAMICAL SYSTEMS

K.R. Sreenivasan and P.J. Strykowski
Mason Laboratory, Yale University, New Haven, CT 06520

We briefly study turbulence in open flow systems in the context of concepts developed in studies of chaotic dynamical systems. Although several flows have been examined, particular attention will be focussed on the question of transition to turbulence in coiled pipes; some degree of correspondence with the Ruelle-Takens-Newhouse route to chaos is indicated. Using the Grassberger-Procaccia algorithm, the dimension of the attractor for velocity signals during and immediately after transition to turbulence has been computed. Our results, such as they are, indicate that the dimension is relatively low. Brief comments will be made on the difficulties of computing the dimension, as well as on the relevance of strange-attractor theory to fully-developed turbulence.

INTRODUCTION

Recent studies of the dynamics of nonlinear systems with finite (and small) number of degrees of freedom have produced profound results with probable implications to the very notion of chaos – for example, in kinetic theory of gases in the context of the Boltzmann equation – but the interest of fluid dynamicists in these studies stems primarily from the notion of genericity, that is, the expectation that the qualitative properties of the Navier-Stokes equations are shared also by these simpler systems. A related important (and, to our knowledge, as yet untested) expectation is that turbulence, at least not too far away from transition, behaves like a strange-attractor. Without going into details, we may restate the above supposition to mean that turbulence has a manageably small number of 'dynamically significant' degrees of freedom, despite the overwhelming complexity it displays, or that one may be able to extract a finite-dimensional projection out of an infinite-dimensional phase space.

As we know today, three distinct 'scenarios' of chaos have been indentified; more will no doubt be discovered. In the first scenario, chaos sets in abruptly following very few (most probably, three) Hopf bifurcations [1,2]. In the second, the onset of chaos occurs via an infinite cascade of period doubling [3,4,5] with certain well-defined universal characteristics. The third, less-studied, route envisages chaos through gradual merging of decreasingly intermittent chaotic regions [6]. Obviously, these scenarios of chaos have at least qualitative resemblence to transition to turbulence in one or the other of the fluid flows; considerable work [7-10] in the last few years has shown that the correspondence is more than superficial in highly constrained 'closed flow systems', that is, fluid flows which are totally confined within a closed boundary (for example, the narrow-gap Taylor-Couette flow, or convection in a finite box of small dimension). Although it appears certain that many aspects of transition, even in confined

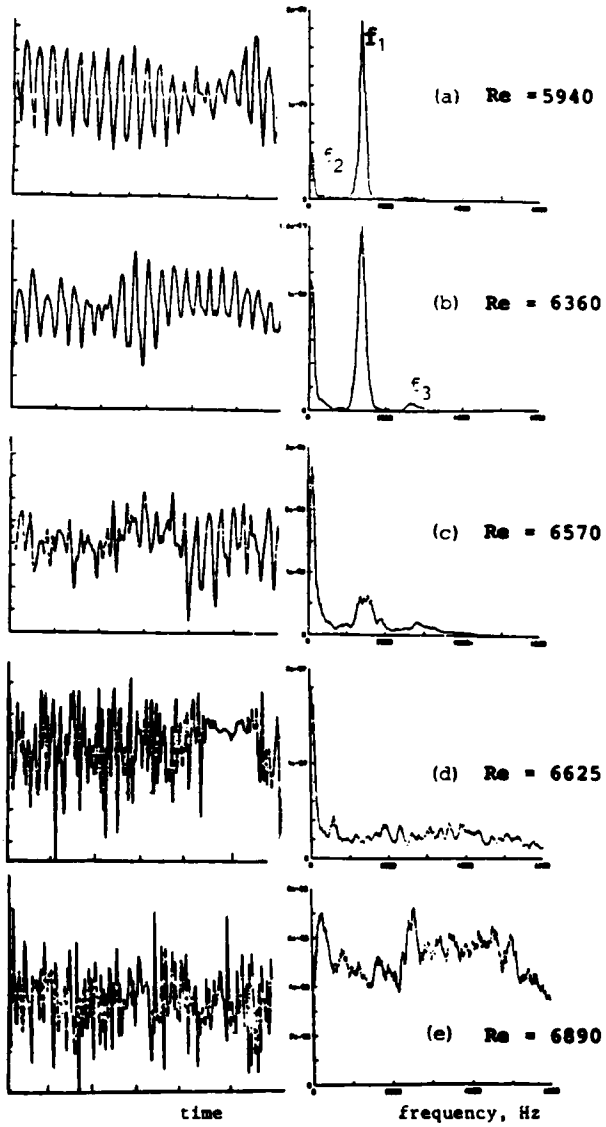

Figure 1. Time traces (duration 15 ms) and power spectral densities of the fluctuating velocity u on the pipe centerline of a coiled pipe; pipe diameter = 3.18 mm, coil radius = 42 mm. Same gain for all cases. Note that the spectral ordinates do not all have the same scale. In general, open systems are characterized by the presence of sizeable noise in the initial conditions, which is why we have chosen to plot the power on a linear scale. Some averaging has been performed on the power spectra.

fractal dimension D, an adaptation of the Hausdorff dimension. (The fractal dimension may be viewed as a measure of the information necessary to specify the location of a fractal set. For classical cases with self-similarity, it coincides with the usual notion of dimension.) Calculating D using box-counting algorithms is not practical if $D \gtrsim 2$ (see [13]), as is surely the case for turbulence (see below). Another dimension ν, related to the fractal dimension $D(\nu \leq D)$, as well as the information-theoretic entropy, has been proposed [14]. If $\underset{\sim}{v}$ is the n-dimensional vector in time domain, one computes first the quantity C(r) given by

$$C(r) = \lim_{N\to\infty} \frac{1}{N^2} \sum_{i,j=1}^{N} H(r - |\underset{\sim}{v}_i - \underset{\sim}{v}_j|), \qquad (1)$$

where $\underset{\sim}{v}_i = \underset{\sim}{v}(i\tau')$, τ' being the sampling interval, and H is the Heaviside step function. For r not too large, it can be shown that $C(r) \sim r^{\nu}$. Grassberger & Procaccia [14] have shown that $\nu = D$ for several chaotic attractors commonly discussed in the literature on dynamical systems, and have argued that, where it is smaller than D, ν is in fact the more appropriate quantity to consider. We shall not discuss this further but only note that D is a quantity related to geometry, while ν has a probablistic content in it. In our computations of ν, we used real-time data of the axial velocity component to construct a multidimensional vector using the delay coordinates $(u_t, u_{t+\tau}, \ldots, u_{t+(d-1)\tau})$ with increasing values of d, and evaluated ν as indicated above; τ is an integral multiple of τ'. Initially, ν increases with d but settles down eventually. It is this asymptotic value

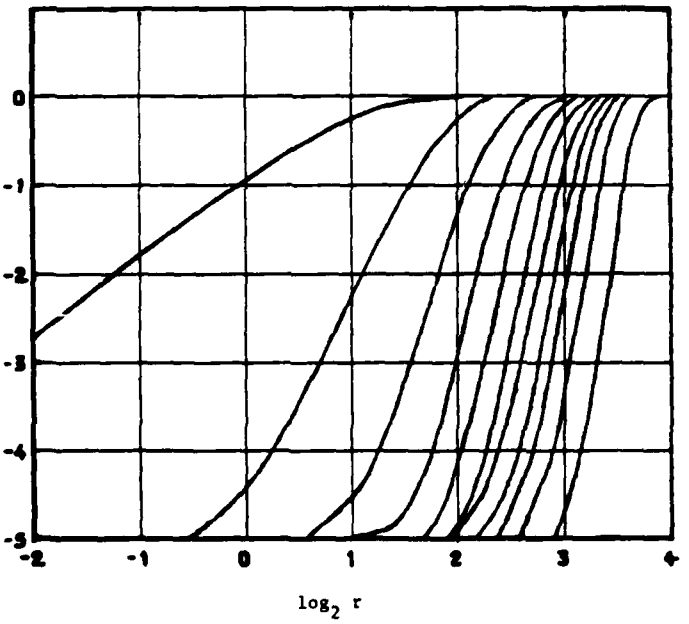

Figure 2. The quantity $\log_2 C(r)$ vs $\log_2 r$, r in arbitrary units. Re = 6625. Different curves correspond to different d. From left to right, d = 1, 5, 10, 15, 20, 25, 30, 20, 50 and 70.

of ν that is of interest to us. If ν is relatively small, the concept of strange attractors may be very useful in turbulence; otherwise, it is hard to assess its significance.

As a check on our computational procedure, we may note that ν was found to be 1 for a sine wave and 0.63 for a Cantor set, as expected. Since a purely random signal, such as the output of a white-noise generator, has a space-filling attractor, $\nu \approx d$ for all d.

Figure 2 shows several curves of log C(r) vs log r, computed with increasing values of d, from the velocity data for Re = 6625 just after the onset of the broadband spectral behavior. Typically, these curves have a linear region; the levelling off of the curves for large r is the result of the finiteness of the attractor, while deviation from linearity towards the very low end of the curves arises from resolution problems. The slope of the linear region increases with d initially but appears to settle down to a constant beyond a certain d. This can be seen more directly from figure 3. The asymptotic value of ν is around 6.

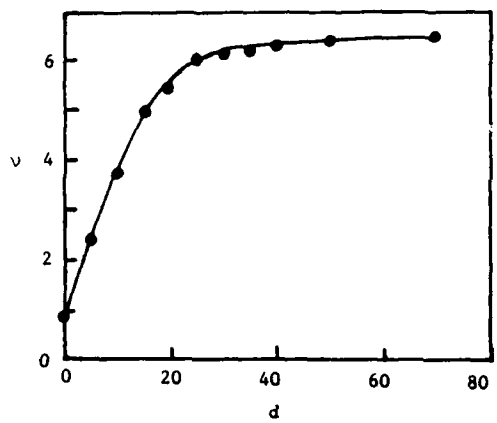

Figure 3: The slope ν of the straight regions of curves in figure 2, vs the dimension of the phase space, d. The asymptotic value is around 6.

The data presented in figures 2 and 3 are typical of our computations, which extend to Reynolds numbers on either side of 6625. However, they are not sufficiently systematic at this point to be included here as conclusive results. This is so chiefly because we have not yet made the various sensitivity tests on ν. First, before the signal is digitized, some low-pass filtering is necessary; we have not investigated the effect of varying this cut-off on ν. We have also not investigated very thoroughly the effect of varying τ on ν. Typically, however, this latter effect is not significant over a fairly wide range of τ. With these reservations noted, we may mention that, for Re < 6625, the value of ν is less than 6, while being a rather strongly increasing function of Re at higher Re; in fact, at the highest Reynolds number of our computations, we have not yet seen ν settle down even for d as large as 100. (Our initial results presented at the meeting in Kyoto were necessarily at lower Reynolds numbers than 6625.)

DISCUSSION AND CONCLUSIONS

The results of the previous two sections represent only a small part of a largely unyielding investigation. In relation to transition and the scenarios of chaos, our experience is that none of the above-mentioned routes to chaos occurs during

transition to turbulence in open systems like jets or wakes. While it is of course possible that more than one of the above scenarios operate simultaneously, it looks certain that turbulence, unless constrained severely, does not behave like a simple dynamical system. On the other hand, we would like to make a specific mention of the fact that our initial experience with coiled pipes was disappointing too; it was only after some modifications of the flow were made, primarily in the form of a smoother inlet to the upstream straight section, that we could observe the evolution discussed earlier. Can we then make the sweeping generalization that, by making 'appropriate' changes to the flow, perhaps by way of restricting initial conditions to a suitable (but unknown) 'basin of attraction', we can nudge transition to follow some well-defined scenario of chaos?

What specifically has our work shown in relation to fully developed, or, at least, 'nascent' turbulence? While much work needs to be done, it suggests that, at least at Reynolds numbers not too far above the transition value, the attractor for turbulent signals is relatively low-dimensional. It may thus justify attempts at extracting for the Navier-Stokes equations a finite-dimensional projection out of the seemingly infinite-dimensional phase space. We should, however, note that the dynamical systems approach will at best represent a small part of the total picture in turbulence unless the spatial chaos and order, as well as the relation between these latter characteristics and temporal behavior, are discussed.

ACKNOWLEDGEMENTS

KRS would like to thank Professor E.T. Onat for initiating his interest in this area, Professor R. Jensen for a useful conversation, and Dr. H. Oertel and his colleagues in DFVLR, Göttingen, for their interest; he also acknowledges the award of the Humboldt fellowship. This paper originated from work begun on an AFOSR grant on turbulence control.

REFERENCES

[1] Ruelle, D. and Takens, F., Commun. Math. Phys. 20 (1971) 167-192.

[2] Newhouse, S., Ruelle, D. and Takens, F., Commun. Math. Phys. 64 (1978) 35-40.

[3] May, R.M., Nature, 261 (1976) 459-467.

[4] Feigenbaum, M.J., J. Stat. Phys. 21 (1979) 669-706.

[5] Feigenbaum, M.J., Commun. Math. Phys. 77 (1980) 65-86.

[6] Manneville, P. and Pomeau, Y., Physica 1D (1980) 219-226.

[7] Gollub, J.P. and Swinney, H.L., Phys. Rev. Lett. 35 (1975) 927-930.

[8] Fenstermacher, P.R., Swinney, H.L. and Gollub., J. Fluid Mech. 94 (1979) 103-129.

[9] Ahlers, G. and Behringer, R.P., Phys. Rev. Lett. 40 (1978) 712-715.

[10] Libchaber, A. and Maurer, J., J. de Physique 41 (1980) c3-51 — c3-56.

[11] Sreenivasan, K.R. and Strykowsky, P.J., Experiments in Fluids 1 (1983) 31-36.

[12] Mandelbrot, B., In: Turbulence and Navier Stokes equation (ed: R. Temam) Lecture Notes in Math., 565 (1976) 121-145.

[13] Greenside, H.S., Wolf, A., Swift, J. and Pignataro, T., Phys. Rev. 25 (1982) 3453-3456.

[14] Grassberger, P. and Procaccia, I., Phys. Rev. Lett. 50 (1983) 346-349.

Transition and Turbulence in Fluid Flows and Low-Dimensional Chaos

K.R. Sreenivasan

Department of Mechanical Engineering, Yale University
New Haven, CT 06520, USA

Recent studies of the dynamics of low-dimensional nonlinear systems with chaotic solutions have produced very interesting and profound results with several implications in many disciplines dealing with nonlinear equations. However, the interest of fluid dynamicists in these studies stems primarily from the expectation that they will help us understand better the onset as well as dynamics of turbulence in fluid flows. At this time, much of this expectation remains untested, especially in 'open' or unconfined fluid flows. This work is aimed at filling some of this gap.

Measurements made in the wake of a circular cylinder, chiefly in the Reynolds number range of about 30-10^4, have been analyzed to show aspects of similarity with low-dimensional chaotic dynamical systems. In particular, it is shown that the initial stages of transition to turbulence are characterized by narrow windows of chaos interspersed between regions of order. The route to the first appearance of chaos is much like that envisaged by Ruelle & Takens; with further increase in Reynolds number, chaos disappears and a return to three-frequency quasiperiodicity occurs. This is followed in turn by the reappearance of chaos, a return to four-frequency quasiperiodicity, reappearance of chaos yet again, and so on. We have observed several alternations between order and chaos below a Reynolds number of about 200, and suspect that many more exist even in the higher Reynolds number region. Each window of chaos is associated with a near-discontinuity in the vortex shedding frequency and the rotation number, as well as a dip in the amplitude of the vortex shedding mode. It is further shown that the dimension of the attractor constructed using time delays from the measured velocity signals is truly representative of the number of degrees of freedom in the ordered states interspersed between windows of chaos; it is fractional within the windows of chaos, and is higher than those in the neighbouring regions of order. Our measurements suggest that the dimension is no more than about 20 even at a moderately high Reynolds number of 10^4, and that it probably settles down at about that value.

1. Introduction

a. General remarks

The principal parameter of incompressible viscous flows, in situations free of body forces, is the Reynolds number, Re. Observations show that for given (fixed or time-independent) boundary conditions (and external forces if applicable), the flow

is unique and steady for $Re < Re_{cr}$, where Re_{cr} is a certain critical value of Re; this is the steady laminar motion. As Re increases, the fluid motion may first become periodic, quasiperiodic, and 'eventually' chaotic. (Chaos is defined better in section 3 and in the appendix, but we shall also loosely use the word to designate a state in which the details of motion are not reproducible.) This chaotic state is not necessarily turbulence as generally understood – and we shall discuss this shortly – but it is believed that one attains the turbulent state if the Reynolds number is taken to a sufficiently high value. The goal of the stability theory is to understand how the evolution from the laminar to the turbulent state occurs, while turbulence theories aim at unearthing and predicting the mysteries of the (fully) turbulent state itself.

It is generally believed that the key to both these problems lies in the Navier-Stokes (NS) equations, and that no additional hypotheses of fundamental nature are required for describing either the onset of turbulence or its dynamics. Much effort has thus been spent on mastering the NS equations. However, the difficulties, both analytical and computational (at high enough Reynolds numbers), remain intimidating.

In the recent past, claims have been made that autonomous dynamical systems with small number of degrees of freedom, typified by

$$\frac{db_i}{dt} = f(b_i;\ \varepsilon_i), \tag{1.1}$$

where the b_i characterize the state of the system (the so-called 'state variables'), i is a small integer, and ε_i are the so-called control parameters (analogous to Re in the NS equations), help us towards attaining both the goals mentioned above. It is to a discussion of aspects of these claims, via an example of fluid flow behind circular cylinders, that this paper is devoted.

b. Remarks on degrees of freedom, genericity, and spatial chaos

Several questions arise immediately. One natural question concerns the relevance to fluid flows of low-dimensional dynamical systems. To give some meaning to the concept of degrees of freedom in fluid flows, let us *approximate* the velocity vector u_j appearing in the NS equations as

$$u_j = \sum_{\underset{\sim}{k}} a_j(\underset{\sim}{k};t)\, e^{i\underset{\sim}{k}\cdot\underset{\sim}{x}} \quad (j = 1,2,3), \tag{1.2}$$

where the wave number vector $\underset{\sim}{k}$ is an element of a discrete (finite or infinite) set. The NS equations can then be written formally as

$$\frac{\partial a_i(\underset{\sim}{k};t)}{\partial t} = F(a_i;\ Re),\ i = 1,2,\ldots.N\ (\text{large}). \tag{1.3}$$

The number of the coefficients a_i which, for given boundary conditions for the fluid flow, are capable of variation in time can now be called the degrees of freedom of the fluid flow governed by the NS equations (to within the approximation implied in (1.2) and (1.3)). Since the laminar flow is uniquely specified by the boundary (and external force) conditions, this number is zero. If Re increases just past

Re_{cr}, only a few degrees of freedom are excited, and hence it appears that, at least in the positive neighbourhood of Re_{cr} (to be called transcritical region henceforth), consideration of these few degrees of freedom is adequate.

An interesting hypothesis (which we shall examine in this paper) is that the number of degrees of freedom (not necessarily in the sense described above) remains small even in (certain type of) high Reynolds number turbulence.

Assuming that the number of degrees of freedom excited in the transcritical region is indeed small, we must ask whether the behavior in this transcritical region does not depend on the broad nature of the right hand side of equations (1.1) and (1.3). The most often cited justification for the belief that this dependence is in some sense of secondary importance comes from the work of Ruelle & Takens [1] and Newhouse, Ruelle & Takens [2] which indicates that chaos sets in abruptly following a few Hopf bifurcations, and that this behavior is 'generic' or 'typical'.

The words 'generic' and 'genericity' find their frequent use in the literature on dynamical systems, and so, it is perhaps useful to discuss the concept briefly. Ruelle & Takens make this concept quite specific for the vector fields they were considering, but we shall be content with a rather loose qualitative description. Consider as an *example*, a class of functions possessing continuous derivatives up to a certain order, and satisfying differential equations of the type (1.1). Properties of this class of functions which are the rule and not the exception, and which do not depend on the precise nature of the right hand side of (1.1), are called generic. The conclusions of Ruelle & Takens strictly hold for an idealized mathematical system, and whether the concept of genericity is powerful enough to embrace fluid systems is not clear. One should attempt to answer this question by looking at the specific form of F in (1.3) and/or by observing the actual bifurcations in experiments on laminar-turbulent transition.

Even if the concept of genericity does hold for fluid flows, it is not obvious that interesting nongeneric phenomena do not occur. To make this notion specific, let us consider the following rather far-fetched example. Suppose we link (as in our example above) genericity to the existence of velocity fields possessing continuous derivatives of a certain order. Those generic properties may be irrelevant to a turbulent boundary layer since one cannot exclude the possibility that at some moment during bursting near the wall (a key event sustaining turbulence production) this smoothness condition is destroyed in spite of viscosity. It is therefore sensible to keep in mind that nongeneric behavior is neither uninteresting nor unlikely, especially when conditions such as configurational symmetry, vicinity to wall, play an important role in the evolution of the flow.

Finally, one must mention the predominant role played by spatial chaos (and order!) in turbulent flows of fluids. An important characteristic of fluid turbulence is random vorticity, whose presence necessarily implies that the velocity vector is a random function of *position*. Autonomous dynamical systems of the type (1.1), on the other hand, do not contain any space information. While temporal chaos in fluid turbulence may in some sense be symptomatic of spatial chaos, it is clear that

autonomous dynamical systems have little to say directly about the latter, at least at the current state of development.

c. 'Closed' and 'open' flow systems

Notwithstanding these remarks, it is necessary to note that several beautiful experiments now exist in the Taylor-Couette flow (e.g., Refs. 3, 4 and 5) and the convection box (e.g., Refs. 5 and 7) which have lent support to the notion that the behavior of fluid flows in the transcritical region could be similar to that of low-dimensional dynamical systems. This in itself is undoubtedly remarkable, but it should be remembered that these two flows are special in the following sense. In all 'closed flow' systems — of which the convection box and the Taylor-Couette flow are two popular examples — the boundary is fixed so that only certain class of eigenfunctions can be selected by the system; this does not hold for another class of flows we may call 'open flow systems' — for example, boundary layers, wakes, jets — in which the flow boundaries are continuously changing with position. Thus, while in closed flow systems each value of the control parameter (for example, the rotation speed of the inner cylinder in the Taylor-Couette problem) characterizes a given state of the flow globally, this is not true of open systems. Consider as an example the near field of a circular jet. For a given set of experimental conditions, the flow can be laminar at one location, transitional at another and turbulent at yet another (downstream) location. This usually sets up a strong coupling between different phenomena in different spatial positions in a way that is peculiar to the particular flow in question. Secondly, the nature and influence of external disturbances (or the 'noise', or the 'background or freestream turbulence') is more delicate and difficult to ascertain in open flows: the noise, which is partly a remnant of complex flow manipulation devices and partly of the 'long range' pressure perturbations, is not 'structureless' or 'white', no matter how well controlled. Finally, it is well known that closed flow systems can be driven to different states by means of different start-up processes; for example, different number of Taylor vortices can be observed in a Taylor-Couette apparatus depending on different start-up accelerations [8]. This type of path-sensitivity in a temporal sense does not apply to open systems, where the overriding factor is the path-sensitivity in a spatial sense (i.e., the 'upstream influence').

d. Scope of the paper

On balance, all these considerations suggested to us that it is desirable to look at some open flows to determine the extent to which dynamical systems can assist us in our goals of understanding transition and turbulence in fluid flows. This is the motivation for the work described in this paper, which is to be viewed more as a progress report than as a complete account; obviously much more remains to be done. Our approach is to select well-known flows and follow the bifurcations as closely as possible. (We reported some of our earlier work in pipe flows in [9] and wake work in [10].) Surprisingly, while much work has been done in these flows in the past, an

amazing amount of new information can still be acquired that will facilitate clarifying the relation between low-dimensional chaotic systems and fluid flow transition and turbulence. Part of the reason for this is undoubtedly that the details one looks for are often dictated by contemporary concerns.

2. Experiments

a. Experimental conditions

Although we have conducted experiments in wakes, jets and pipe flows, we choose to discuss here only our wind tunnel experiments in two-dimensional wakes behind circular cylinders. The Reynolds number range covered is from about 30 (slightly below the vortex shedding value) to about 10^4. Two wind tunnels — one of the blower type and one of the suction type — were used. Nylon threads, stainless steel wires and aluminium tubes, stretched tightly across the width of the wind tunnels, were used as wake generators. The aspect ratio varied between about 70 and 2000. The basic experimental conditions are summarized in Table 1.

Table 1. The flow configuration and experimental conditions

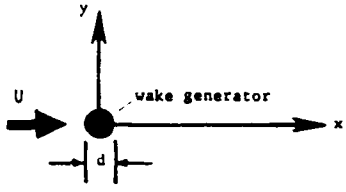

d (mm)	≈x/d	≈y/d	aspect ratio	wind tunnel characteristics
0.24	5	1	2000	suction type; turbulence level ≈ 0.2% at speeds of interest
0.24	50	1	2000	
0.36	5	1	1330	
4.0	5	1	170	
0.36	11	1	70	blower type; turbulence level varied from 0.68% at speeds ≈ 1 m/s to 0.06% at speeds ≈ 10 m/s

All velocity signals were obtained with a hot-wire operated on a DISA 55M01 constant temperature anemometer. The speed of the tunnel was monitored with a Pitot tube connected to a calibrated MKS Baratron with adequate resolution (and an averager). The hot-wire and the Pitot tube were mounted on a specially designed slim holder.

Some of the data to be presented in this and later sections is in the form of power spectral density of the streamwise velocity component, u. Nearly all the signals were digitized at sufficiently high frequency (60 kHz or more) to ensure that, whenever the signal was periodic, at least 30 digitized points were contained in one

period of the basic frequency (so that it was a good representation of the analog signal). Further, the entire length of the signal (which contained at least 100 cycles of the basic frequency) was Fourier transformed at once using the Cooley-Tukey FFT algorithm. The overriding criterion was that the spectral resolution should be as good as possible (here, between 0.5 Hz and 2 Hz compared with shedding frequencies of the order of 2000 Hz or more) and that one must not miss any low frequency modulations.

b. The background turbulence

We have worked with varying levels of background turbulence, and found that the occurrence of different stages of transition reported here is in itself not terribly sensitive to the turbulence level as long as it is not too high; larger turbulence levels blur the distinction between different stages and alter the details somewhat erratically. One should, however, strive to eliminate all strong discrete frequency components in the background turbulence structure.

Figure 1a shows a typical power spectral density of u in the freestream at Re = 60. (The ordinate is the logarithm to base 10 of the power.) The 'noise' (though

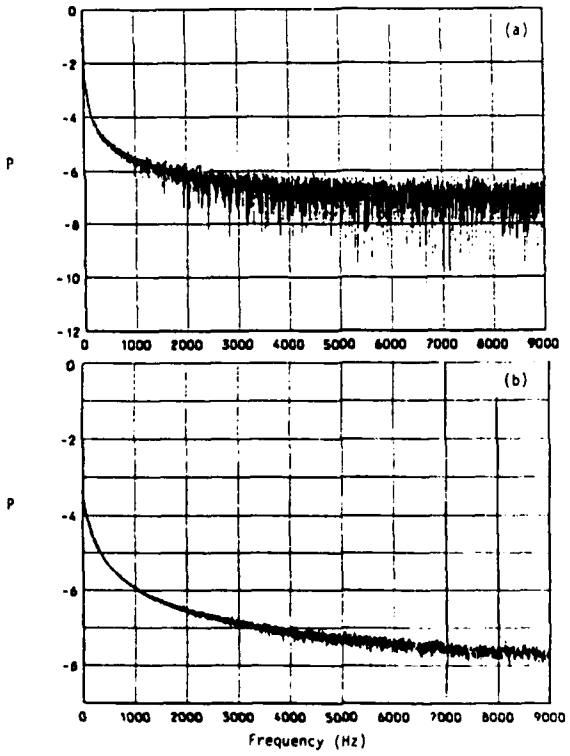

FIGURE 1: Normalized power (or frequency) spectrum of (a) noise of the instrumentation and digitizer, plus freestream disturbances, Re = 60; (b) instrumentation and digitizer noise only with no flow.

devoid of any disc
low frequency comp
the flow completel
erating the same w
content is not rep
noise. Allowance
spectral data to f

3. Results from

Figure 2 show
sity of u at a Rey
of the cylinder) o
ding. Notice that
the peak of the sp
quency behind the
than the noise lev
the right of f_1 wh

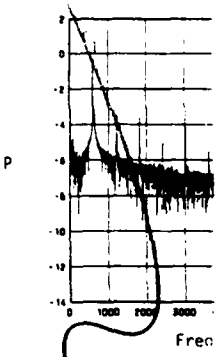

At a somewhat
the spectrum (figu
can be identified
basic vortex shedd

At an Re = 66
ingly strong discr
2 and 3. One migh

The sequence
in the Ruelle-Take
digression *roughly*
troduction to the

devoid of any discrete peaks) does not appear to be 'white' but has a much larger low frequency component. Figure 1b shows the power spectral density measured with the flow completely shut off, but the hot-wire and other electronic instruments operating the same way as before. It is clear that the anomalously high low frequency content is not representative of the flow itself, but of electronic and computer noise. Allowance should thus be made for this fact in the interpretation of the spectral data to follow.

3. Results from Spectral Measurements

a. Route to chaos: the first appearance

Figure 2 shows the logarithm (to base 10) of the normalized power spectral density of u at a Reynolds number (based on the freestream velocity and the diameter of the cylinder) of about 36, which is approximately the onset value for vortex shedding. Notice that the instrumentation and other noise level is around 10^{-8}, while the peak of the spectrum (marked f_1), corresponding to the basic vortex shedding frequency behind the cylinder, is at round $10^{-0.5}$, about 7½ orders of magnitude higher than the noise level! The sharpness of the peak (as well as of the other peaks to the right of f_1 which are the harmonics of f_1) is excellent.

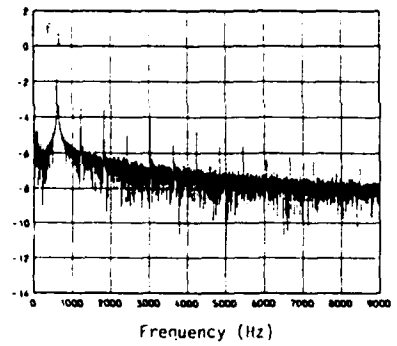

FIGURE 2: Normalized frequency spectrum of u at Re ≈ 36. Note that the power P is plotted on a logarithmic scale (to base 10). The peak at $f_1 \approx 590$ Hz corresponds to the vortex shedding, and the subsequent strong peaks above the noise level are simply harmonics of f_1.

At a somewhat higher Reynolds number of 54, there appear a number of peaks in the spectrum (figure 3a); as shown in the expanded version (figure 3b) all the peaks can be identified precisely in terms of the interaction of the two frequencies — the basic vortex shedding frequency f_1 and another incommensurate frequency f_2.

At an Re = 66 the spectrum (figure 4) shows broadened peaks with no overwhelmingly strong discrete components — quite a different situation from that of figures 2 and 3. One might say, in the language of dynamical systems, that chaos has set in!

The sequence of events leading to chaos are so far literally like that envisaged in the Ruelle-Takens-Newhouse (RTN) picture of transition to chaos, and so, a brief digression *roughly* describing this picture is quite useful. (The appendix is an introduction to the basic terminology.) With increasing Re, the steady laminar motion

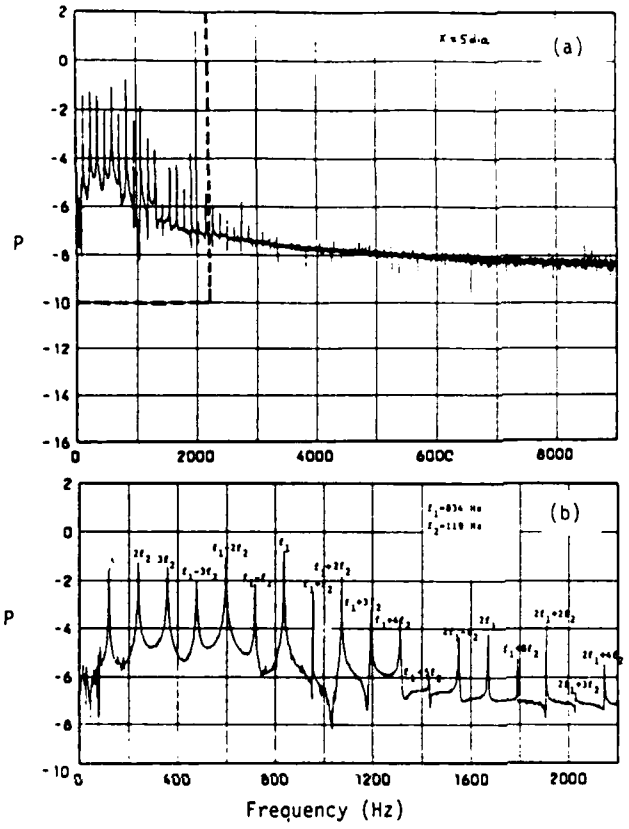

FIGURE 3: (a) Normalized frequency spectrum of u at Re = 54. In (b), the frequency range 0-2200 Hz is expanded. All significant peaks in (b) are simple combinations of the vortex shedding frequency f_1 (corresponding to the most dominating peak), and another incommensurate frequency f_2. After satisfying ourselves that there are no subharmonics of f_1 (and that 119.02 Hz is unrelated to the line frequency or spurious oscillations of the cylinder) we have picked f_2 by hypothesizing that the peaks nearest f_1 must be $f_1 \pm f_2$. The value of f_2 thus obtained accounts for every other significant peak as shown in (b) — actually to 4 or 5 decimal places for reasons we do not understand! At least part of the reason for the relatively low noise level (compared with figure 2) is the increased signal level.

loses stability and becomes periodic with frequency f_1 (say); the power spectral density will have (as in figure 2) a peak at f_1 (and its harmonics), and the phase diagram will show a limit cycle behavior. Loss of stablility of this new state yields a quasiperiodic motion with two independent frequencies, f_1 and (say) f_2. The spectral density will now show f_1, f_2 and various combinations $mf_1 \pm nf_2$ (as in figures 3a, b), and the phase portrait will be a two-torus. Further increase in Reynolds

number yields a quasiperiodic motion with three frequencies (three-torus). Newhouse, Reulle & Takens [2] argue that even a weak nonlinear coupling (of a certain variety!) among the three frequencies is likely to result in chaos or a strange attractor (see appendix), one of whose symptoms is an increased broadband content (see figure 4). This contrasts the classical picture of Landau, according to which turbulence is the asymptotic state of increasingly higher order quasiperiodicities.

Phase diagrams provide complementary information on the sequence of events leading to chaos. To construct phase diagrams, it would seem that one would require the *measurement of N independent variables* (in general, a hopeless task!), but embedding theorems like those of Takens [11] justify the use of a single measured variable. From the measured local velocity $u(t)$ – for example – one constructs a d-dimensional diagram from the vectors $\{u(t_i), u(t_i + \tau), \ldots. u(t_i + (d-1)\tau)\}$, $i = 1, \ldots\infty$, τ being a time delay whose precise value in a certain wide range seems to be immaterial. According to the embedding theorems, the phase diagrams constructed in the above manner will have essentially the same properties as the one with N independent variables, as long as $d \geq 2N + 1$ (although exceptions to this now commonly assumed philosophy are not hard to concoct). In practice, d is increased by one at a time until the properties of interest become independent of d.*

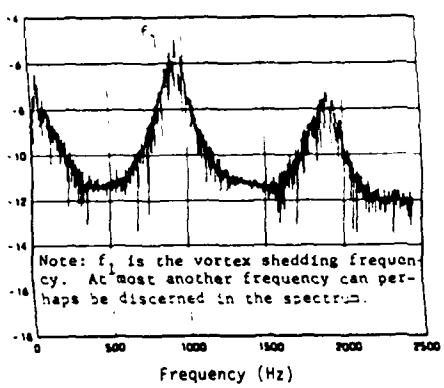

FIGURE 4: The first appearance of chaos at Re = 66. The broadband nature implies chaos; onset of chaos does not rule out the existence of spectral peaks. (Note: This does not signify some high order quasiperiodicity as dimension and entropy calculations of section 4 show.)

Figures 5, 6 and 7 show respectively the plot of $u(t_i + \tau)$ vs $u(t_i)$ at Re = 36, 54 and 66, and can be considered as projections of the phase diagrams on a two-dimensional plane. The limit cycle behavior at Re = 36 is evident, the scatter visible in the figure being partly due to experimental noise (see figure 2) and partly due to the jitter in the signal. Further, a Poincaré section reveals no discernible structure. The situation is thus basically periodic.

* About two years ago (October 1982) when we first started constructing phase diagrams in this manner, we were unaware of any literature on embedding theorems, but were guided solely by elementary *ad-hoc* considerations.

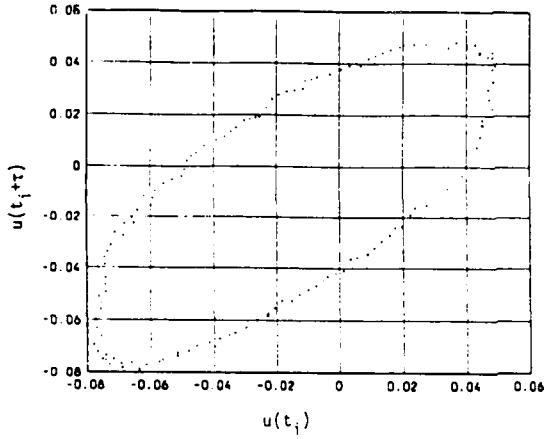

FIGURE 5: The phase plot from the velocity signal u at Re ≈ 36, showing limit cycle behavior. The time delay τ = 10 sampling intervals; the starting point t_1 is arbitrary.

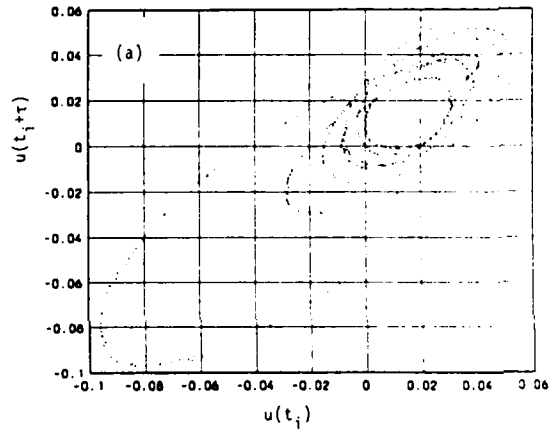

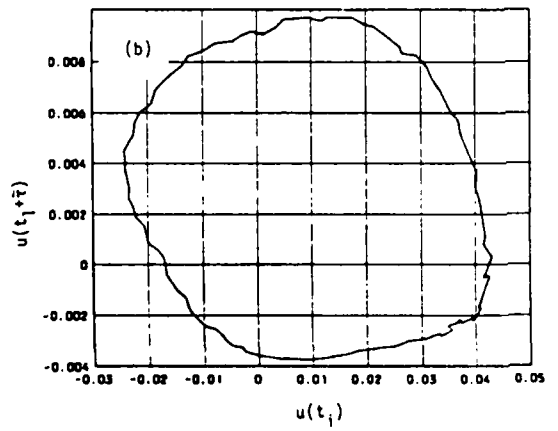

FIGURE 6: (a) The phase plot from u at Re ≈ 54. τ = 10 sampling intervals. (b) Poincaré section for the phase plot of (a). This is simply a plot of $u(t_i+\tau)$ vs $u(t_i)$ with τ spaced exactly $1/f_2$ apart.

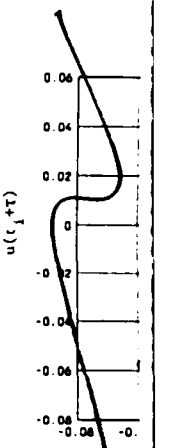

At Re =
pearance* fi
cing the fac
only is the
its Poincaré
tional dimen
chaotic.
(As equ
(characteris
entropy (whi
Limitations
– such measu
[5] – but we
This pr
attractor –
is thus extra
idealized ma
fluid dynami
It shou
the *signal* w
flow must po
flow at Re =
Reynolds num
nomenon (as
present turb
with an ever

* Note that
rarely str
can be rel

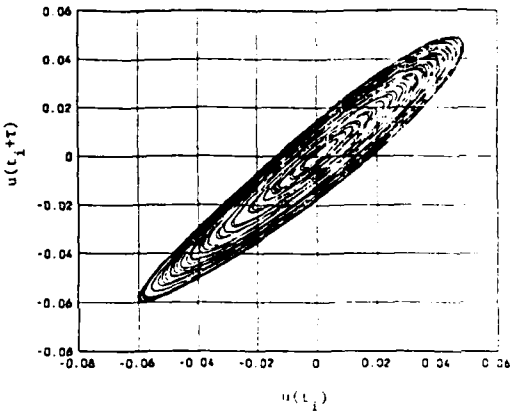

FIGURE 7: The phase diagram for Re = 66. τ = 10 sampling intervals. The continuous curve is now the result of joining successive data points (done for clarity).

At Re = 54, although the projection of the phase diagram is complicated in appearance*(figure 6a), a Poincaré section (figure 6b) yields a limit cycle, reinforcing the fact that only two degrees of freedom are present. On the other hand, not only is the projection of the phase diagram at Re = 66 complex (figure 7), but also its Poincaré sections (not shown), no matter how defined. This, as well as the fractional dimension of the attractor (see section 4a) show that the signal is indeed chaotic.

(As equally valuable measures of chaos, one could evaluate the Lyapunov exponent (characterising the exponential divergence of nearby trajectories) or the Kolmogorov entropy (which, for typical systems, equals the sum of positive Lyapunov exponents). Limitations of various kinds have prevented us from measuring the Lyapunov exponent – such measurements for a Taylor-Couette flow have been made by Brandstäter et al. [5] – but we do discuss some entropy measurements in section 4d.)

This progression towards chaos – underlying the possible presence of a strange attractor – proceeds much like that proposed by Newhouse, Ruelle & Takens [2]. It is thus extraordinary that the 'generic' behavior indicated by Ruelle & Takens for an idealized mathematical system should have a nontrivial bearing on a rather complex fluid dynamical system!

It should be noted that few would feel comfortable in designating as turbulent the *signal* we have recognized as chaotic. Clearly, to the extent that a turbulent *flow* must possess *spatial* randomness, we cannot say much of value as to whether the *flow* at Re = 66 is turbulent or not without a global survey of the flow field at this Reynolds number. Further, if one *defines* turbulence as a high Reynolds number phenomenon (as is often done!), it is tautologically true that the signal does not represent turbulence. Further, a look at the signal (figure 8) would prevent someone with an everyday familiarity with high Reynolds number turbulence from accepting it

* Note that the trajectory resides most often in the upper right quadrant, but only rarely strays away into the lower left quadrant. This behavior in the phase plane can be related to the finite skewness of the signal.

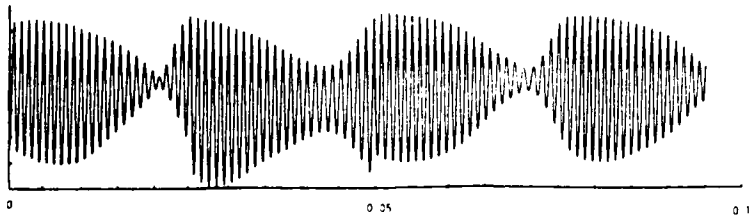

FIGURE 8: The signal u(t) at Re = 66.

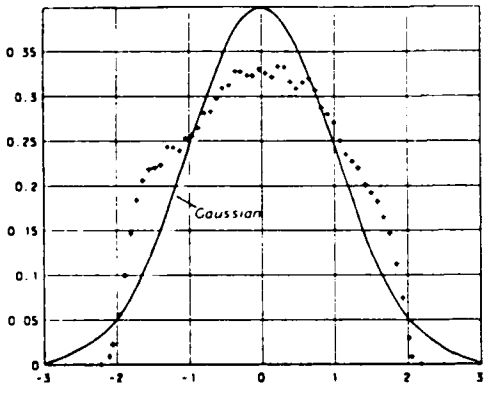

FIGURE 9: The measured probability density of u at Re = 66. The abscissa is the amplitude about the mean normalized by the root-mean-square of the signal, and the ordinate is the probability density. The signal has a skewness of near zero and a flatness of about 2.4.

as turbulent. Nevertheless, we would like to suggest that the signal shown in figure 8 is indeed random (for example, in terms of algorithmic complexity required to specify it [12]) with a well-defined probability density (see figure 9; for a comparison with similar data at 'large' Reynolds numbers in the far wake, see Thomas [13]). What this means is that even at low enough Reynolds numbers, the interaction of only a few degrees of freedom leads to randomness! It is also pertinent to point out that at least in some respects the signal of figure 8 resembles a narrow band pass filtered turbulent signal at high Reynolds numbers. (Perhaps the word 'preturbulence' also used commonly in dynamical systems literature, is sufficiently useful to designate the signal such as the one shown in figure 8, and its dynamics.)

b. Chaos and its aftermaths

No qualitative change occurs between Re = 66 and about 71. Soon thereafter the system becomes reordered. For example, the spectral density at Re = 76 shows (essentially) nothing but discrete peaks again (figure 10a). These peaks, shown in detail in figure 10b, can all be identified with great precision as arising from the interaction of *three* irrational frequencies. (That there are definitely three independent frequencies can also be seen from Poincaré sections (not shown here) and the dimension of the attractor discussed in section 4b). After a small increase in Reynolds number to about 81, one can see the onset of the broadband spectral content (figure 11), and we may consider chaos to have set in again!

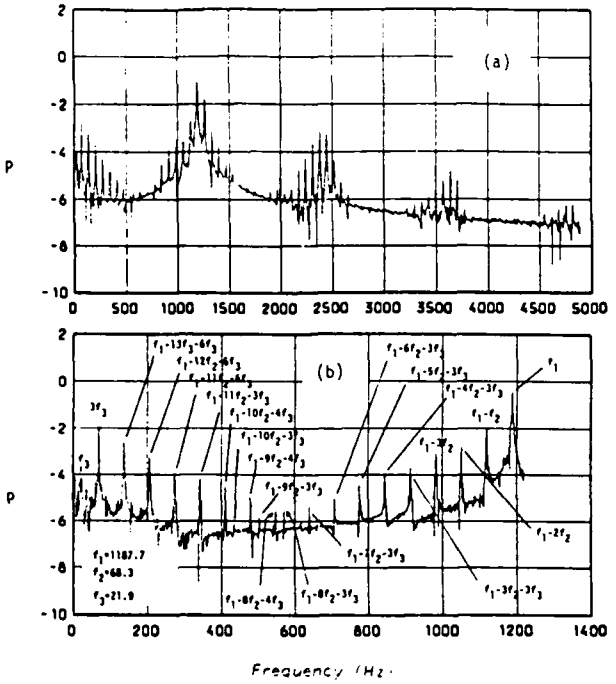

FIGURE 10: Reordering at Re = 76. (a) The measured power spectral density of u, and (b) its details in the frequency range 0-1250 Hz. Note that all peaks above noise level can be represented by combinations of three frequencies f_1, f_2 and f_3. This conclusion can certainly be influenced by the finite FFT resolution, but our belief in the accuracy of this statement comes also from dimension calculations (section 4).

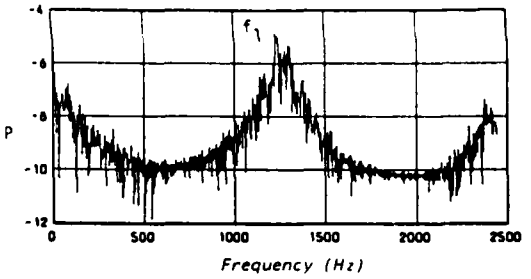

FIGURE 11: Chaos at Re = 81. f_1 is the vortex shedding frequency.

The system reorders itself around an Re of about 90, and we have discussed elsewhere [10] that this reordered state is quasiperiodic with four frequencies. (That this is the case will be demonstrated also by dimension measurements in section 4d.) Chaos sets in again at an Re = 140, followed by yet another reordering around an Re = 143. In fact, this sequence of return to chaos and reordering continues for much higher Reynolds numbers although it becomes progressively more difficult with increasing Re to distinguish experimentally between the two states.

Two related points of importance emerge. First, there do exist quasiperiodic motions with three or four independent frequencies; just like Landau's quasiperiodicities, the Ruelle-Takens picture of transition is also not the whole story. Second, transition to turbulence (at least in the temporal sense) is characterized by regions of chaos interspersed between regions of relative order. Each of these deserves at least a brief discussion.

c. Note on quasiperiodicities with more than two frequencies

We have shown that the route to the lowest Reynolds number chaos occurs in our experiments precisely as postulated in the RTN picture of transition. On the other hand, our experiments also show that quasiperiodicities with three (and possibly four) frequencies do exist. This type of disagreement with the RTN scheme has been noted earlier in the Taylor-Couette flow [14] and the convection problem [15]. It is thus pertinent to inquire whether there are (in some sense) exceptional conditions to be satisfied for the RTN scheme to hold. Greborgi et al. [16], who address this question in a specific numerical experiment, suggest that the three frequency quasiperiodicity is indeed quite likely to occur in practice, and that the special perturbation required to destroy this state (as in the RTN scheme) is unlikely. Haken [17] discusses this issue at some length and concludes that if the frequencies possess a certain kind of irrationality with respect to each other (or, more precisely, the so-called Kolmogorov - Arnold - Moser condition holds), bifurcation from a two-torus to a three-torus is possible. Both these discussions are strictly relevant to systems with no externally imposed noise (or fluctuations), a condition that does not strictly obtain in experiments (especially open systems). Our own experience is that the precise nature of even small amounts of noise (some of which is controllable in our wind tunnels and some of which is not!) has an influence on the evolution of the system (for a brief discussion of this influence, see subsection 3e). It is not hard to visualize that in our experiments the detailed conditions of intrinsic noise itself could have altered from before to after the first occurrence of chaos. Clearly, this is an area for further work, both experimentally and theoretically.

d. Windows of order and chaos

Figure 12 summarizes the changes occurring in the low end of the Reynolds number range we have considered. The shaded regions indicate windows of chaos, and the question marks indicate the uncertainty and difficulty in quantifying what we believe are reordered states.

At least two questions arise: What is the mechanism that permits the reordering of a chaotic state? What determines the length and location of the windows of chaos? Our understanding of these matters is rather limited, but even within these limits, some comments seem called for. Let us consider the first question now, and relegate the second one to the next subsection. The observed alternation between chaos and order has been known to occur in several low-dimensional dynamical systems; for ex-

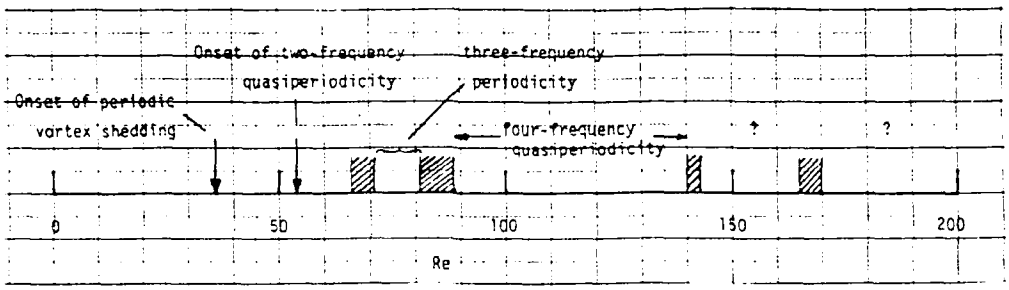

FIGURE 12: Window of chaos and order

ample, Lorenz equations [18], and spherical pendulum [19]. In these systems, the occurrence of reordering is independent of *external* noise. The numerical experiments of Matsumoto & Ysuda [20] show that chaotic orbits could be unstable to external noise, and noise addition to deterministic chaos (i.e., chaos characteristic of deterministic dynamical systems) yields an ordered state in some cases. They specifically consider the so-called Belousov-Zhabotinskii (BZ) reaction and some variants of the logistic model. Roux et al. [21] find windows of chaos and order in their experiments on the BZ reaction.

In experiments on open systems, it is hard to ascertain whether the return to order is tied intimately to external noise or the increased degrees of freedom associated with the appearance of chaos itself. In any case, the analogy between this situation and increased eddy viscosity in turbulent flows appears to be more than superficial: addition of high frequency modes results in a lowering of an effective Reynolds number and increased stability of the flow.

Though we have not made detailed spectral measurements at higher Reynolds numbers, it is our contention that the succession of order and chaos in a wake continues indefinitely even at very high Reynolds numbers (with the caution that order must now be interpreted to mean spectral sharpening). Roshko [22] pointed out several years ago that order reappears in the Reynolds number range of 10^6. More recently, the fluctuating lift force measurements of Schewe [23] on a circular cylinder showed that the spectral density of the lift coefficient was broad at $Re = 3.7\times10^6$ (upper end of transition) and became increasingly narrow until, at $Re = 7.1\times10^6$, it was quite sharp, rather like a narrow-band-pass filtered signal. Although the fluctuating lift force can at best be related to the squared fluctuating velocity filtered via the transfer function corresponding to the response of the circular cylinder, its behavior is nevertheless indicative of the flow itself in the vicinity of the cylinder.

e. The vortex shedding frequency and windows of chaos

Consider now the variation of the vortex shedding frequency f_1 with Reynolds number (figure 13). The frequency does not vary monotonically with Re but shows several more or less distinct breaks. Such breaks have been noted before [24,25,26], and perhaps most convincingly demonstrated in a beautiful experiment by Friehe [27].

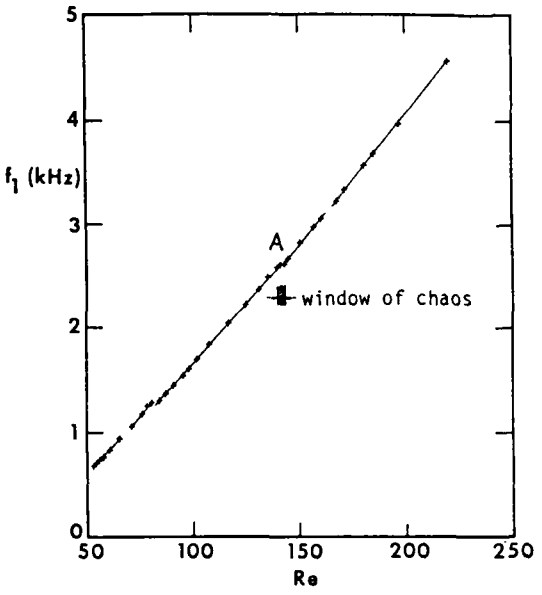

FIGURE 13: Variation of vortex shedding frequency with Re. Notice discontinuities, and their coincidence with windows of chaos, as illustrated near A.

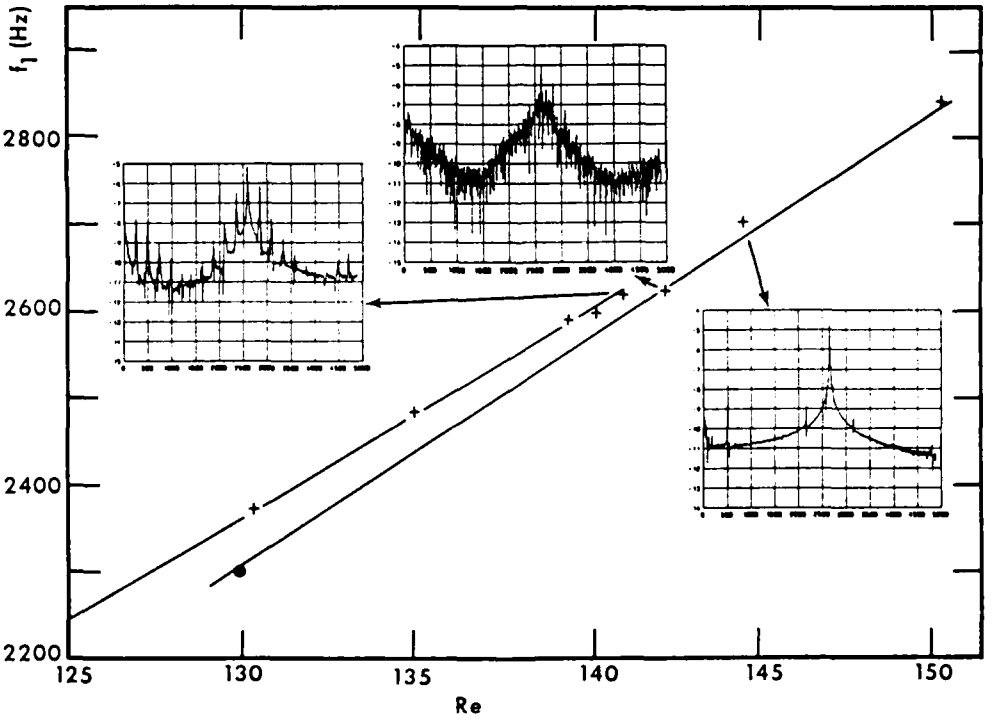

FIGURE 14: Expanded version of figure 13 near A. • shows a data point in another series of experiments where the window of chaos began at an Re ≈ 130.

Friehe varied the Reynolds number continuously at a small rate and obtained on an x-y plotter the frequency-Re variation directly. Although the appearance of the breaks has been disputed [28], our own data, presented here and elsewhere [10], support the conclusion that discontinuities do indeed appear.

Our interest here is in pointing out that the occurrence of these breaks coincides with the windows of chaos. To establish the connection better, we may consider in figure 14 the details of the break marked A in figure 13. Just upstream of the break, the spectral density is quite ordered (four-frequency quasiperiodicity) while it is broadband until the end of the break region coinciding with the upper end of the window of chaos; to the extent we can ascertain, the frequency spectrum shows a reordering immediately after the break.

The data shown by crosses in figures 13 and 14 were all obtained from one experimental run. In a repeat of the experiment the following day (for example) we found the same general features, except that chaos set in at different Reynolds numbers; the windows of chaos were also of different widths. The filled circle in figure 14 was obtained in a second series of experiments. It is seen that this point falls below the first set of data at the same Re, but it falls on the backward extrapolation of the line corresponding to the reordered state (Re $\geq$ 143) in the first set. It is hard to tell the differences between conditions in the two experiments without extensive documentation, but there are reasons to believe that the second experiment was conducted in a somewhat noisier environment. We thus speculate that the location as well as the widths of the windows of chaos are to some extent determined by noise characteristics – in a way that is not well understood at present.

It is interesting to note from figure 14 that the ratio f_2/f_1 (the so-called rotation number), where f_2 is the second largest independent frequency, changes its value abruptly across the narrow windows of chaos. Figure 15 is a plot of the rotation number with Re. It is seen that the number changes abruptly across all the windows of chaos, but only slowly within regions of order.

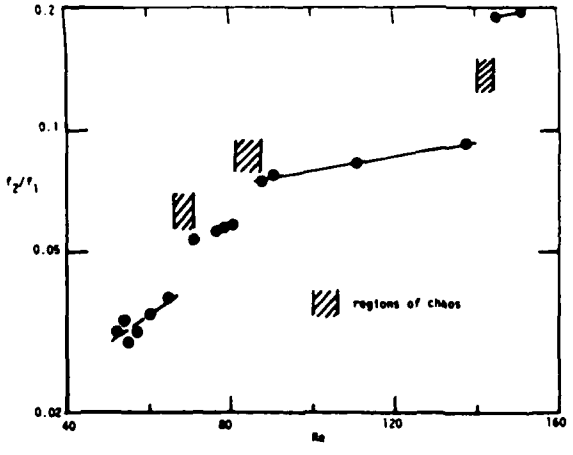

FIGURE 15: The variation of the rotation number with Reynolds number.

f. The amplitude of the vortex shedding mode and chaos

Since reordering is associated with the reemergence of stronger spectral peaks, it is natural to expect that there must be some relation between the amplitudes of the various modes and the occurrence of order and chaos. Figure 16 shows the amplitude of the vortex shedding mode (or the f_1 frequency) as a function of velocity. (The amplitude A_1 is expressed as a fraction of the freestream velocity U, but is given here to an arbitrary scale.) It is clear that O indicating order coincides with a local peak in A_1, C indicating the onset of chaos coincides with a local minimum, and, finally, RO indicating reordering coincides with the reappearance of a peak. Except for the first time that reordering occurs, every successive reordering is associated with a general lowering of the amplitude of the vortex shedding mode.

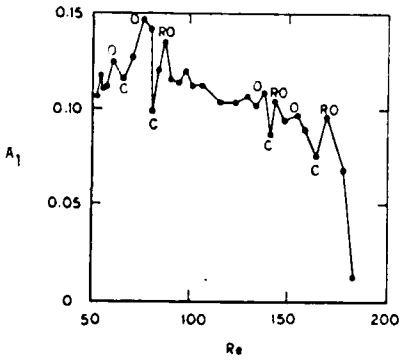

FIGURE 16: The amplitude of the vortex shedding mode as a function of Re. O is order, C chaos and RO is reordering; within a window of chaos, O and RO may in general indicate different states of order.

4. Results from the Dimension of the Attractor

a. The dimension

It is clearly worth inquiring whether there is any property of the attractor that successfully describes in some way the many subtle changes that occur in the frequency spectra and the related properties discussed in section 3. It appears that there indeed is such a quantity, namely the dimension of the attractor. Loosely speaking, the dimension of the attractor is related to the number of degrees of freedom — and hence its importance. The concept of the dimension is highlighted in studies of dynamical systems, and we may briefly digress here to discuss its meaning before presenting results from our measurements. It should be pointed out that, apart from our own earlier measurements of the dimension for turbulence attractors [9,10], such measurements have been made by others in the Taylor-Couette flow [5] and in the convection cell [29].

Let us consider an attractor (constructed as already discussed in section 3) from a measured temporal signal u(t) that is embedded in a (large) d-dimensional phase space. Let $N(\varepsilon)$ be the number of d-dimensional cubes of linear dimension ε required to cover the attractor to an accuracy ε. Obviously, making ε smaller renders N larger, but if the limiting quantity

$$D = \lim_{\varepsilon \to 0} \frac{\log N(\varepsilon)}{\log(\frac{1}{\varepsilon})} \tag{4.1}$$

exists, it will be called the dimension of the attractor. An important characteristic of a strange attractor is that D is small even though d is large. We should be interested in knowing whether transitional and turbulent signals have this property.

To see what the dimension means, let us write (4.1) as

$$N(\varepsilon) \sim \varepsilon^{-D}; \tag{4.2}$$

that is, if one specifies D and the accuracy ε to which we need to determine the attractor, we automatically know the number of cubes required to cover the attractor. The only missing information will now be the position of the cubes in the phase space. Thus, D can be considered as a measure of how much more information is required in order to specify the attractor completely; the larger the value of D, the larger is this missing information.

In general, the dimension D, as defined in (4.1), is fractional for strange attractors, and it has been called the fractal dimension by Mandelbrot [30] who has contributed a lot to our understanding of the quantity. As defined in (4.1), D is a geometric property of the attractor, and does not take into account the fact that a typical trajectory may visit some region of the phase space more frequently than others. Several measures, taking this probability into account, have been defined — and are believed to be closely related to the dynamical properties of the attractor. The most well-known among them are:

(a) the pointwise dimension

(b) the Grassberger-Proccacia dimension.

If the attractor is uniform, that is, every region in the phase space is as likely to be visited by the trajectory as every other, then the above two measures equal D defined by (4.1). Otherwise, they are generally smaller than D.

Let $S_\varepsilon(x)$ be a sphere of radius ε centered about a point x on the attractor, and let μ be the probability measure on the attractor. Then, the pointwise dimension is defined [31] as

$$d_p(x) = \lim_{\varepsilon \to 0} \frac{\log \mu[S_\varepsilon(x)]}{\log \varepsilon} \tag{4.3}$$

or

$$\mu[S_\varepsilon(x)] \sim \varepsilon^{d_p} \tag{4.4}$$

Grassberger & Procaccia [32] have defined another measure ν which is related to the dimension of the attractor, as well as the entropy (see section 4d). The procedure for computing ν is as follows:

(i) Obtain the correlation sum $C(\varepsilon)$ from:

$$C(\varepsilon) = \lim_{N \to \infty} \frac{1}{N^2} \sum_{\substack{i=j=1 \\ i \neq j}}^{N} H[\varepsilon - |u_i - u_j|] \tag{4.5}$$

where H is the Heaviside step function and $\underset{\sim}{u}_i - \underset{\sim}{u}_j$ is difference in the two vector positions $\underset{\sim}{u}_i$ and $\underset{\sim}{u}_j$ on the phase space. Basically, what C does is to consider a window of size ϵ, and start a clock that ticks each time the difference $|\underset{\sim}{u}_i - \underset{\sim}{u}_j|$ lies within the box of size ϵ. Thus, one essentially has

$$C(\epsilon) = \lim_{N\to\infty} \frac{1}{N^2} \{\text{number of pairs of points } (i,j) \text{ with } |\underset{\sim}{u}_i - \underset{\sim}{u}_j| < \epsilon\}$$

(ii) Obtain ν from the relation [32]

$$C(\epsilon) \sim \epsilon^{-\nu} \quad \text{as } \epsilon\to 0 \tag{4.6}$$

In practice, not all components of $\underset{\sim}{u}$ are known for constructing the phase space, but perhaps only one component, say u_m. As we discussed in section 3, one constructs a d-dimensional 'phase space' using delay coordinates

$$\{u_m(t_i),\ u_m(t_i+\tau),\ \ldots,\ u_m(t_i+(d-1)\tau)\},\ i = 1,\ \ldots, k,$$

where, again, τ is some interval which is neither too small nor too large and k is large (in principle, infinity!). Since one does not *a priori* know ν, one constructs several 'phase spaces' of increasingly large value of d and evaluates ν for each of them; ν will first increase with d and eventually asymptote to a constant independent of d. This asymptotic value of ν is of interest to us as a measure of the dimension of the strange attractor.

We have computed both d_p and ν as described above, using the streamwise velocity fluctuations u up to an Re of 10^4, and the delay coordinates. Our confidence in the numerical values of these measures of dimension is very good when they are less than about 5 or 6, but becomes increasingly shaky at higher values. However, we do believe that they are reasonable, judging from their repeatability and the several precautions we have taken (such as taking the proper limit as $\epsilon\to 0$ and using, in a couple of cases, double precision arithmetic in our computations). It would be interesting and useful to evaluate the dimension at high Reynolds numbers, but such calculations are likely to be of uncertain value (unless perhaps some carefully selected combination of experimental and computational conditions obtains): with increasing Re, the newly excited degrees of freedom can be expected to be of smaller and smaller scales, and to properly accommodate them in the dimension calculations requires that one must in practice look at increasingly smaller values of ϵ (see equation 4.6). Such efforts will very soon be frustrated by instrumentation noise and digitizer resolution problems.

b. Data for Re $\lesssim$ 100

It is convenient to consider first the data for Re $\lesssim$ 100 (figure 17). Concentrating on the data in the ordered states only, we may conclude the following. At Re = 36, where there is only one independent degree of freedom (corresponding to the periodic vortex shedding) — see figures 2 and 5 — the dimension of the attractor turns out to be about 1. When only two frequencies are present (figures 3 and 6) at Re =

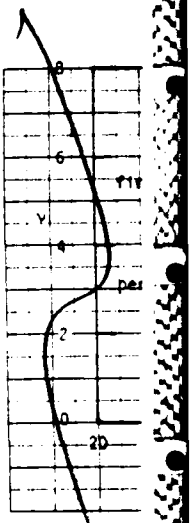

FIGURE 17:
numbers. Not
36), about
frequencies
to higher

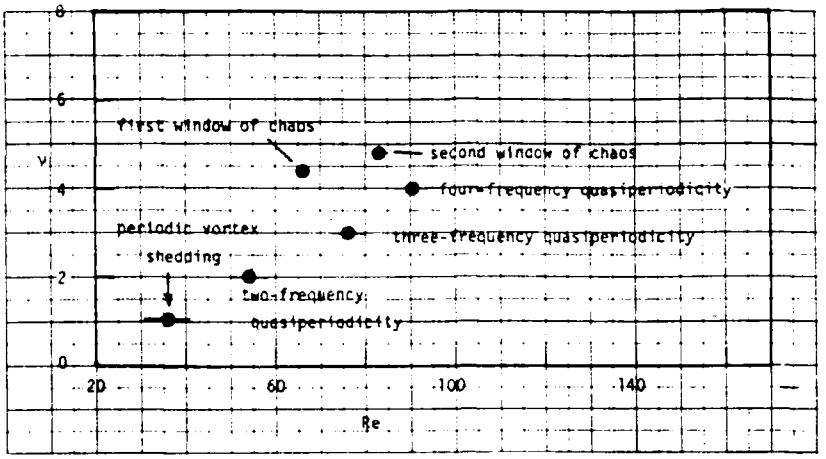

FIGURE 17: Variation of the dimension of the attractor with respect to Reynolds numbers. Note that the dimension is about 1 when there is only vortex shedding (Re = 36), about 2 when there are only 2 frequencies (Re = 54), about 3 when there are 3 frequencies (Re = 76), about 4 when there are 4 frequencies. The dimension jumps to higher noninteger values in the windows of chaos.

54, the dimension is about 2. At Re = 76 where there are three dominant frequencies (figure 10), the dimension is three to within experimental uncertainty. Lastly, at Re = 91 where there are four frequencies present, the calculated ν is very close to 4. Thus, to within computational uncertainties, it is seen that the dimension of the attractor is a reasonable representation of the number of degrees of freedom.

Now getting back to measurements in the windows of chaos, it is clear that the first appearance of chaos at Re = 66 is characterized by a jump in the dimension (to about 4.4 from 2 characteristic of the two-frequency quasiperiodicity), followed by a return to a value of 3 in the region of three-frequency quasiperiodicity. Similarly, the dimension of the attractor in the second chaotic window is about 4.8. As we discussed earlier, the dimension of the attractor in the chaotic windows is a fraction.

c. Higher Reynolds number data

Figure 18 shows the results of the dimension calculations up to an Re of about 10^4. Both ν and d_p increase to about 20 or so at an Re of 10^4, although the increase is not always monotonic. In fact, our calculations seem to suggest that the dimension settles down to about a value of 20!

If it is true that the dimension of the attractor retains, even at high Reynolds numbers, its meaning as an indicator of the number of dynamically significant degrees of freedom, common wisdom tells us that the dimension of the attractor should generally increase with Re. In contrast, the dimension does not increase continuously; further, its value is far lower than $Re^{9/4}$, which is the classical estimate (see Landau & Lifshitz [33])for the number of degrees of freedom in a turbulent *flow*. It

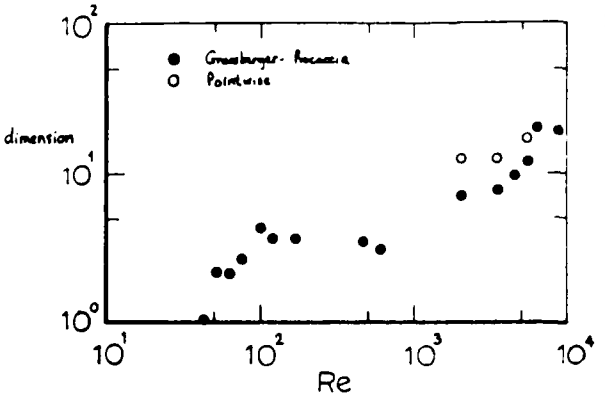

FIGURE 18: Dimension data for Re up to 10^4.

may be that the constancy of the dimension at higher Re is simply an artifact of resolution and computational problems, but if the result is genuine instead, it should provide an incentive for a suitable reformulation of 'turbulence problem'.

d. The Kolmogorov entropy

The Kolmogorov entropy has the property that it is positive for a chaotic signal, zero for ordered signals and infinite for a random signal with a space filling attractor. As already mentioned, there are conjectures that the entropy equals the sum of positive Lyapunov exponents, and hence, unlike the dimension D, is a dynamic measure of unpredictability of the motion.

Suppose the d-dimensional phase space housing the attractor is partitioned into boxes of size ε^d. Let $p(i_1, i_2, \ldots, i_d)$ be the joint probability of finding $\underset{\sim}{u}$ at time $t = \tau$ in box i_1, $\underset{\sim}{u}$ at time $t = 2\tau$ in box i_2, ..., $\underset{\sim}{u}$ at time $t = d\tau$ in box i_d. The Kolmogorov entropy is then defined [34] as

$$K = -\lim_{\varepsilon\to 0}\lim_{\tau\to 0}\lim_{d\to\infty}\frac{1}{d\tau}\sum_{i_1,\ldots i_d} p(i_1,\ldots i_d)\ln p(i_1,\ldots i_d). \qquad (4.7)$$

Grassberger & Procaccia [35] have defined a quantity K_2 which is close to K and further has the property that $K_2 > 0$ is a sufficient condition for chaos. Without going into too many details, we follow [35] and note that it can be computed by first obtaining $C(\varepsilon)$ as in Eq.(4.5) in section 4a for various d, and forming the ratio

$$K_{2,d}(\varepsilon) = \frac{1}{\tau}\ln\frac{C_d(\varepsilon)}{C_{d+1}(\varepsilon)}, \qquad (4.8)$$

where C_d indicates C for dimension d. In the limit,

$$\lim_{\substack{d\to\infty\\ \varepsilon\to 0}} K_{2,d}(\varepsilon) = K_2.$$

Table 2 gives K_2 for Re = 66 and 81 within the first two windows of chaos. For comparison, the table also lists K_2 for the Hénon map from [35].

Table 2: The Kolmogorov entropy

Signal	K_2
u at Re = 66	≈ 0.22
u at Re = 81	≈ 0.24
The Hénon map	0.325 ± 0.02

5. Discussion of Results

We have shown that several features of transition to turbulence behind circular cylinders are in essential agreement with the behavior of low-dimensional dynamical systems. We emphasize that many details discussed above in the near-wake region hold also at around x/d = 50, although less conspicuously.

One particularly important feature of this work is the discovery of windows of chaos interspersed between regions of order: these latter regions are three and four-frequency quasiperiodicities in the low Reynolds number range up to about 140 (possibly even higher!). Not all observations we have made can be understood within the present framework of chaos and dynamical systems, but we find it amazing that the dynamics of fluid motion which we believe are particularly governed by the NS equations should be at all represented by extremely simple systems. One aspect of this work is the fine resolution (in Reynolds number, frequency domain, as well as in the phase space) with which measurements have been made. It seems to us that even finer resolution, especially within the windows of chaos and regions bordering them, will perhaps disclose even more interesting aspects.

We have shown that, during early stages of transition, a strong connection (speculated previously, but never shown to be true conclusively) exists between the dimension of the attractor and the degrees of freedom as inferred from power spectral densities. Provided this interpretation is true also in windows of chaos and (moderately) high Reynolds number turbulence, our results suggest that the degrees of freedom are not too many even up to Reynolds number of the order of 10^6. Our numerical calculations based on Schewe's data lead us to expect that the dimension of the attractor, as computed according to (4.4) and (4.5), is not high even at higher Reynolds numbers corresponding to the fully turbulent state ($Re \approx 10^6$). If the attractor is sufficiently low-dimensional, a clever projection of it can perhaps be used to our advantage. (If the attractor dimension is even as high as 20, however, no matter what projection one devises, it will perhaps look uniformly dark!) At this stage it is not clear how one could use this information, but, without entering into a detailed discussion, we may point out that it lends credence to concepts embodied in renormalization group theory, slaving principle, or, closer to home, large eddy simulation or orthogonal decomposition techniques.

We thus believe that there is much that we can learn about transition and turbulence from chaos theories. In the immediate future, these theories provide a strong

motivation for looking into newer aspects of fluid flow phenomena; discoveries of close correspondence between fluid flows and low-dimensional chaotic dynamical systems will undoubtedly prove useful in the sense that the rich variety of results from dynamical systems can be brought to bear on fluid flow transition and, perhaps, even turbulence. In the long run, the hope is that they will help us in coming to grips with the eternal problem of turbulence, namely, the enormous amount of 'information' that seems to be available to us! Perhaps we can then model, even at high Reynolds numbers, at least local behaviors by low-dimensional dynamical systems.

Do we then conclude that the key to the understanding of transition and turbulence lies totally in low-dimensional dynamicsl systems? We think that such statements are optimistic at best and misguided at the worst. Apart from the fact that the spatial structure of turbulent flows, which is their single most important characteristic, lies outside the scope of dynamical systems theories — at least as they stand today — there is a lot that they do not or, perhaps, cannot, tell: for example, they do not tell us anything about the origin and physical structure of the various bifurcations that can occur, or how the drag coefficient varies with Reynolds number. To answer these and similar questions of practical interest, we suspect that we have to revert to the NS equations!

One final comment should be made. It would be useful to make a concurrent flow visualization study and relate the various findings reported here to the spatial characteristics of the flow. It is unfortunate that we cannot use much the extensive flow visualization observations made by others (for example, Gerrard [36]) because the details from one experiment to another do not precisely match.

ACKNOWLEDGEMENTS

For their helpful comments during this work or on an earlier draft of the manuscript, it is my pleasant duty to thank [illegible] Arel, Peter Bradshaw, B.-T. Chu, Rick Jensen, John Miles, Mark Morkovin, Turan Onat, David Ruelle, Paul Strykowski, Harry Swinney and Peter Wegener. I am indebted to Mike Francis who patiently accommodated this pursuit within an AFOSR grant [illegible] for turbulence control work. Finally, presentation of these results in Evanston and preparation of this manuscript for this volume honoring Stan Corrsin has been a labor of love, and an expression of indebtedness I have for him.

Appendix

Let $b_1, b_2, \ldots, b_n$ be the state variables of the system (1.1). In an n-dimensional space spanned by $b_1, b_2, \ldots, b_n$, each point determines the state of the system completely at a given time, t. As t evolves, we obtain a continuous sequence of points which form the trajectory of the system. As $t \to \infty$, the b_i's need not go to infinity, but may terminate (in two dimensions) either at a node or a focus or on a limit cycle or, in higher dimensions, on to a more complicated object. This object

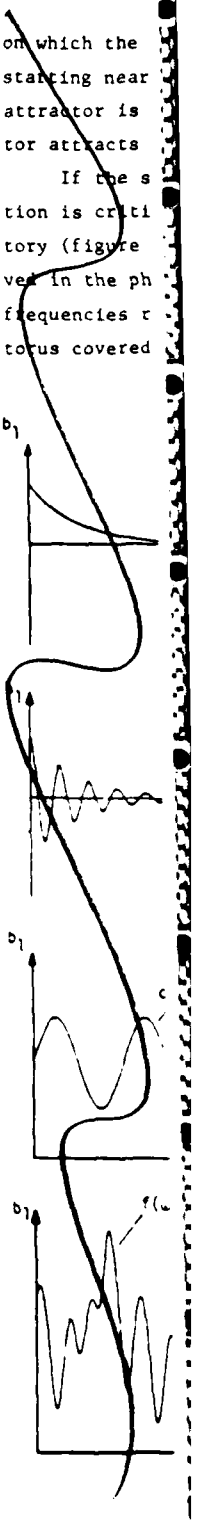

on which the trajectory terminates is called an attractor if all other trajectories starting near the said trajectory converge to the same object as $t \to \infty$. (That is, the attractor is the limit set of a representative point in phase space. Thus, an attractor attracts all nearby trajectories.)

If the system is stable and steady the attractor is a point – a node if the motion is critically damped (figure A1) or a focus if the motion is damped but oscillatory (figure A2). If the system executes a periodic motion, a limit cycle is observed in the phase plane (figure A3). Quasiperiodic motion with two incommensurate frequencies results in a two-torus (see figure A4), with the entire surface of the torus covered by the trajectory eventually. A projection of the torus on to a plane

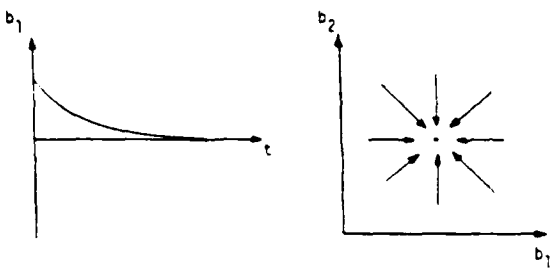

FIGURE A1: Stable node. (point attractor)

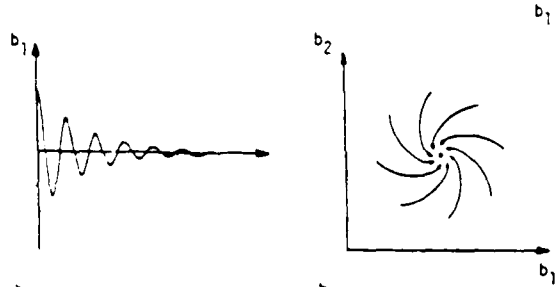

FIGURE A2: Stable focus. (point attractor)

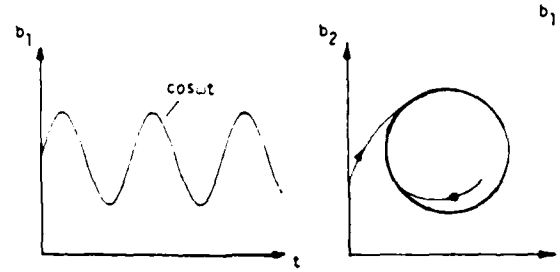

FIGURE A3: Limit cycle.

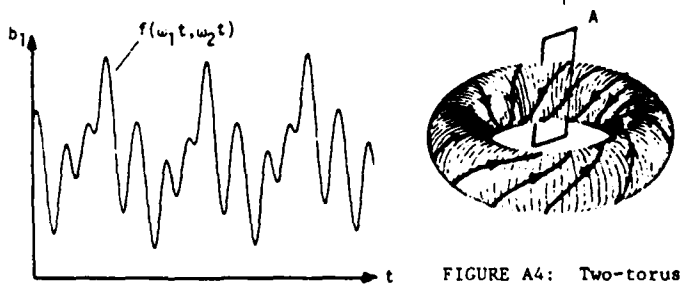

FIGURE A4: Two-torus. (perspective view)

may have different shapes depending on the orientation of the plane, but it is clear that a section of the torus, say, by the plane A in figure A4 (the Poincaré section) will yield a limit cycle. To obtain such a section in practice, one has to intercept the trajectory each time it crosses the plane (or 'sample' the system at the frequency f_1 and at fixed phase), and plot b_1 and b_2 (say) corresponding to these periodically sampled data. The phase portrait corresponding to the quasiperiodic motion with three frequencies is a three-torus, and so on.

The attractor has been called a 'strange attractor' if (roughly speaking) it is a complex surface repeatedly folded onto itself in such a manner that a line normal to the surface intersects it in a Cantor set. That is, if one successively magnifies regions of this intersection which appear, at some level of resolution, to be entirely 'filled', one sees regions of 'emptiness' interspersed between regions of 'occupation'. One cannot test this property of the strange attractor directly if it is constructed from experimental data (because of noise and the finite resolution of the instrumentation), and so, one uses several of its other properties to determine its occurrence. For example, any two neighboring trajectories on the strange attractor will diverge exponentially apart for small t (the so-called sensitivity to initial conditions, measured by positive Lyapunov exponents or the Kolmogorov entropy); the so-called dimension of the attractor (see section 4) is generally a non-integer; the spectral density of the temporal signal used to construct the attractor will have broadband components orders of magnitude above the instrumentation and other noise levels.

References

1. Ruelle, D. & Takens, F., Commun. Math. Phys. 20, 167 (1971).
2. Newhouse, S., Ruelle, D. & Takens, F., Commun. Math. Phys. 64, 35 (1978).
3. Gollub, J.P. & Swinney, H.L., Phys. Rev. Lett. 35, 927 (1975).
4. Fenstermacher, P.R., Swinney, H.L. & Gollub, J.P., J. Fluid Mech. 94, 103 (1979).
5. Brandstäter, A., Swift, J., Swinney, H.L. & Wolf, A., Phys. Rev. Lett. 51, 1442 (1983).
6. Libchaber, A. & Maurer, J., J. de Physique 41, C3-57 (1980).
7. Libchaber, A., In Chaos and Statistical Methods (ed. Y. Kuramoto, Springer 1984), p.221.
8. Coles, D., J. Fluid Mech. 21, 385 (1965).
9. Sreenivasan, K.R. & Strykowski, P.J., In Turbulence and Chaotic Phenomena in Fluids (ed. T. Tatsumi), to appear.
10. Sreenivasan, K.R., In Nonlinear Dynamics of Transcritical Flows (ed. H. Oertel), to appear.
11. Takens, F., In Lecture Notes in Mathematics 898 (eds. D.A. Rand and L.S. Young, Springer-Verlag 1981), p.366.
12. Chaitin, G.J., Scientific American, 246, 47 (May issue, 1982).
13. Thomas, R.M., J. Fluid Mech. 57, 549 (1973).
14. Gorman, M., Reith, L.A. & Swinney, H.L., Ann. N.Y. Acad. Sci. 357, 10 (1980).

15. Gollub, J.P., & Benson, S.V., J. Fluid Mech. 100, 449 (1980).
16. Greborgi, C., Ott, E. & Yorke, J.A., Phys. Rev. Lett. 51, 339 (1983).
17. Haken, H., Advanced Synergetics, Springer 1984.
18. Sparrow, C., The Lorenz Equations, Springer 1982.
19. Miles, J.W., Physica D (to appear), 1984.
20. Matsumoto, K. & Tsuda, I., J. Stat. Phys. 31, 87 (1983).
21. Roux, J.-C., Turner, J.C., McCormick, W.D., & Swinney, H.L., In Nonlinear Problems: Present and Future (eds. A.R. Bishop, D.K. Campbell, B. Nicolaenko, North-Holland Publishing Co., 1982), p.409.
22. Roshko, A., J. Fluid Mech. 10, 345 (1961).
23. Schewe, G., J. Fluid Mech. 133, 265 (1983).
24. Tritton, D.J., J. Fluid Mech. 6, 241 (1959).
25. Berger, E., Z. Flugwiss. 12, 41 (1964).
26. Tritton, D.J., J. Fluid Mech. 45, 749 (1971).
27. Friehe, C.A., J. Fluid Mech. 100, 237 (1980).
28. Gaster, M., J. Fluid Mech. 38, 565 (1969).
29. Malraison, B., Atten. P., Berge, P. & Dubois, M., J. Physique Lett. 44, L-897 (1983).
30. Mandelbrot, B., The Fractal Geometry of Nature, Freeman & Co., New York, 1983.
31. Farmer, J.D., Ott, E. & Yorke, J.A., Physica 7D, 153 (1983).
32. Grassberger, P. & Procaccia, I., Phys. Rev. Lett. 50, 346 (1983).
33. Landau, L.D. & Lifshitz, E.M., Fluid Mechanics (volume 6 of the Course of Theoretical Physics), Pergamon Press, 1982.
34. Barrow, J.D., Phys. Reports, 85, 1 (1982).
35. Grassberger, P. & Procaccia, I., Prepublication report (1983).
36. Gerrard, J.H., Phil. Trans. Rov. Soc. Lond. 288A, 29 (1978).

Chaos in Open Flow Systems

K.R. Sreenivasan

Center for Applied Mechanics, Mason Laboratory, Yale University,
New Haven, CT 06520, USA

We discuss briefly some aspects of 'open flow systems' in the context of deterministic chaos. This note is mostly a statement of the difficulties in characterizing such flows, especially at high Reynolds numbers, by dynamical systems. Brief comments will be made on the fractal geometry of turbulence.

1. Introduction

One of the most fascinating phenomena in fluid mechanics is the transition from a steady laminar state to a turbulent state. Our concern here is a brief discussion (in the context of deterministic chaos) of this transition process (or processes), and of aspects of the fully turbulent state itself. We shall concentrate entirely on 'open flow systems', or 'unconstrained' flows, e.g., wakes, jets, boundary layers, channel and pipe flows, etc.

It is not obvious in what sense one can think of open flow systems as genuine dynamical systems. We recall from [1] that such flows could behave in generically different ways from the 'closed flow systems'. In all closed flow systems the boundary is fixed so that only certain class of eigenfunctions can be selected by the system; this does not hold for open flow systems in which the flow boundaries are continuously changing with position. Thus, while in closed flow systems each value of the control parameter (for example, the rotation speed of the inner cylinder in the Taylor-Couette problem) characterizes a given state of the flow globally, this is not true of open systems. Consider as an example the near field of a circular jet. For a given set of experimental conditions, the flow can be laminar at one location, transitional at another and turbulent at yet another (downstream) location. This usually sets up a strong coupling between different phenomena in different spatial positions in a way that is peculiar to the particular flow in question. Secondly, the nature and influence of external disturbances (or the 'noise', or the 'background or freestream turbulence') is more delicate and difficult to ascertain in open flows: the 'noise', which is partly a remnant of complex flow manipulation devices upstream and partly of the 'long range' pressure perturbations, is not 'structureless' or 'white', no matter how well controlled. Finally, it is well-known that closed flow systems can be driven to different states by means of different start-up processes; for example, different number of Taylor vortices can be observed in a Taylor-Couette apparatus depending on different start-up accelerations [2]. This type of path-sensitivity in a temporal sense does not apply to open systems, where the overriding factor is the path-sensitivity in a spatial sense (i.e., the 'upstream influence').

These remarks notwithstanding, it has been shown in Refs. 1 and 3 that it is worthwhile examining transition in open flow systems from the point of view of low-dimensional chaos. The usual way of establishing this connection is via the analysis of the time history of a single dynamical variable such as a velocity component obtained at a fixed (Eulerian) point in the flow [4]. We should stress that this procedure is inadequate especially for the open flow systems. Two re-

marks ought to suffice. First, since the dynamical instabilities in open flows are most often convective in nature, analysis of temporal Eulerian quantities does not carry with it much information on the evolution of the system. Deissler & Kaneko [5] have pointed out that a flow which gives every appearance of being chaotic may nonetheless have no positive Lyapunov exponents in the Eulerian frame of reference. Perhaps a more relevant method of characterizing the evolution of the flow in terms of a dynamical system would be to use the Lagrangian information obtained, say, by measuring the velocity of a fluid particle as it moves about in the flow. To say the least, accurate measurements of this type are hard to make.

The second point to be made is that most open flow systems possess strong spatial inhomogeneities in a direction normal to the flow. (Indeed, these inhomogeneities are responsible for processes that maintain the flows against viscous dissipation.) For this reason, it is a priori unclear to what extent the temporal information obtained at one selected point fixed in the flow can represent the global dynamics. One might think that a simultaneous measurement (at a given time or as time sequences) of a dynamic quantity such as velocity, made at many spatial points in the flow, might solve this problem. This is not so: one does not even know how to construct a dynamical system from such empirical data.

It therefore appears worth enquiring explicitly whether, in open flow systems, attractors constructed from Eulerian point measurements, using the usual time delay techniques, are chaotic; that is, whether they are characterized by low dimensions, and possess (at least!) one positive Lyapunov exponent. This is done in section 2. In section 3, we examine the variation with the flow Reynolds number of the dimension of the attractor, and comment briefly on the dimension at large Reynolds numbers. In section 4, brief remarks will be made on two aspects of turbulence that can be ascribed fractal dimensions.

2. Chaotic attractors for open flows: low Reynolds numbers

Chaotic attractors are characterized by at least one positive Lyapunov exponent and by relatively low dimensions that do not continously increase with the embedding dimension. We have made point measurements of velocity signals in several different flows and constructed attractors using the time delay technique; we have obtained the correlation dimension ν according to the Grassberger-Procaccia algorithm [6], and the largest Lyapunov exponent according to the algorithm given in Wolf et al. [7]. (Spurred by a talk that Harry Swinney gave in Kyoto in 1983, we wrote versions of a program to calculate the largest Lyapunov exponent, but have now switched over to the method of Ref. 7.) Since both these procedures are now well-known, we shall not describe them here.

In Table 1, we list some basic information for four flows. A crucial factor in obtaining the correlation dimension is the choice of the optimum time delay τ. We simply varied τ over a wide range, and used a τ in the range where its precise value is not critical. We show in Fig. 1 the correlation dimension as a function of τ. Clearly, too large a τ will result in the increase of ν.

Figure 2 shows the convergence with the number of iterates of the largest Lyapunov exponent for the wake, calculated using an embedding dimension of 6; other embedding dimensions yield essentially the same asymptotic value, even though the initial behaviors could be quite different. It should be remarked that the dimension and the Lyapunov exponents usually converge (for the calculations typified by Table 1) relatively fast; total signal durations of the order of $2000\tau_o$, where τ_o is the zero-crossing time scale of the auto-correlation function, was found to be usually sufficient.

Table 1: Typical data for low Reynolds number open flow systems

Flow	$Re=U_o d/\nu$	Correlation dimension, ν	Largest Lyapunov exponent, λ_1
wake behind circular cylinder[1]	67	2.6	0.65 bits/orbit
axisymmetric jet (unexcited)[2]	1000	6.3	0.95 bits/orbit
axisymmetric jet (excited)[3]	1000	3.2	——
curved pipe[4]	6625	6.0	0.40 bits/orbit

[1] d = diameter of the cylinder, U_o = upstream flow speed; data were obtained 10 diameters downstream, 1 diameter off-axis.

[2] d = diameter of the nozzle, U_o = nozzle exit velocity; data were obtained in the potential core 2 diameters downstream of nozzle exit.

[3] no Lyapunov exponent was computed because we lost the data sets immediately after computing the dimension.

[4] d = pipe diamter, U_o = section average velocity; the data correspond to the centerline of the pipe.

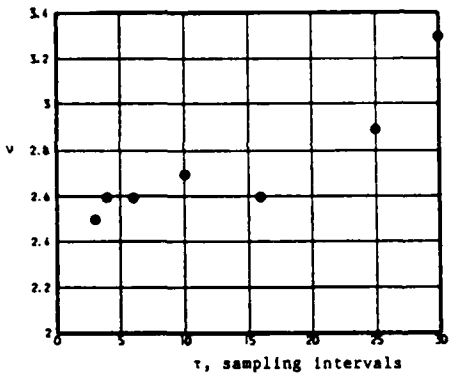

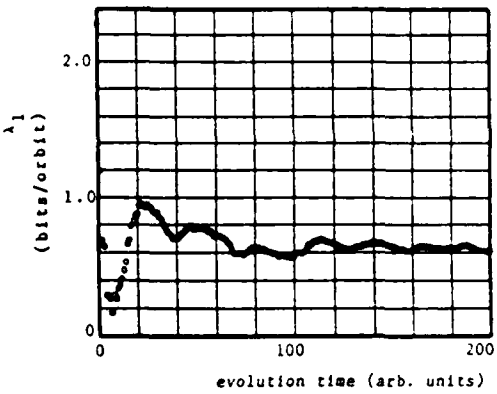

Fig. 1 The variation of the correlation dimension as a function of the time delay τ used to construct the attractor.

Fig. 2 Variation of the largest Lyapunov exponent with the evolution time.

From many such calculations, we conclude that if one constructs attractors using a single Eulerian dynamical quantity via time delay techniques, such attractors do possess (at low Reynolds numbers) characteristics of chaotic dynamics. Perhaps, Eulerian quantities do preserve some information on the dynamical evolution, in some loose sense akin to Poincaré sections!

We shall remark that these calculations do not unequivocally establish that tubulence is chaotic (in the sense of extreme sensitivity to initial conditions). Our findings could perhaps be interpreted equally well in terms of 'external noise amplification' in the system. Much more work is needed before one can determine the extent to which

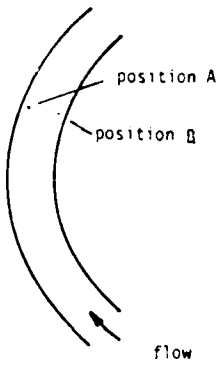

Fig. 3a Measurement stations for the curved pipe. Flow at the measurement stations is fully developed. Configuration details can be found in [3].

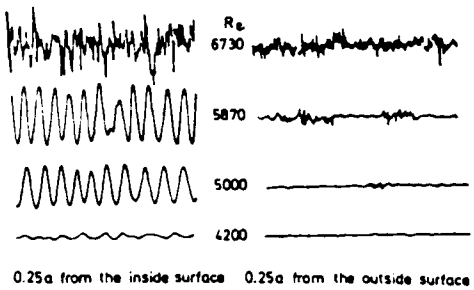

Fig. 3b Streamwise velocity fluctuations at several Reynolds numbers at position A (the right set of signals, measured 0.25 radius from the outer wall) and position B.

this last mentioned factor competes with the intrinsic sensitivity to initial conditions as the mechanism for the generation of turbulence. We should also reiterate the variation with spatial position of the characteristics of the 'Eulerian attractors'. For the curved pipe, Fig. 3 shows samples of streamwise velocity history at two spatial locations (but at the same streamwise section in the so-called fully developed region). Clearly, attractors constructed from signals at these two different locations can be expected to have different dimensions and spectra of Lyapunov exponents. For an Re of 6625, the data are as shown in Table 2. At the least, these data suggest that the interpretation of the dimension as an indicator of the dynamically significant degrees of freedom of flow needs some qualification.

Table 2: The spatial variation of the characteristics of the 'Eulerian attractors' at two different spatial positions in the same flow at the same streamwise location at the same Re. Data are for curved pipe; details as in Fig. 3.

position A		position B	
ν	λ_1, bits/orbit	ν	λ_1, bits/orbit
6.0	0.4	2.7	0.17

3. Dimension calculations at higher Reynolds numbers

If we persist with dimension calculations at higher Reynolds numbers — using the same technique, in spite of its shortcomings — they become uncertain because:

(a) The number of data points required for convergence, and the number of steps involved in dimension calculations go up;

(b) One cannot in general find a proper range of time delays over which the results are sensibly independent;

(c) There is no guarantee that the dimension calculations asymptote to constant values as the embedding dimension increases.

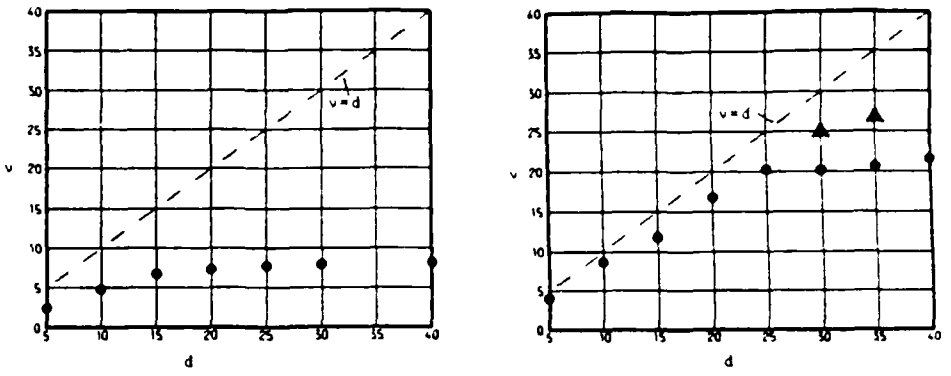

Fig. 4a The variation of the correlation dimension ν with the embedding dimension d. Re = 500, approximately 5 diameters downstream of the cylinder. A space-filling attractor is expected to have the behavior shown by the dashed line.

Fig. 4b The variation of the correlation dimension ν with the embedding dimension d. Re = 2000, approximately 5 diameters behind the cylinder. ν = d line holds for a space-filling attractor. The ▲'s indicate the values of ν computed for the random noise from a commercial random noise generator. Notice that the asymptotic value of ν is definitely below the noise data, although only by a small margin. The nearness of the noise data to the flow data shows why we cannot place too much emphasis on high dimension computations.

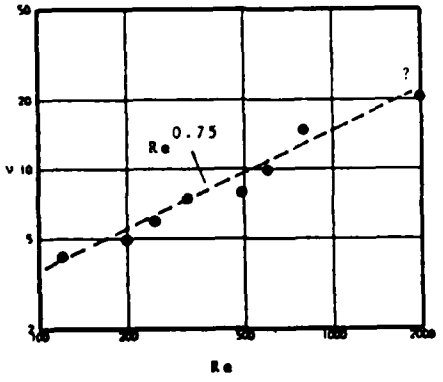

Fig. 5 The variation of the dimension with Reynolds number. Data are for the wake of a circular cylinder.

Figures 4a and b illustrate this last point; Fig. 4b is the upper limit on the Reynolds number at which some credibility (already rather low!) can be ascribed to the dimension calculations. If we believe the numbers obtained from such calculations, we may deduce that a power law relation like $Re^{3/4}$ is not unlikely (Fig. 5).

It is worth mentioning that Constantin et al. [8] have placed the upper bound on the dimension of Navier-Stokes attractors to be of order $R^{9/4}$ (and higher if self-similarity in the Kolmogorov range does not obtain!), where the Reynolds number R = u'L/ν, u' being a

root-mean-square velocity fluctuation, and L is an integral state of turbulence. The precise relation between R and the Reynolds numbers Re used in Table 1 depends on the flow, but it is clear that if the present finding of a 3/4 - power law is true, it is of undoubted significance in spite of our earlier reservations on the meaning of the dimension obtained in this way.

Fully turbulent flows are characterized by temporal and spatial chaos. Temporal dynamics is thus merely a part of the whole story; this in itself is hard to come to grips with, even if the dimension were to increase 'only' according to a 3/4 power of the Reynolds numbers. Is there then any connection between real turbulent flows and finite-(and low-) dimensional dynamical models which one hopes one can construct? (That, presumably, is the practical motivation for studies of this type.) The answer would have been an unequivocal 'no' were it not for the fact that some (perhaps strong?) spatial coherence appears to exist at least in some classes of fully turbulent flows. One might, in some way that remains unclear, be able to decompose the motion into two components, one of which consists of this coherent element and the other, its complement. One can then think of a low-dimensional attractor characterizing the coherent motion, the attractor being made fuzzy by the small scale motion whose effect is to reduce the correlation. Unfortunately, it is not clear whether this loosely worded picture is consistent with facts.

Elementary tests of this hypothesis can be made if one is able to separate the incoherent motion from the coherent part. This might be possible, for example, by some kind of ensemble averaging methods such as used in [9]. The simplest (by no means the most correct) way is to filter out linearly in the frequency domain the coherent motion from the rest. To avoid many conceptual difficulties associated with filtering as the technique for separating the coherent and incoherent motions we choose a (relatively) high Reynolds number flow where the coherent part is clearly contained within a narrow band of frequencies; we then enquire whether the motion associated with this narrow band is low dimensional.

Figure 6a shows the streamwise velocity fluctuation in the wake of a circular cylinder, measured about 2 diameters behind the cylinder and a diameter off-axis; the flow Reynolds number of 10,000 is considered moderately high. Computing the dimension of the attrac-

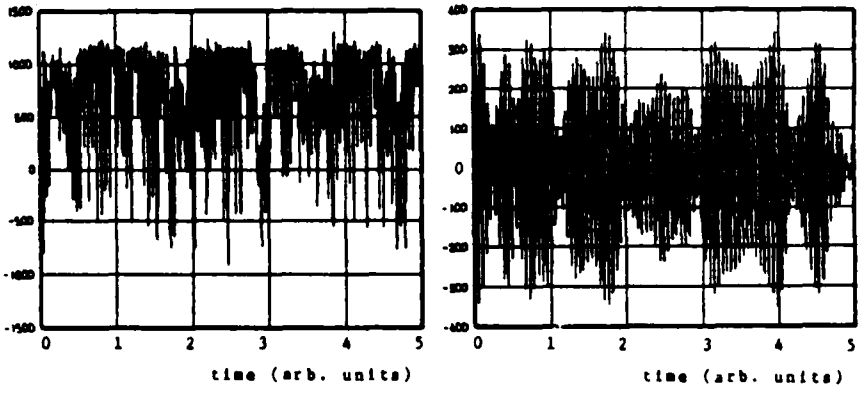

Figs 6a,b: The total (unfiltered) and the coherent part respectively of the streamwise velocity fluctuation in the wake of a cylinder; Re = 10,000. Both the ordinate and abscissa are arbitrary but the same in the two figures.

tor constructed from this signal is doomed to be meaningless in view of the remarks made earlier. (If the $Re^{9/4}$ dependence is valid, the extrapolated estimate for ν is of the order of 30!) We do know from power spectral measurements that this signal has a peak at a frequency f of about 550 Hz; this peak, corresponding to a Strouhal number fd/U_o = 0.21, characterizes the coherent part of the motion. If we band-pass filter this signal between, say, 500 and 600 Hz, the resulting signature is given in Fig. 6b. Calculations show that the corresponding attractor has a dimension of about 3.5!

It is appropriate to end this discussion with the statement that the coherent part, as we defined it here, contains a significant fraction of energy.

4. The fractal geometry of turbulence: a brief note

We have indicated that measurements of attractor dimensions are beset with increasing uncertainties at increasingly high Reynolds numbers. But there are other fractal dimensions whose measurement becomes increasingly definitive as Reynolds number increases. It is to a mention of two of these aspects that this section is devoted; more details should be forthcoming in [10]. The results of this section are essentially spurred by Mandelbrot's remarks on several occasions that many facets of turbulence are fractal.

4a. The fractal dimension of the turbulent/non-turbulent interface

Observations suggest that in high Reynolds number free shear flows (i.e., open flow systems with no constraining boundary) a sharp front or interface demarcates the turbulent and non-turbulent regions. Although a completely accepted view of the detailed nature of this interface does not seem to exist, a visual or spectral study suggests that contortions over a wide range of scales occur. This leads one to the natural expectation that the interface is a fractal surface.

By illuminating a thin section of a flow, and by digitizing the resulting picture, one can evaluate the fractal dimension of the curve that separates the turbulent from the non-turbulent regions; a threshold set on the intensity of illumination separates the two regions. The fractal dimension of the surface bounding turbulent regions is then one more than that of the curve.

Several methods can be adopted to measure the fractal dimension [11]. We shall describe only one rather briefly. Assign to each point in the digitized image of the flow a number 1 when the point lies within the turbulent region, and a number 0 when it lies within the non-turbulent region. Let the boundary shown in Fig. 7 represen

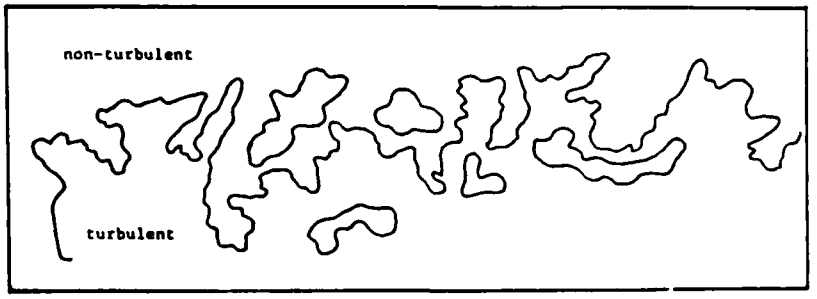

Fig. 7 The boundary between the turbulent and non-turbulent regions. If a circle of radius ϵ drawn around a given point in the digitized image crosses the boundary, the point is considered to be within a distance ϵ from the boundary.

the boundary between the 1's and the 0's. Count the number $N_b(\epsilon)$ of the digitized points which are within a distance ϵ from the boundary. If this boundary is a fractal of dimension D, then it is easily shown from the basic definition of D that

$$N_b(\epsilon) \sim \epsilon^{2-D} \quad . \tag{1}$$

Measurements to be described in [10] show that (1) holds for scales ranging from the Kolmogorov scale to a fraction of the integral length scale (but excluding scales of the order of the integral scale and higher). The measured value of the fractal dimension for the interface varies between 2.3 and 2.4; there is no identifiable variation from one type of flow to another.

4b. The fractal dimension of the velocity and scalar dissipation fields

Another aspect of turbulence that is a candidate for fractal behavior is its dissipative (or internal or small) structure. It has been well-known for some time that the small structure of turbulence is intermittent. The essence of scale-similarity arguments in this context is the following. Within a given field of (fully developed) turbulence, consider a cube with sides of length L_o, where L_o is an integral scale of turbulence. If we divide this cube into arbitrarily large number ($n \gg 1$) of smaller cubes of length $L_1 = L_o\, n^{-1/3}$, the density of dissipation rate in each of these smaller cubes is distributed according to a probabilistic law. Further subdivision of these cubes into second-order ones of length $L_2 = L_1^{-1/3}$ leaves the probability distribution unaltered. This similarity extends to all scales of motion until one reaches sizes directly affected by viscosity. Clearly, this case cries out for fractal description.

Using methods discussed in [11], we have obtained the results shown in Table 3.

One concludes from here that the dissipation field is not space-filling (less space-filling in the high Reynolds number regime) and that (c) is less space-filling than (b) — a result consistent with observations in oceanography. Note that the result (b) is only at slight variance with Mandelbrot's [11] original estimate of 2.6.

Table 3: Summary of the fractal dimensions of the dissipation fields

	Field	Fractal dimension
(a)	Kinetic energy dissipation (low Reynolds number)*	2.9
(b)	Kinetic energy dissipation (high Reynolds number)	2.7
(c)	Passive scalar (e.g., temperature) dissipation (high Reynolds number)	2.6

* The boundary between the low and high Reynolds number regimes is not well-defined. A convenient boundary occurs at a microscale Reynolds number of about 150.

Theoretical explanations of these fractal dimensions, as well as of the connections that might exist among them, would be of fundamental interest.

Acknowledgements: I am indebted to Mr. R. Ramshankar and Mr. P.J. Strykowski for their help with programming, and to Dr. J. McMichael and AFOSR for the financial support.

References:

1. K.R. Sreenivasan, In 'Frontiers in Fluid Mechanics' (eds. S.H. Davis and J.L. Lumley, Springer-Verlag 1985), p.41.

2. D. Coles, J. Fluid Mech. 21, 385 (1965).

3. K.R. Sreenivasan & P.J. Strykowski, In 'Turbulence and Chaotic Phenomena in Fluids (ed. T. Tatsumi, North-Holland 1984), p.191.

4. F. Takens, In 'Lecture Notes in Mathematics 898 (eds. D.A. Rand and L.S. Young, Springer-Verlag 1981), p.366.

5. R.J. Deissler & K. Kaneko, Submitted to Phys. Rev. Lett. (Sept. 1985).

6. P. Grassberger & I. Procaccia, Phys. Rev. Lett. 50, 346 (1983).

7. A. Wolf, J.B. Swift, H.L. Swinney, & J.A. Vastano, Physica 16D, 285 (1985).

8. C. Constantin, C. Foias, O.P. Manley & R. Temam, J. Fluid Mech. 150, 427 (1985).

9. K.R. Sreenivasan, R.A. Antonia, & D. Britz, J. Fluid Mech. 94, 745 (1979).

10. K.R. Sreenivasan, The fractal facets of turbulence, in preparation, 1985.

11. B. Mandelbrot, The Fractal Geometry of Nature, Freeman and Co., New York, 1982.

J. Fluid Mech. (1986), *vol.* 173, *pp.* 357–386
Printed in Great Britain

The fractal facets of turbulence

By K. R. SREENIVASAN AND C. MENEVEAU

Center for Applied Mechanics, Yale University, New Haven, CT 06520, USA

(Received 25 March 1986)

Speculations abound that several facets of fully developed turbulent flows are fractals. Although the earlier leading work of Mandelbrot (1974, 1975) suggests that these speculations, initiated largely by himself, are plausible, no effort has yet been made to put them on firmer ground by resorting to actual measurements in turbulent shear flows. This work is an attempt at filling this gap. In particular, we examine the following questions: (*a*) Is the turbulent/non-turbulent interface a self-similar fractal, and (if so) what is its fractal dimension? Does this quantity differ from one class of flows to another? (*b*) Are constant-property surfaces (such as the iso-velocity and iso-concentration surfaces) in fully developed flows fractals? What are their fractal dimensions? (*c*) Do dissipative structures in fully developed turbulence form a fractal set? What is the fractal dimension of this set? Answers to these questions (and others to be less fully discussed here) are interesting because they bring the theory of fractals closer to application to turbulence and shed new light on some classical problems in turbulence – for example, the growth of material lines in a turbulent environment. The other feature of this work is that it tries to quantify the seemingly complicated geometric aspects of turbulent flows, a feature that has not received its proper share of attention. The overwhelming conclusion of this work is that several aspects of turbulence can be described roughly by fractals, and that their fractal dimensions can be measured. However, it is not clear how (or whether), given the dimensions for several of its facets, one can solve (up to a useful accuracy) the inverse problem of reconstructing the original set (that is, the turbulent flow itself).

1. Introduction

Starting with Richardson (1922), it has been thought that fully developed turbulence consists of a hierarchy of eddies, or scales of various orders. The mechanism responsible for this situation is assumed to be that eddies of a given order (or size) arise as a result of the loss of stability of larger eddies of the preceding order; these in turn are assumed to lose their stability and generate eddies of a smaller order to which they transmit their energy. This recurring scheme is expected to terminate at scales small enough to be stable – that is, scales whose characteristic Reynolds number is unity. It is well known that this lower bound on the scale size is of the order of the Kolmogorov scale. This theory of cascade, verbalized in a memorable rhyme by Richardson (1922), and cultivated by Kolmogorov (1941, 1962), Obukhov (1941, 1962), Onsager (1945) and Weizsäcker (1948), has made remarkable strides in advancing our understanding of turbulent flows.

It is this description of turbulent flows – namely that they are 'objects' consisting of a hierarchy of scales – that leads to the expectation that the theory of fractals (Mandelbrot 1982, to which reference must be made for an enjoyable and original account of fractals) must be applicable to turbulence. In the most basic sense, fractals

are objects that display self-similarity over a wide range of scales. (We shall return in §5 to the fact that fractals are now used to describe more general class of objects than those displaying strict self-similarity.) Mandelbrot (1982), for example, has remarked that 'turbulence involves many fractal facets' and claimed that a proper investigation of the geometric aspects of turbulence – which has been ignored all along in the vast literature on turbulence – must necessarily involve fractals; concepts from Euclidean geometry are totally inadequate. He has also led the way by his own investigations (Mandelbrot 1974, 1975) but, in his own words (Mandelbrot 1982), 'they involve suggestions with few hard results as yet'. The intention of this paper is to remedy this situation by resorting to actual measurements in turbulent flows.

Analogous to the Euclidean dimension of classical (or ordinary) objects, each fractal object is associated with a characteristic dimension called the fractal dimension which forms a basic measure of it fragmentation or roughness; it has the property that it is strictly greater than the object's topological dimension. It appears as a certain exponent $D = \log N / \log (1/\epsilon)$, characteristic of a self-similar object which is made of N parts, each of which is obtained from the whole by a reduction of ratio ϵ. (We hope that this inadequate explanation here, to be amplified in later sections, will not hinder the readability of this paper.) Of course, a complete description of fractal sets demands a specification of other quantities such as lacunarity (Mandelbrot 1982) – which, loosely speaking, is a measure of how far the fractal object is from being dust-like – or the entire spectrum of scaling functions (Halsey *et al.* 1986) only one of which is the fractal dimension. (Even more appropriately, one may use scaling functions of the type introduced by Feigenbaum 1983; these scaling functions contain all the geometric information about the object in question, but they are nowhere differentiable and are awkward to handle – even assuming that they can be constructed somehow.) Our primary effort in this paper will be confined to the determination of the fractal dimensions (if they exist) of the turbulent/non-turbulent interface (§2), iso-velocity surfaces (§3), and regions of active dissipation (§4). In §5, we briefly discuss several other avenues, studied to date in less detail than the issues of the preceeding three sections. In each section, we lay sufficient foundation for the specific issues to be discussed there. Section 6 will put these various measurements in the overall context of what additional insight one may acquire about turbulent flows.

2. Fractal dimension of the turbulent non-turbulent interface

2.1. *Background*

Observations (Corrsin & Kistler 1954) suggest that in high-Reynolds-number unbounded turbulent shear flows a sharp front or interface demarcates the turbulent and non-turbulent regions (see figure 1). The free edge of a boundary layer shows much the same behaviour. Townsend (1956) suggested that large eddies of turbulence contort the interface, but a visual or spectral study of the interface suggests that contortions over a range of scales occur. In the framework of scale similarity alluded to above, this leads to the natural expectation that the interface is a fractal surface. The aim in this section is to determine the fractal dimension (if one exists) of the turbulent/non-turbulent interface in several classical shear flows.

It is generally understood that turbulent/non-turbulent interface means the surface separating the vortical and non-vortical regions of the flow; the vortex-stretching mechanism inherent in three-dimensional motion can be thought of as

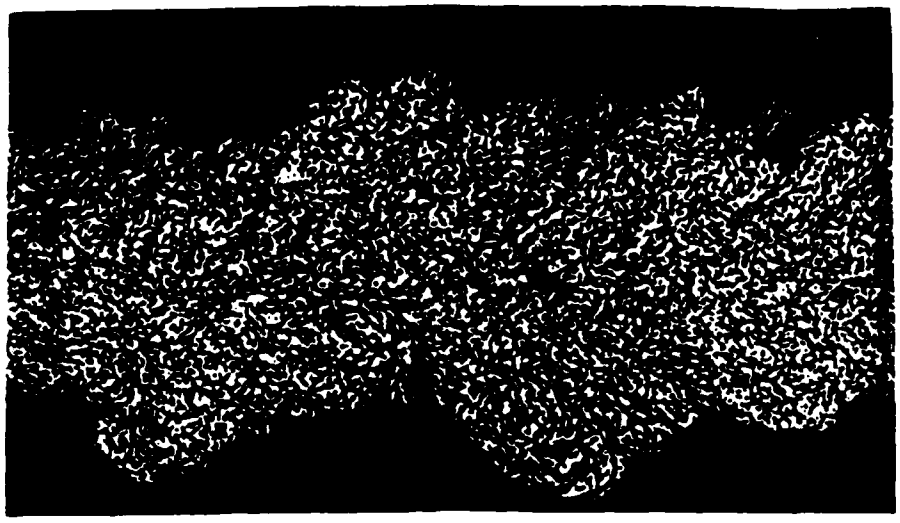

FIGURE 1. A short duration shadowgraph of the wake of a projectile shot through the atmosphere at supersonic speed. This classic photograph made at the Ballistic Research Laboratories, Aberdeen Proving Ground, first appeared in Corrsin & Kistler (1954), and has since been reproduced many times. The remarkably sharp boundary between the turbulent region in the wake and the outside air has led to the notion of a contiguous interface whose properties were explored by Corrsin & Kistler, and several others later.

being responsible for maintaining a sharp separation between the two regions. That such a surface can be defined was demonstrated by Corrsin & Kistler (1954), who also studied its properties in some detail. It is by no means obvious that the interface observed in flow-visualization pictures such as figure 1 and the vortical/non-vortical interface are the same. We shall return to this point later but, until required, we shall not be specific about which interface we are discussing.

The prescription for determining the fractal dimension of the interface (surface) is to cover it with area elements of decreasing size, and note how the area changes with the resolution ϵ of these square elements. For a surface that is highly contorted with squiggles of ever-increasing fineness, the measured area estimates will increase indefinitely with increasing resolution. If the surface has no regularity associated with it, one cannot in general specify the manner in which the area will increase with increased resolution. However, if some order prevails in the sense that the surface observes scale similarity – that is, the surface looks the same (at least *statistically*) at all levels of resolution, or, equivalently, it is a self-similar fractal – the area increase will follow a power law; in general, power laws are symptomatic of self-similar or fractal behaviour. For a true fractal surface of dimension D_3 (the suffix 3 indicating that the interface is embedded in a three-dimensional physical space) the area will indefinitely increase according to the relation

$$N = \epsilon^{-D_3}. \tag{2.1}$$

One can rewrite (2.1) as

$$D_3 = \frac{\log N}{\log (1/\epsilon)}. \tag{2.2}$$

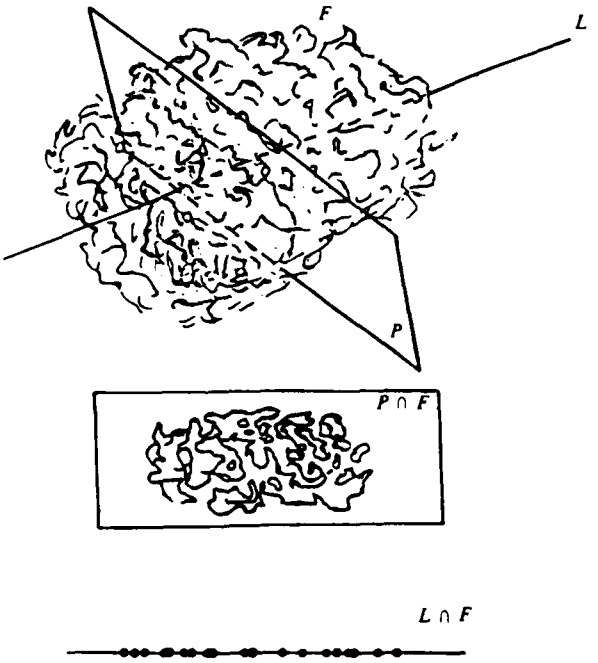

FIGURE 2. A schematic of an object F with a fractal interface, and its intersections with a plane and a line. The intersection with the plane leads to an object whose border has a dimension D_2, one less than D_3, the dimension of F embedded in the three-dimensional space. The dimension of the line intersection leads to a Cantor set whose fractal dimension D_1 is 2 less than D_3.

This is the standard relation used in fractal-dimension calculations. The meaning of the dimension becomes clearer if we apply this above procedure to classical surfaces, say a square of unit area. Let us cover the square with 16 area elements each of which is of length $\frac{1}{4}$. Then D_3 will be $\log 16/\log \frac{1}{4} = 2$, which is the dimension of the area of surface in Euclidian geometry. It is trivial to convince oneself that covering the square with increasingly finer area elements will always give $D_3 = 2$ for the square. From this simple example and other similar ones, one concludes that for classical surfaces the dimension calculated from (2.2) has the usual meaning associated with the dimension. For fractals, the dimension as calculated from (2.2) will in general not be an integer – and hence the name fractal – but it retains the meaning as the exponent specifying the rate at which the number N of area elements increases with ϵ. As already noted, a characteristic of a fractal surface is that its fractal dimension will be larger than its Euclidian dimension of 2. What this implies is that a fractal surface covers something between an area and a volume, a fact for which the large degree of convolutedness of the surface is responsible.

What use is the fractal dimension of a fractal surface since its surface area is undefined? From (2.1) it is seen that, given the accuracy (or the resolution) to which the area needs to be specified, the dimension D_3 will provide the number of the area elements of prescribed resolution required to cover the fractal surface. This goes some way in describing the fractal surface. A complete specification of the fractal surface no doubt requires additional information, such as the location and the orientation of these little area elements, but the dimension is the basic quantity related to the

convolutedness of the surface. A measure of the convolutedness of a surface is of importance, for example, in the contexts of combustion.

2.2. *Dimension from sections with lower-dimensional subspaces*

To measure the fractal dimension of a surface by the direct procedure described above is difficult, and so we adopt alternative procedures based on sections with lower-dimensional subspaces (Mandelbrot 1982). To explain this, it is convenient to refer to figure 2. Let F be an object (e.g. a turbulent jet) in three-dimensional space with a fractal interface of dimension D_3. Let P be a plane intersecting the object. In analogy with our experience in Euclidean geometry, we may expect that the fractal dimension D_2 of the boundary of the resulting object $P \cap F$ and the dimension D_3 are related by

$$D_3 = D_2 + 1. \tag{2.3}$$

Similarly, an intersection of the object F with a line element gives a set of isolated points – akin to the Cantor discontinuum – whose dimension D_1 can be measured. Again, in analogy with classical objects, we expect that

$$D_3 = D_1 + 2. \tag{2.4}$$

Although there are exceptions to this rule (Mandelbrot 1982, p. 135), it is known to hold if the sections taken are independent of the fractal itself. Equivalently, the orientation of the intersecting plane or line will be irrelevant if the fractal is isotropic. More discussion and a brief circumstantial justification of this point will appear in §§2.3 and 2.4.

It is appropriate to mention here that the interface cannot be a true fractal because the scale similarity at all scales, leading to one fixed value of D_3, does not strictly obtain. Clearly, it will be truncated on the low end by the Kolmogorov scale: that is, if one measures the area of the interface with resolutions better than the Kolmogorov scale, it behaves like a classical surface of finite area (because surface convolutions on even finer scales do not exist). On the upper end, it can be expected to be bounded by scales comparable with or smaller than the large scale of the flow. Thus, the interface can be expected to be fractal-like only in an intermediate range of scales†. This is not a highly restrictive situation because, in all practical circumstances, there are inevitable scale cutoffs, and any meaningful application of the fractal concept to real circumstances will have to live with this fact. At large flow Reynolds numbers, the range of scales over which similarity can be expected to hold is large; and, naturally, it is easier to identify the fractal-like behaviour. As will be described more fully at appropriate places, instrumentation constraints restricted our experiments to moderate Reynolds numbers (the integral to Kolmogorov scale ratio no more than a few hundreds). Even so, the results are sufficiently convincing to justify their publication: besides making the important connection between fractals and fluid flows, they shed new light on some classical problems of turbulence.

2.3. *Dimension by intersection with a plane*

The practical way of obtaining two-dimensional sections or slices would be to seed the flow with some passive markers (e.g. smoke), illuminate a section of the flow by a thin sheet of light, and photograph the section for later analysis, namely measuring

† It is worth pointing out that, while the large scale is set by the flow boundary conditions and the small scale by the viscosity of the fluid, the equations of motion themselves do not set any new scales, which is what renders the scaling expectations plausible.

FIGURE 3. A smoke photograph of a turbulent boundary layer developing on a flat plate. The momentum thickness Reynolds number is around 2000. The thickness of the intersecting light sheet is of the order of the Kolmogorov thickness.

the dimension of the 'border' between the turbulent and non-turbulent regions. Although the intersecting plane must in principle be mathematically thin, it may in practice be of finite thickness without violating this principle, provided the thickness is smaller than or comparable with the Kolmogorov lengthscale η. The rationale for this assertion is that the 'fuzzing' due to the finite thickness of the plane is negligible because the Kolmogorov thickness represents the smallest scale of motion relevant to turbulence dynamics.

We have already alluded to the fact that smoke pictures (or pictures obtained by any other means of flow visualization) do not mark vorticity regions (which they should, to be truthful to the interface) for the following two reasons, both related to the diffusivity of the passive marker. If we remember that smoke is composed of aerosols (= oil fog) whose diffusivity is small compared with the molecular viscosity, the relatively large value of the effective Schmidt number will create a disparity between the smallest dynamical scale (i.e. η) and the smallest scale visible in the flow. This is not too worrisome as long as the latter is smaller than the former. The second, and more important, point is that to mark the interface satisfactorily, one has to put smoke exactly where vorticity is being generated, which is strictly impossible. Obviously, if one puts smoke very far upstream of the observation point, the pattern one sees is in general a remnant of the integrated memory that a given streakline experiences, and not necessarily a reflection of the local dynamics and geometry. Because turbulence diffuses smoke rather rapidly, there is some hope, however, that it will *roughly* mark the interface if carefully injected in the fully turbulent region reasonably close to the region of visualization, but not so close that it does not have time to diffuse.

Even if one grants the plausibility of this last statement, even roughly marking the interface by smoke is admittedly a trial-and-error procedure in practice. The issue is worth exploring in detail – which we have not done – but there are reasons of precedence which are somewhat reassuring. For example, the statistics of the interface obtained by marking it with hydrogen bubbles (Kim, Kline & Reynolds 1971) and by heat (Sunyach & Mathieu 1969) agree favourably with those obtained by momentum and other means; we ourselves have recorded elsewhere (Sreenivasan, Antonia & Britz 1979) some simultaneously obtained traces of two components of fluctuating velocity, Reynolds shear stress and the temperature fluctuation in a

FIGURE 4. A section of an axisymmetric jet made visible by laser-induced fluorescence, from Dimotakis *et al.* (1981). Scales down to the Kolmogorov limit have been resolved in this picture.

slightly heated jet, which confirm that passive scalars are useful for marking the interface. The final point must no doubt be that, although our procedure is believed to mark the interface roughly it is the smoke/no-smoke interface that we are strictly studying.

Another concern is that a streamwise section is somehow preferential, thus biasing the results. To test this, one ought to take plane sections of the interface at several orientations and demonstrate the invariance of the results. For the anisotropic flows of the sort studied here, it is possible that the scale-invariance concept must be thought through more thoroughly, and that one may come up with more than one fractal dimension depending on which planar section one is measuring. Our work in this direction is continuing, but our argument is that the present results are representative.

Figure 3 shows a section of a boundary layer made visible by injecting smoke. This figure appears to suggest that there is no contiguous interface, and that there are islands of non-turbulent regions surrounded by turbulent ones, just as there are isolated pockets of turbulence sticking out. The reason that photographs like figure 1 do not show this feature is that they have been obtained by optical means which integrate along the path of light. Obviously, this will smooth out the interior 'holes', and what one sees as a contiguous interface is the horizon of a large number of images

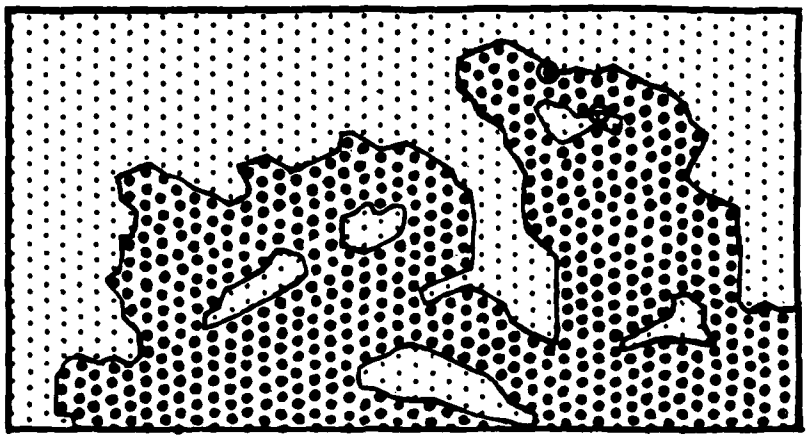

FIGURE 5. A schematic of a part of a digitized image. The dark dots represent the points with intensity above threshold (turbulent regions, by definition here), the light ones representing non-turbulent regions. We want to measure the fractal dimension of the border between the two regions. The little circles of radius ϵ drawn around a dark and a light dot in the upper right corner are two examples of boundary points within the distance ϵ.

superposed on each other. Dimotakis, Lye & Papantoniou (1981) pointed out this fact first, and produced several fascinating pictures of a turbulent jet, one of which is reproduced here as figure 4. (No analysis was attempted by us on the pictures obtained by these authors.) Plane sections by themselves cannot deny the existence of out-of-plane connections of what appear as islands or holes, and we should emphasize that to prove the non-contiguity of the interface one has to produce at the very least simultaneous pairs of pictures in perpendicular planes. In the absence of such work, the point is made here for the sole purpose of indicating that, if the interface is indeed non-contiguous, the fractal dimension one obtains will not lose its meaning but will have to be interpreted as a measure of both its 'roughness' and 'fragmentation', and not merely of the former, as would be the case for a contiguous interface.

We may now discuss several ways in which the fractal dimension D_2 of the border can be measured. The length of the border, in analogy with the coastline of an island cluster, increases with increasing resolution according to the relation

$$L = K\epsilon^{1-D_2}, \tag{2.5}$$

where ϵ is the lengthscale relating to the fineness of resolution, and K is a constant related to the lacunarity of the fractal set. This direct method has so far eluded us chiefly because of the algorithmic complexity in faithfully following the highly contorted, multivalued and disconnected interface (see figures 3 and 4), and alternatives seem called for. We have adopted a simple alternative spelt out in Mandelbrot (1982) and Grebogi *et al.* (1985), but summarized here with the anticipation that they may be unfamiliar to a number of the Journal's readers.

Considering both regions (turbulent and non-turbulent) that are within a distance ϵ from the border, one can form a strip of width 2ϵ about the border, which will have an area of $2\epsilon L$, where L is the length of the border. This area clearly goes like ϵ^{2-D_2}, from (2.5). One measures this area for varying ϵ, and obtains D_2 from the slope of a log–log plot. The implementation of this idea involves the following procedure. One

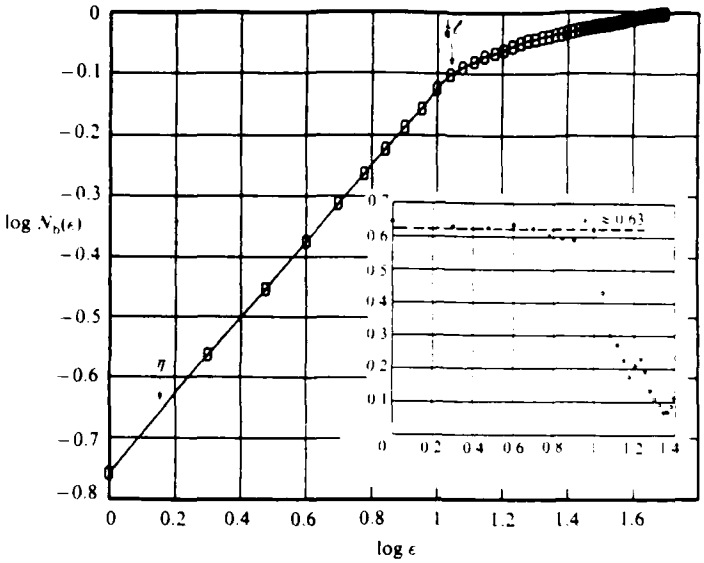

FIGURE 6. The logarithm (to base 10) of the number of boundary points N_b (see figure 5) as a function of the distance ϵ from the boundary. The flow is a heavily tripped boundary layer, thickness about 10 cm, $U_\infty = 2.5$ m s^{-1}. The Kolmogorov and the integral scales are shown for reference. The inset showing the slope gives $D_2 = 2 -$ mean slope $= 1.37$; D_3 is thus expected to be 2.37.

digitizes the image of the flow obtained as described previously, and obtains an assignment of light intensity at each of the digitized points. One then sets a judicious threshold for the light intensity which demarcates the turbulent (above-threshold) from the non-turbulent (below-threshold) regions. (Naturally, one has to ascertain that the precise value of the threshold is not important for the results to follow, and evidence to this end will be presented at the appropriate place.) One then obtains a digitized image, schematically shown in figure 5, where each dark dot is a digitized image point in the turbulent region and each light dot in the non-turbulent. It is the dimension of the border between the two regions that we want to measure. The conceptual equivalent of the data processing on the computer is the following. Draw around each of these digitized points (dark as well as light) circles of radius ϵ. Whenever a circle drawn around a point crosses the border, obtained by interpolation between the neighbouring light and dark dots, the point is counted as a border point within a distance ϵ from the border. Count the number of all border points $N_b(\epsilon)$ within the distance ϵ from the border. Repeat the process for varying ϵ, and determine the variation of $N_b(\epsilon)$ with respect to ϵ. From the earlier discussion in the paragraph, we have

$$N_b(\epsilon) \propto \epsilon^{2-D_2}. \tag{2.6}$$

For future reference, we may note that the quantity $2 - D_2$ (or in general $d - D_d$, where D_d is the fractal dimension of the object's interface in the embedding space of dimension d) is called the codimension. In most well-behaved (i.e. integrable or non-chaotic) systems, a small amount of uncertainty ϵ in the initial state will translate to a comparable final-state uncertainty. For fractal objects, the final-state uncertainty is large and proportional to ϵ^{D_c}, where D_c is the codimension (Grebogi *et al.* 1985). The codimension appears again in §4.

Figure 6 shows a plot of $\log N_b(\epsilon)$ *vs.* $\log \epsilon$ obtained from the digitized image of the

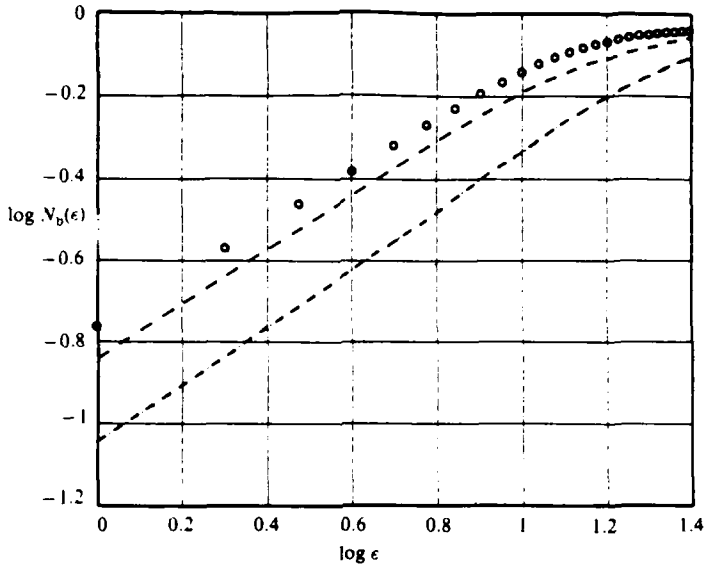

FIGURE 7. The effect of threshold setting on the codimension. The threshold (in the notation of the text) varies by a factor of 1.5 with no perceptible change in the slope. In the units described in the text, the thresholds are (from top to bottom) 3000, 3500 and 4000.

type shown in figure 3: the inset shows the slope of the curve. Clearly, there is a region of constant slope as expected for a fractal interface. Several comments must be made before interpreting the result. First, the low end of the constant-slope region is comparable with the Kolmogorov scale†. The high cutoff seems to occur around $\frac{1}{6}\ell$, where ℓ is the transverse integral scale of turbulence in the boundary layer. (This integral scale was obtained from two-point correlation measurements with the fixed probe at $y/\delta = 0.4$ and the other probe moving outwards.) The obvious conclusion that the scale similarity extends only up to $\frac{1}{6}\ell$ on the high end is not correct because, as we shall soon show, the high cutoff occurs prematurely because of the limitations of the image processing procedure. To obtain reliable statistics on the high end, one has to include many large scales in the digitized image, which is usually hard (especially if the fine resolution requirements are to be satisfied also) because of the finite capacity of the image digitizer. We have not been able to do that, which means that the apparent termination of scale similarity at $\frac{1}{6}\ell$ is artificial. This shortcoming is overcome in the line-intersection method of §2.4.

The second comment relates to the effect of the threshold setting on the slope in figure 6. At least within the threshold range of 3000–4000 for the light intensity (the units being such that 12000 indicates the brightest spot in the picture and 0 the darkest), the power of ϵ in (2.7) is essentially constant (figure 7); the threshold of figure 7 is about $\pm 15\%$ of that used in the boundary-layer work. The third relevant

† There is some concern that to detect similarity on scales of the order of η, the resolution of the digitized image must be substantially smaller (at least by a factor 2). Figure 6 shows that this factor is about 1.5 for present measurements. We may remark that estimating η to an accuracy better than a factor 2 is beset with many uncertainties; among other things, it depends on the precise location in the flow, the assumptions made in obtaining the energy dissipation, the probe size, etc. The number quoted in figure 6 is thus a representative value.

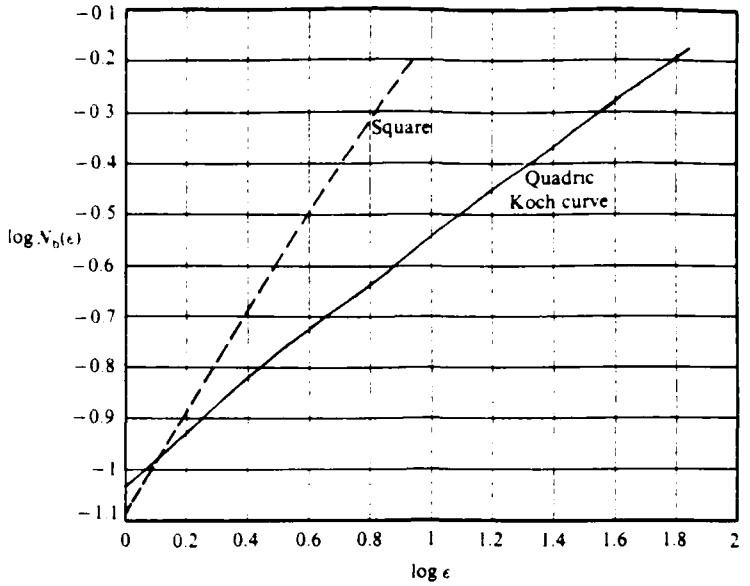

FIGURE 8. Calibration experiments for the imaging method. The continuous line (mean slope = codimension = 0.5) is for a quadric Koch island, and the dashed line (codimension = 1) is for a square. Their respective dimensions are in good agreement with the theory.

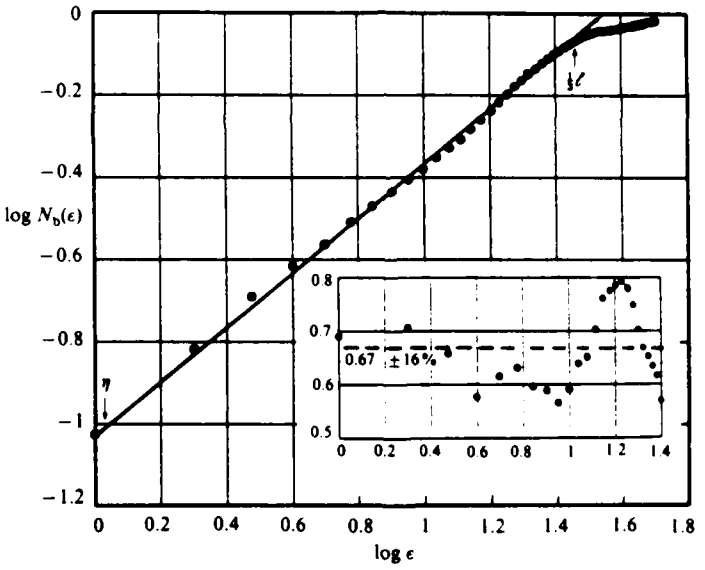

FIGURE 9. The logarithm (to base 10) of the number of boundary points N_b (see figure 5) as a function of the distance ϵ from the boundary. The flow is a round water jet seeded with polystyrene spheres. Jet exit Reynolds number is about 2500, diameter $D = 5$ mm; $x/D = 30$. The inset shows that the slope of the line is $0.67 \pm 15\,\%$.

comment concerns the 'calibration' experiments on some well-known fractals (e.g. a quadric Koch island, Mandelbrot 1982, p. 50) and regular objects (such as a black square). As shown in figure 8, it is clear that the codimension (mean slope of the curves) is 0.5 for the Koch island (i.e. $D_2 = 1.5$, the theoretical value), and 1 for the square ($D_2 = 1$).

Putting all this together, we conclude from figure 6 that scale similarity extends from η up to a fraction of ℓ (the precise value to be determined shortly), and that we have $D_2 = 2$-slope $= 1.38$ (for the border), leading to the conclusion that $D_3 = 2.38$ (for the interface surface).

Figure 9 shows similar data for an axisymmetric jet of water flowing vertically down into a large tank of still water. The jet was seeded with polystyrene microspheres; both seeding and gravity effects were considered negligible. A part of the jet in the developed region (in the vicinity of $x/D = 30$) was intersected by a thin sheet of light, photographed and digitized as before. Again, scale similarity extends all the way from η to a fraction of ℓ; for reasons already mentioned, we think little of the fact that the high cutoff occurs at $\frac{1}{3}\ell$ (instead of $\frac{1}{6}\ell$ in the boundary layer) or that the slope is slightly different from the boundary-layer case. This latter is well within the scatter of the data (about which more will be said in §2.4).

In determining the dimension, we have chosen to digitize certain regions of the cross-section that are neither too close to wall (or jet axis) nor too far away from it. Both for the jet and the boundary layer, the digitized image spans (approximately) $0.6 < \gamma < 0.1$, where γ is the intermittency factor representing the fraction of time the flow is turbulent at a given point in the flow. We empirically found the region just mentioned to be optimum given the image-processor constraints.

2.4. *Dimension by line intersection*

As discussed earlier, the dimension of the set resulting from line intersection of the interface (yielding simply a 'truncated' Cantor set of dimension less than 1) is expected to be two less than that of the interface, D_3. In practice, we have interpreted that this statement holds true for the one-dimensional cut obtained by intersecting a *moving* interface with a small (i.e. η or smaller) stationary hot-wire probe. This assumes the validity of Taylor's frozen-flow hypothesis, which we know is not strictly true, but much can be learnt in spite of this shortcoming.

As is standard in the turbulence literature, we formed the intermittency function from the measured velocity signal by setting a convenient threshold and a hold time. The reasonableness of the threshold as well as the hold time was ascertained by a comparison of the resulting intermittency function with the original signal. The set of intersection points between a horizontal line and the intermittency function results in a 'truncated' Cantor set whose dimension D_1 we want to measure. To obtain D_1, the so-called box-counting algorithm, which is merely the application of (2.2) for line elements, has been employed. It makes direct use of the definition of fractal dimension by counting the number N_ϵ of the line segments of length ϵ required to cover the set for several values of ϵ.

Figure 10 shows a typical set of data for N_ϵ *vs.* ϵ for the boundary-layer flow. It is seen that there is a sizeable region of constant slope, giving in this instance $D_1 = 0.4$; we infer that $D_2 = 1.4$ and $D_3 = 2.4$. It should be noted that D_1 inferred from one-dimensional cuts is approximately one less than D_2 inferred from intersections with planes, thus providing some circumstantial justification for the method of sections with lower-dimensional subspaces discussed in §2.2. Note also that the region of self-similarity does not extend all the way down to η as in the two-

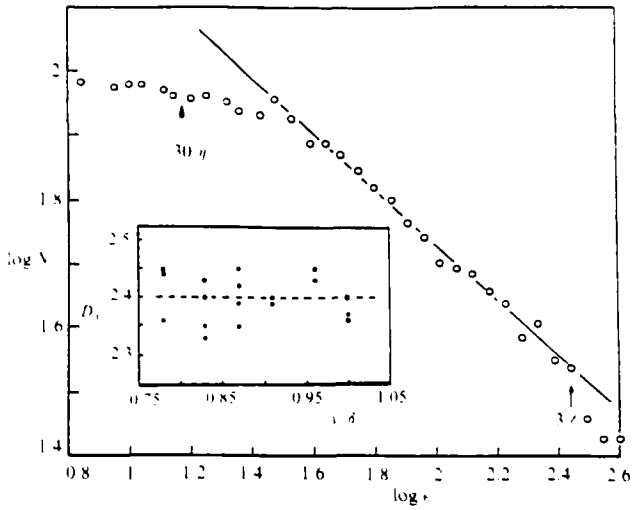

FIGURE 10. The logarithm (to base 10) of the number of segments N_ε of length ε needed to cover the Cantor discontinuum formed by the intersection between a horizontal line and the intermittency function (turbulent boundary layer, $y/\delta = 0.91$, $U_\infty = 12$ m s^{-1}). The inset shows the dimension D_1 as a function of the position of the line intersection, or probe height from the wall in the boundary layer, obtained for several chunks of data. Corresponding intermittency factors, from the highest to the lowest, are 0.41, 0.24, 0.19, 0.13, 0.10, 0.08.

dimensional slice method of §2.1, and even scales up to 30η do not fall on the straight part. Part of the reason is clearly the problem related to Taylor's hypothesis and the size of the hot-wire, which is several η long (approximately 10η in this case) both of which will bias the results at small scales. A more basic problem is related to the inappropriateness of using the streamwise velocity for constructing the intermittency function. One should ideally use a vorticity probe (which gives a much clearer on–off signal), or a passive scalar that is uninfluenced by the long-range effects of the turbulent pressure field. However, the outer cutoff does not occur until ℓ or beyond. Combining this result with the inner cut-off of the previous subsection, we might conclude that scale similarity extends between η and 3ℓ. (The outer cutoff is thus approximately the streamwise integral scale, which is of the order of the boundary-layer thickness.)

It is now helpful to examine the sensitivity of the dimension results with respect to position in the intermittent region where the one-dimensional slice was obtained. The inset in figure 10 shows the data as a function of the probe height in the intermittent region of the boundary layer. Because the interface is rarely found deep in the flow, not surprisingly, we cannot compute the dimensions for $y < 0.5\,\delta$ (corresponding to a γ of almost unity). In fact, calculations become uncertain for $y < 0.7\,\delta$ (or, roughly, $\gamma > 0.6$), say, and hence we have not presented any results there. The variability of D_1 is about 10% in the region $0.75 < y/\delta < 1.0$ where the measurements are trustworthy; further, it is approximately in this region that the two-dimensional slices were taken. Clearly, then, this latter method may be expected to represent an average of values obtained from one-dimensional slicing; it is somewhat reassuring that this is indeed the case. We conclude that one-dimensional cuts offer a reasonably valuable tool. The main contribution of this method has been

Flow	Fractal dimension of interface (surface) by: two-dimensional slicing	Fractal dimension of interface (surface) by: one-dimensional slicing
Boundary layer	2.38	2.40†
Axisymmetric jet	2.33	2.32†
Plane wake	—	2.37‡
Mixing layer	—	2.40‡

† Typical average over a range of the outer flow
‡ Single value at some typical location in the outer region

TABLE 1. Summary of the fractal dimensions of the turbulent/non-turbulent interface in several classical turbulent flows

to show that scale similarity extends all the way up to about the integral scales of motion. Recalling that the larger eddies, which are highly dependent on the boundary conditions for the flow, are a few integral scales long, we infer that the scale similarity does not include the biggest scales in the flow. Our conclusions about the interface are summarized in table 1.

From here, the interface dimension of about 2.3–2.4 is seen to be essentially independent of the type of flow. What this means is that one cannot conveniently assign a distinct fractal dimension to each of the different classes of flows. We reiterate that this is not surprising because scale similarity does not encompass the largest scales, which are the ones that depend strongly on the geometric aspects of the flow.

To the extent that in both methods we have examined the interface approximately in the region $0.6 < \gamma < 0.1$, we are not completely justified in talking about the dimension of the interface as a whole, although we expect that what is true of the part is true of the whole. We have already commented on the constraints in the plane-intersection method. One runs into two problems in the line-intersection method. Outside the region we have covered, the infrequent appearance of the interface there would demand the inclusion of data for long intervals of time in order to obtain reliable statistics, and this violates Taylor's frozen-flow hypothesis. This is relatively easy to overcome, at least in principle, by resorting (for example) to intersection by a suitable laser beam of a fluorescing flow. Although this should be attempted soon, we have not done it immediately because waiting for enormously long times results in a randomization of results that will obscure the fractal nature; this point is best deferred to §3 where it is more fully discussed.

Finally, it may be worth remarking that Maxworthy (1986) finds $D_2 = 1.37$ for the interface of the flattened bubbles of air injected into a viscous fluid contained in a Hele-Shaw experiment.

2.5. *Fractal dimension of clouds: a brief comparative study*

Lovejoy (1982) obtained the fractal dimension of clouds using the so-called area-perimeter rule (Mandelbrot 1982, p. 112). For classical objects, the perimeter P and the area A are related through $P \propto A^{\frac{1}{2}}$. For an object with a fractal boundary of dimension D_{2p}, the relation is modified to $P \propto A^{(\frac{1}{2})D_{2p}}$. Thus, if one has different sizes of statistically similar fractal objects, this area-perimeter rule (both P and A evaluated to the same resolution) can be used to determine D_{2p}. Lovejoy used digitized images of satellite and rain-pattern pictures of clouds with sizes varying

between 1 km and 1000 km, and obtained the fractal dimension of about 1.34. It is the coincidence of this number with that obtained by us for D_2 in laboratory turbulent flows that calls for specific comment. Recall that we took a slice of the flow to obtain D_2, whereas Lovejoy was looking at the boundary of the projection of a cloud onto a horizontal plane. The key question then is the difference between the two techniques. We know of no rigorous analysis of this point. However, a projection can be thought of as superposition of a large number of sections, each section being separated from the other by distances of the order η.

Going back to figures 3 and 4, we may qualitatively perceive the effect of superposition of several sections. One effect is obviously to reduce the interior fragmentation (leading to a reduced fractal dimension), but the other effect is to increase the boundary roughness (leading to an increase in fractal dimension). It is the net effect in which we are interested. If the fractal dimension is small (that is, neither the interior fragmentation nor the boundary convolutedness is very large), D_2 and D_{2p} cannot be very different. While taking sections of clouds is not within our capability, superimposing sections of boundary-layer or jet flows can easily be done by increasing the thickness of the light sheet. This has been done, and the result is that increasing the relative size of the light-sheet thickness (from between 1 and 2η to about 5η) increases the dimension D_2 (from 1.37 to 1.43), suggesting that $D_{2p} > D_2$. In doing this experiment we could not unfortunately hold the Reynolds number constant, but if we believe that the primary effect of increasing the Reynolds number is to increase the range of scale similarity (but not alter the dimension), this increase in D_2 is conclusive enough. If this reasoning holds for clouds, we may conclude that $D_2 < 1.34$. It is interesting that Carter *et al.* (1986), using an entirely different procedure from Lovejoy's, arrive at a number of 1.16 for D_2.

We have become aware from a preprint by Lovejoy & Schertzer (1986) that smaller dimensions than 1.34 have in fact been obtained for clouds by setting the threshold to higher values. The result that the more intense regions of a fractal are distributed on sets with lower fractal dimensions is described in §§ 3 and 4.3, and is apparently quite general (Halsey *et al.* 1986).

3. Dimension of iso-velocity surfaces in boundary layers

Here, we seek the fractal dimension of surfaces separating regions of velocity above and below a certain chosen level, say u_1 in figure 11. One can similarly (and more satisfactorily) address the issue of iso-concentration surfaces. We have used the line-intersection method described in §2.4. As before, we get Cantor discontinua whose dimension can be obtained by the box-counting method. The hope is that adding 2 to the numbers obtained will yield the fractal dimension of iso-velocity surfaces; again, one should keep in mind the various aspects discussed in §2. Figure 12 shows results from a box-counting algorithm implemented on a signal obtained in a boundary layer at a height of 0.35δ. The different curves are for different segments of the same (long) signal. To within the variability of about 12%, the line drawn through these various curves represents a mean behaviour. Such results can be obtained for several velocity levels of the same signal (the uncertainty is largest for levels near the mean velocity) and for signals obtained at several heights in the boundary layer, all of which are consolidated in figure 13. The dimension is highest for the iso-surface for the local mean velocity, and drops off on both sides. Further, the peak value of the dimension goes up slowly towards 3 as the distance from the wall increases (see inset).

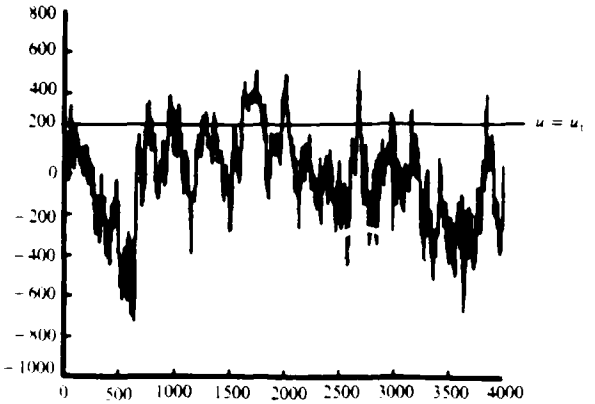

FIGURE 11. A turbulent velocity signal, $u(t)$, and the level u_1 defining the iso-velocity surface. The units are arbitrary.

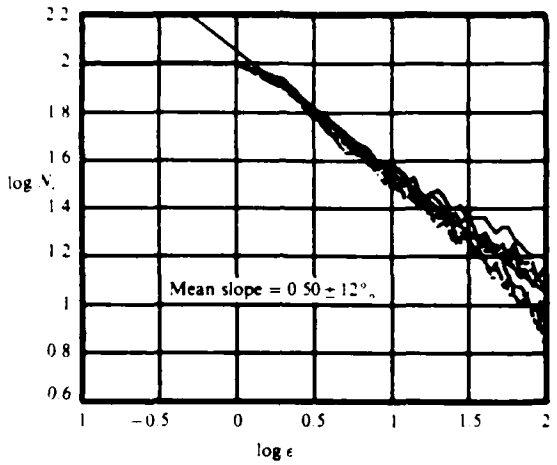

FIGURE 12. The logarithm (to base 10) of the number N_ϵ of the line segments of length ϵ required to cover the Cantor discontinuum obtained by the intersection of the threshold level u_1 ($= 0.75\,U_\infty$) with the velocity signal; $y/\delta = 0.35$, $U_\infty = 20$ m s^{-1}, $\delta = 4$ cm. Each line in the figure corresponds to a different segment of the velocity signal, each of which is of the order of 100 transverse integral scales long (see text). The mean slope (D_1) is 0.50 with a variation of $\pm 12\%$, giving a $D_3 = 2.50$.

A complete interpretation of these curves must take into account several factors. We expect the dimension to be largest for the most space-filling iso-velocity surface, or the velocity with the largest number of 'level crossings' (which roughly translates as the largest probability density – see, for example, Sreenivasan, Prabhu & Narasimha 1983). In the fully turbulent regions of the boundary layers, the peak of the probability density of the velocity signal occurs roughly at the mean velocity. Far into the boundary-layer free stream (i.e. $y \gg \delta$), we should ideally expect nothing but the free-stream velocity to prevail everywhere; thus the set $u_1 \neq U_\infty$ is a null set and its complement, namely the set $u_1 = U_\infty$, is really a classical volume for which the dimension must equal 3. In practice, the presence of some overriding noise on the free-stream velocity will reduce the peak dimension to something smaller than 3 and produce a spread onto the neighbouring velocity levels. In the intermittent regions, where laminar chunks of signal are interspersed between the turbulent ones, the

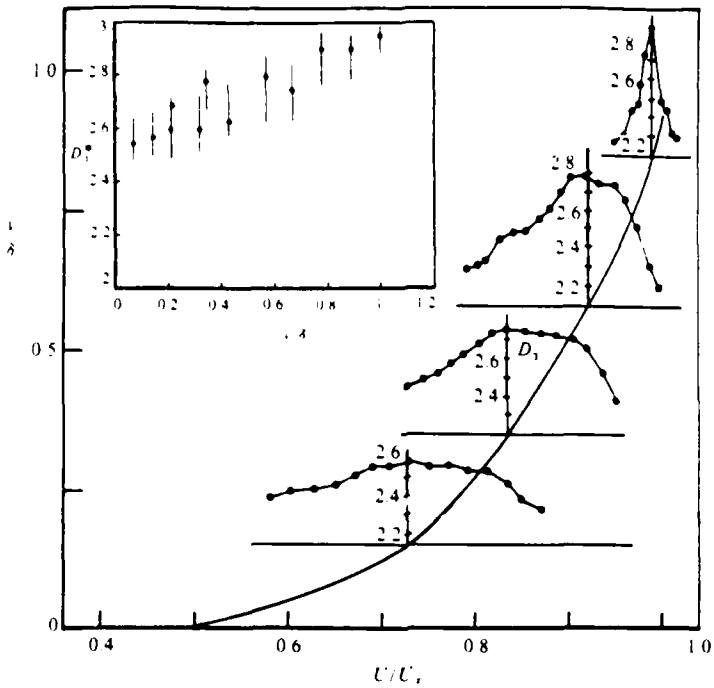

FIGURE 13. The dependence of the dimension of iso-surfaces of streamwise velocity as a function of both its magnitude and the distance from the wall. The spread is smaller as one goes away from the wall, while the peak magnitude D^* (shown in the inset) increases. The solid curve with no data is the mean velocity distribution in the boundary layer. The scales for the abscissae for each of the dimension plots is the same as that for the mean velocity.

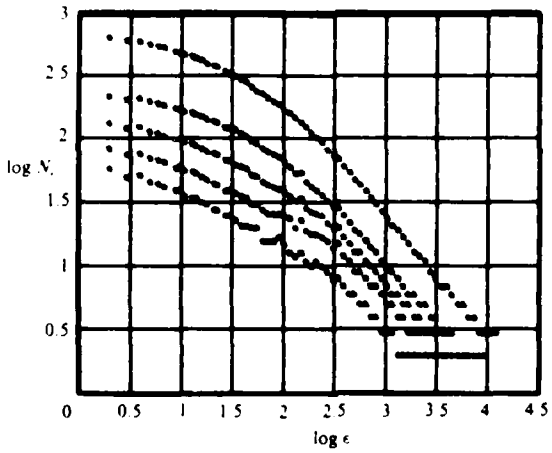

FIGURE 14. The effect of increasing the data segment length used for computing the dimension. The data segment length is, from bottom to top, $.50\ell$, $.83\ell$, 1.32ℓ, 2.00ℓ and 4.30ℓ, where ℓ is the transverse integral lengthscale. For small lengths, there is a distinct constant-slope region over the scales of interest; this becomes less conspicuous as the signal length increases. For large data segments, one can find a constant-slope region in the scale region far larger than the integral scale; the dimension D_1 is very nearly 1, however.

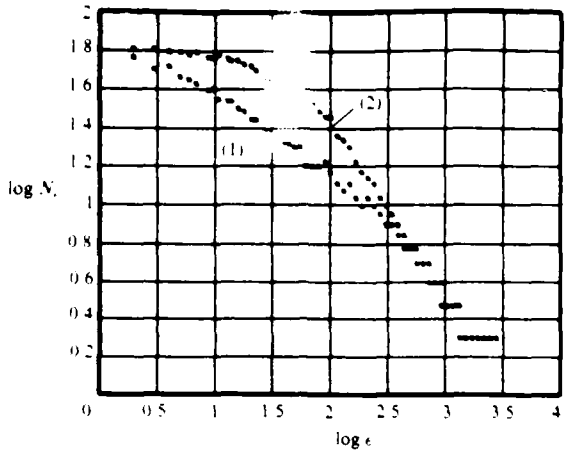

FIGURE 15. The box-counting algorithm applied to a typical iso-velocity intersection (curve 1) and to the same amount of points randomly distributed on a line, curve (2). For curve 2 there is no self-similarity range; only at large scales, for which the set looks like a solid line, do we get $D_1 = 1$.

dimension of an iso-velocity surface must be a weighted average between those of the same iso-surface in the turbulent and non-turbulent regions: the dimension will now peak at around the mean velocity in the non-turbulent region because the distribution of the Cantor-set elements is much denser there than anywhere else (with or without noise); according to the measurements of Kovasznay, Kibens & Blackwelder (1970), the mean velocity in the non-turbulent region is approximately the same as the overall mean velocity (at least to the accuracy appropriate in this context). It is also logical that the dimension must get smallest near the wall because the strong viscous effects will inhibit excessive contortions of an iso-velocity surface. While all these interpretations are consistent with the data of figure 13, note that the data of figure 13 do not apply to iso-surfaces in the non-turbulent regions only, and hence cannot answer questions related, for example, to the dimension of an iso-velocity surface with $u_1 = 0.9U_\infty$ residing entirely in the non-turbulent region.

In figures 12 and 13, we have used many segments of signal that are of the order of 50 transverse integral time scales long, and ensemble averaged over them. This should be quite acceptable because all iso-surfaces are only a few integral scales in streamwise extent and small in the transverse direction. We should point out, however, that if one uses fewer longer chunks of the signal for the calculations (the total length remaining the same), the straight-line regions become more and more ambiguous, until they disappear altogether for signal lengths beyond, say, 500 integral scales long (figure 14). The distribution then takes the shape characteristic of a random process (figure 15). What this implies is that the iso-surfaces are fractal-like when viewed on timescales of the order of 50 integral timescales, but behave more akin to random processes when viewed on timescales an order of magnitude larger.

An operationally helpful comment on the long-time randomization of the self-similar behaviour observed over short times is the following. If two separate segments of data show fractal characteristics but with slightly different fractal dimensions, it is easy to see that the sum of the two segments of data will in general *not* show the fractal behaviour. (The sum of two processes, each of which is hyperbolically

distributed, will also be hyperbolically distributed only if the scaling exponent is the same for both.) The observed randomization is a rough consequence of the central-limit theorem for the collection of a large number of slightly different and nearly independent events. If we argue that fractals are intermediate between complete order and total chaos, we may interpret our findings as revealing short-time order (or order over small extent) and long-time disorder in turbulence – a concept that has support in a variety of circumstances in turbulent flows.

4. Fractal dimensions of dissipative structures of turbulence

Another aspect of turbulence that is a candidate for fractal description is its dissipative (or internal or small) structure. It is known (Batchelor & Townsend 1949) that the small structure of turbulence is intermittent, and that scale-similarity arguments (e.g. Gurvich & Yaglom 1967) are very helpful in describing it. The essence of scale-similarity arguments in this context is the following. Within a given field of (fully developed) turbulence, consider a cube with sides of length L_0, where L_0 is an integral scale of turbulence. If we divide this cube into a number ($n \gg 1$) of smaller cubes of length $L_1 = L_0 n^{-\frac{1}{3}}$, the density of dissipation rate in each of these smaller cubes is distributed according to a certain probability law. Further subdivision of these cubes into second-order cubes of length $L_2 = L_1 n^{-\frac{1}{3}}$ leaves the probability distribution unaltered. This similarity extends to all scales of motion until one reaches sizes directly affected by viscosity. The simplest distribution is the binary one according to which a given high-order box either contains dissipation or does not. It is this simple picture that we shall pursue. The goal in this section is to examine the appropriateness of fractal description for the dissipative structure of both turbulent energy and of a passive-scalar field. Except for the material in the following subsection, which is an update of some earlier work, the rest of the material in this section is new.

4.1. *An update of Mandelbrot's work*

Let $\mathscr{D}$ be the fractal dimension of the dissipative field. (We shall avoid using the subscript 3 in this instance because there is no ambiguity.) When we have resolved the smallest scales η, and determined the number N of boxes of size η required to cover the entire dissipation regions, $\mathscr{D}$ can be calculated according to its definition:

$$\mathscr{D} = \frac{\log N}{\log (L_0/\eta)} \quad \text{or} \quad N = (L_0/\eta)^{\mathscr{D}}. \tag{4.1}$$

Since each cube has a volume of the order $(L_0/\eta)^3$, the total volume occupied by the cubes of active dissipation is $(L_0/\eta)^{\mathscr{D}-3}$. Since all dissipation is contained in these cubes, the level of dissipation in them is $(L_0/\eta)^{3-\mathscr{D}}$ times the global average value. Assuming local isotropy, this means that $(\mathrm{d}u/\mathrm{d}x)^2$ in the dissipating cubes is $(L_0/\eta)^{3-\mathscr{D}}$ times the global mean. Consequently, the kurtosis (or the flatness factor) of $\mathrm{d}u/\mathrm{d}x$, defined as

$$K = \frac{\overline{\left(\frac{\partial u}{\partial x}\right)^4}}{\left(\overline{\frac{\partial u}{\partial x}}\right)^2} \tag{4.2}$$

will be given by $(L_0/\eta)^{2(3-\mathscr{D})}$ times the volume occupied by the dissipating cubes. (Note that this assumes the identity of the set supporting dissipation and that

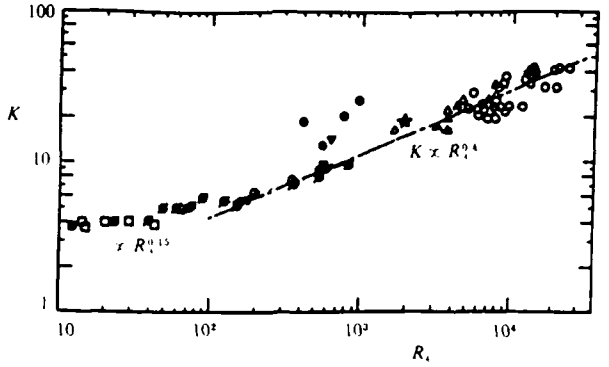

FIGURE 16. The variation of the kurtosis of (du/dt) as a function of the microscale Reynolds number. With minor modifications, this diagram is the same as figure 2 of Van Atta & Antonia (1980). □, Batchelor & Townsend (1947, 1949), grid turbulence; ■, Friehe, Van Atta & Gibson (1971), circular cylinder; ●, Gibson, Stegen & Williams (1970), atmosphere; ○, Wyngaard & Tennekes (1970), mixing layer and atmosphere; △, McConnell (1976), atmosphere; ▲, Park (1976), atmosphere; ◑, Williams & Paulson (1977), atmosphere; ▼, Champagne (1978), atmosphere; ⌀, Kuo & Corrsin (1971), grid turbulence and circular jet; ★, Pond & Stewart (1965), atmosphere

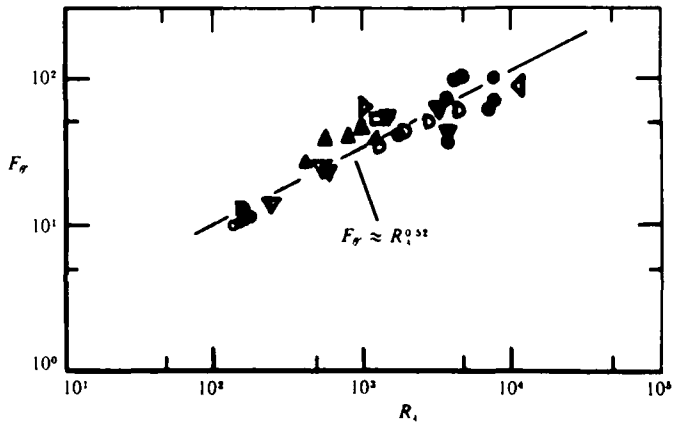

FIGURE 17. The kurtosis of the temperature derivative (dT/dt). ●, McConnell (1976), atmosphere; ◁, Antonia *et al.* (1980), atmosphere; ▯, Antonia & Danh (1977), atmosphere; ○, Sreenivasan, Antonia & Danh (1977), boundary layer; ▲, Gibson *et al.* (1970), atmosphere; ▷, Park (1976), atmosphere; □, McConnell (1976); jet; ▽, Antonia & Van Atta (1975); ◗, Antonia & Danh (1977), jet; ▽, Gibson & Masiello (1972), jet; ▼, Gibson *et al.* (1970), jet.

supporting $(du/dt)^2$. We are strictly calculating the fractal dimension of the latter.) From (2.4), we have

$$K \propto (L_0/\eta)^{3-\mathscr{D}} \propto R_\lambda^{\frac{1}{2}(3-\mathscr{D})}, \tag{4.3}$$

where $R_\lambda = u'\lambda/\nu$, λ being the Taylor microscale and u' the root-mean-square streamwise velocity. If we invoke Taylor's frozen-field hypothesis, the flatness factor of (du/dx) is the same as that of (du/dt); Antonia, Phan-Thien & Chambers (1980) have shown that this is true to within about 7 %. A plot of $\log K$, where now K is the kurtosis of (du/dt), *vs.* $\log R_\lambda$ will yield the co-dimension $(3-\mathscr{D})$.

Mandelbrot used this argument and, from an examination of the kurtosis data from Kuo & Corrsin (1971), estimated $\mathscr{D}$ to be 2.6. More data have become available since

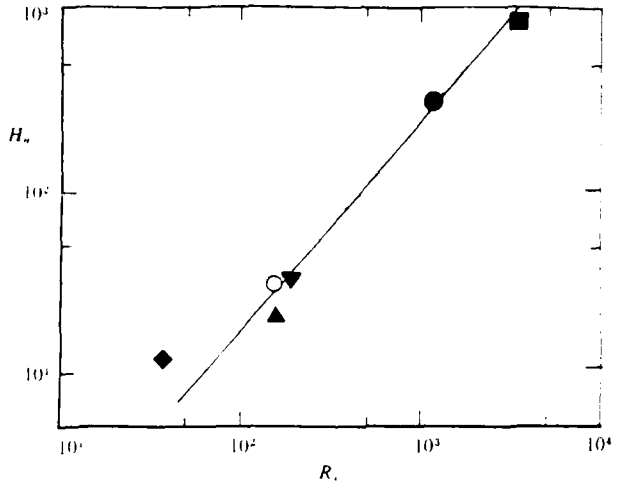

FIGURE 18. The hyperflatness of (dT/dt). ◆, Yeh (1971); ●, Sreenivasan, Antonia & Danh (unpublished) boundary layer; ▼, Antonia & Van Atta (1978), jet; ▲, Antonia & Van Atta (1978), laboratory boundary layer; ○, Antonia & Van Atta (1978), atmospheric boundary layer over land; ■, Park (1976), atmospheric boundary layer over water.

then, and are plotted in figure 16. With small modifications and additions, this figure is essentially a reproduction from Van Atta & Antonia (1980) who first compiled them. Given the difficulties in obtaining the data, they may be considered to collapse on a line with a slope of 0.4, yielding a $\mathscr{D}$ of 2.73, a revision from Mandelbrot's earlier estimate. This means that the fractional volume $(L_0/\eta)^{(\mathscr{D}-3)}$ occupied by the dissipation field is given by $(L_0/\eta)^{-0.27}$. For $R_\lambda < 150$, the slope in figure 16 is decidely smaller (≈ 0.15), which yields a $\mathscr{D}$ of 2.9. This indicates either that the dissipation regions at low Reynolds numbers are less spotty or that local isotropy does not obtain. Both are likely.

4.2. *Fractal dimension of the temperature 'dissipation' field*

Precisely the same arguments show that the kurtosis F_θ for the temperature derivative (dT/dt) is related to the Reynolds number as

$$F_\theta \propto R_\lambda^{\frac{1}{2}(3-\mathscr{D}^*)},$$

where $\mathscr{D}^*$ is the dimension of the temperature dissipation field. From figure 17, where all the available data have been collected, we conclude that $\mathscr{D}^* = 2.6$. (By drawing a line with a slope of 0.52 on figure 16, it is easy to see that the difference between the scalar and momentum dissipation fields is indeed statistically significant.) The temperature dissipation field (and by inference, those of all passive scalars) is less space filling ($\propto (L_0/\eta)^{-0.4}$), or is more intermittent. This result has been known to oceanographers for some time.

Similar arguments suggest that the so-called hyperflatness (i.e. the normalized sixth moment) of (dT/dt) must behave like $R_\lambda^{3(3-\mathscr{D}^*)}$. Figure 18 shows that this is quite consistent with the experimental data for $R_\lambda > 100$.

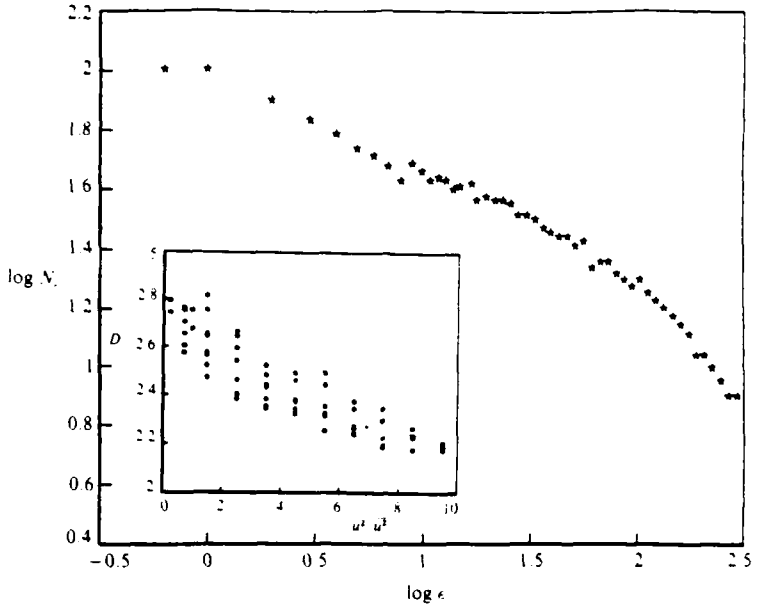

FIGURE 19. Log N_ε *vs.* log ε for the 'dissipation' field in grid turbulence by a line intercept using a threshold of $5\bar{u}^2$. The inset shows the dependence of the resulting dimension on the threshold used to identify the iso-dissipation surface.

4.3. *Dimensions of iso-dissipation surfaces by the line-intersection method*

It is obvious that the volume occupied by the dissipative structures depends on the threshold employed to identify the dissipation regions. There is no explicit mention of any threshold in the above method, which is both its strength and weakness – weakness because one does not really understand the inherent experimental definition of dissipation regions: the probes and the differentiation operations somehow set a threshold of their own. To permit sharper questions about the dependence on the threshold or, equivalently, about the dimensions of iso-dissipation surfaces, it is useful to resort to the line-intersection method. The method here is in principle free of some of the ambiguities raised in earlier sections because of the expected statistical isotropy of the dissipation regions, even in inhomogeneous shear flows. The procedure is exactly the same as in §2.4, except that we replace u by $(\mathrm{d}u/\mathrm{d}t)^2$. Figure 19 gives a typical result in grid turbulence for the threshold setting equal to 5 times the global mean value of dissipation. The slopes in the appropriate regions of similar curves obtained for various thresholds are shown in the inset. The fairly strong dependence of $\mathcal{D}$ on the threshold means that the dissipation regions identified by higher threshold settings are less space filling (obviously!), and the surfaces bounding them are less convoluted. (Similar data for clouds have now been obtained by Lovejoy & Schertzer 1986.) It must be mentioned that the range of scales over which self-similarity can be observed shrinks as we approach lower thresholds, thus making the dimension measurements more uncertain for iso-surfaces containing most of the dissipation (i.e. low threshold); this accounts for the larger scatter there. We observe however that the mean trend is to intercept the $\mathcal{D}$-axis at a value of near 2.7, which compares very well with the value obtained in §4.1.

We saw earlier that the volume occupied by the dissipation structures is small,

equal to $(L_0/\eta)^{-3}$. Fractal sets that occupy a small fraction of the embedding volume are called thin fractals (to be contrasted with fat fractals in §5.5). Mathematically, thin fractals are defined as sets possessing zero volume; in practice, this volume is positive but small because of the finite inner cutoff scale. We are justified in thinking of the dissipative set as a thin fractal because its volume/area ratio is vanishingly small at sufficiently high Reynolds numbers. Needless to say, the turbulent/non-turbulent interface is a thin fractal also.

5. Miscellaneous aspects

In this section, we shall briefly discuss several aspects of turbulence that may usefully be associated with fractals.

5.1. *Fractal dimension of interfaces in the developing region*

If we consider as an example the flow past a circular cylinder, the interface between the vortical and non-vortical regions in the immediate vicinity of the cylinder is expected to be a classical surface (because of the more or less regular vortex shedding), and the dimension will then be 2. This expectation will hold even at high Reynolds numbers except that it will be confined more and more near the 'origin' of the flow. Far downstream, we have shown the dimension of the interface to be about 2.4, which means that in the developing regions the dimension goes up from 2 to about 2.4. We have not made extensive measurements in this region, but scattered measurements (by imaging methods in jets and line cuts in wakes) confirm this suggestion. Naturally, the range of scale similarity is shorter.

5.2. *Evolution of material lines in grid turbulence*

To motivate the discussion here, it is convenient to refer to a 'classical' fractal, like a Koch curve (Mandelbrot 1982, p. 42). Iterations of the type shown in figure 20 on the sides of an initially equilateral triangle will produce smaller and smaller scales; the results of three iterations are shown. The fractal dimension of the boundary of the asymptotic object – the so-called Koch curve – can easily be deduced from its definition to be $\log 4/\log 3$. The relevant point here is that the length of this Koch curve increases exponentially with the number of iterations.

Suppose now that we place a patch of ink in a field of turbulence. The effect of turbulence dynamics, which is to distort the ink patch in a manner visualized schematically by Corrsin (1959), can be thought of as being equivalent to a repetitively occurring iteration scheme (according to some complex algorithm), producing smaller and smaller scales at each iteration. If this is so, the perimeter of the ink blob should increase exponentially. Mundane experimental difficulties have so far prevented us from demonstrating this expectation. However, we have examined a somewhat similar question of the growth of material lines in a turbulence field behind a grid. We generated lines of fine hydrogen bubbles in the developed region behind a grid placed in a water channel, and measured their length as they propagate downstream. Their true lengths have been measured by obtaining two orthogonal projections simultaneously (placing a mirror at 45°); the procedure is explained in the Appendix. Corrsin & Karweit (1969) had earlier measured the increase in length of hydrogen-bubble lines, but their method was indirect and used an equation (Corrsin & Phillips 1961) relating the length to the number of cuts experienced by sampling planes making all angles with the axis of a statistically axisymmetric line

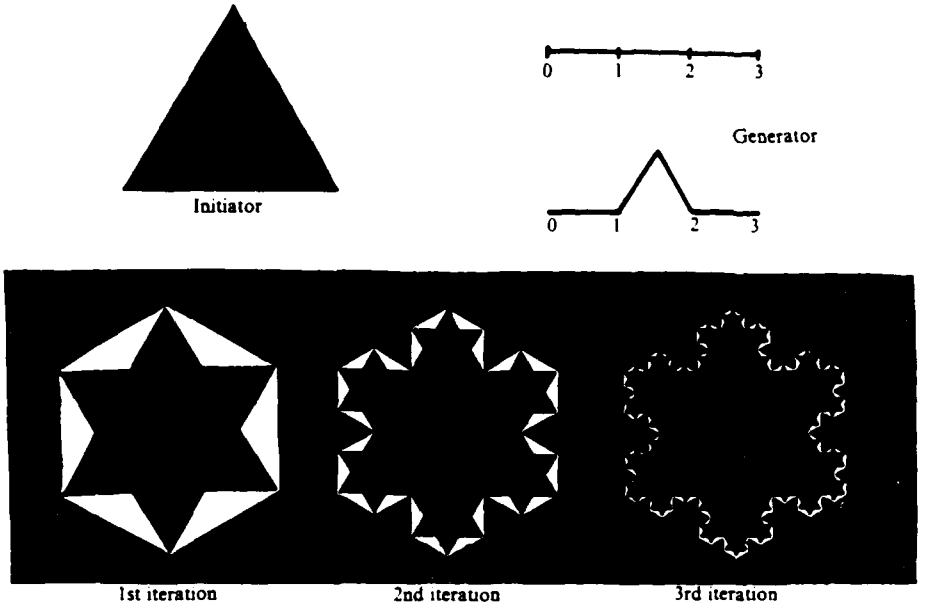

FIGURE 20. The iteration scheme for a triadic Koch island (Mandelbrot 1982) to be performed on an equilateral triangle (the so-called initiator): in each iteration the sides of the triangle are restructured according to the scheme shown on the upper right. The objects resulting from the first three iterations are shown.

element. It is gratifying to note that the two estimates agree where they overlap (figure 21). Clearly, except initially and in the last stages, the growth is indeed exponential. The initial behaviour is not expected to be exponential (Batchelor 1959), and the final levelling off is most likely due to the inadequate resolution of length measurement.

5.3. *Velocity signals*

Figure 22 shows the temperature signal taken on the centreline of a slightly heated axisymmetric jet (Sreenivasan *et al.* 1979). The most striking feature of this signal is the sharp ramp-like structures upon which the small structure is superimposed. Admittedly, this signal is carefully chosen to emphasize the point, but it is not statistically untypical. The temperature and velocity (especially normal component) signals in the boundary layer (even in the non-intermittent parts, see figure 11) show similar behaviour, although not as dramatic. The conclusion is that the fluctuations do not randomly jump about from one level to another, but gradually build up to a level from which they suddenly depart rather sharply. This behaviour is consistent with a power-law behaviour, which is symptomatic of self-similarity (and thus fractals). Following Lovejoy & Mandelbrot (1985), if we artificially construct a sum of randomly placed rectangular pulses whose width w obeys an inverse cumulative distribution $Pr(w > W) \propto W^{-1}$, and their height is $\pm w^{1/\alpha}$, the sign being randomly chosen, we can construct signals that show qualitative semblance to those shown in figure 22; here α is a characteristic exponent.

One useful comment relates to the expectation (Carter *et al.* 1986) that the turbulent signals themselves are fractals. This is obviously not a simple concept

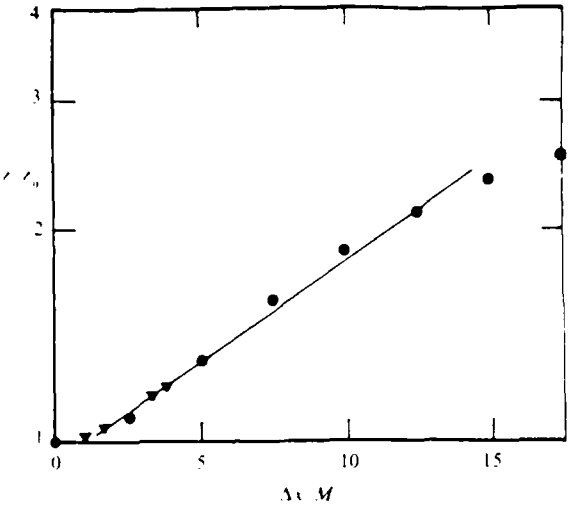

FIGURE 21. The average material line length as a function of the downstream distance from the grid. The circles are the data of Corrsin & Kistler (1969), the triangles the present. For both experiments the hydrogen bubble lines were generated approximately 18 mesh sizes downstream of the grid.

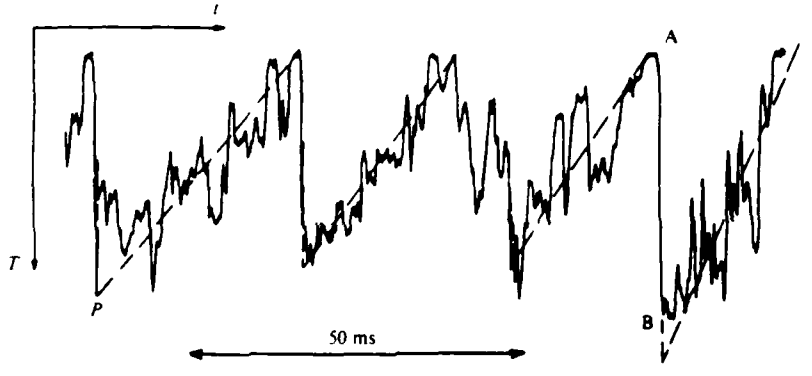

FIGURE 22. A temperature oscillogram in an axisymmetric heated jet, obtained in the region of maximum production of turbulent energy. Intermittency factor = 0.93. The sharp jumps associated with AB (for instance) have been a subject of much study.

because any dimension calculations depend strongly on the scales chosen for plotting the velocity signal. For example, if the signal is expanded to scales comparable with Kolmogorov scales, the signal looks very smooth leading to a dimension close to unity. The expectation is that the signals are self-affine fractals, by which we mean that there are more complex scaling behaviours (invariance under transformations of the type $S(x_1, x_2, \ldots, x_i) \rightarrow S(r_1 x_1, r_2 x_2, \ldots, r_i x_i)$, where all the r are different), and our work in this direction is continuing.

5.4. *Higher-order dimensions*

For the fractal description to be complete, one should be able at least to distinguish between two different fractals which may have the same dimension. Higher-order

dimensions are defined for this purpose (Hentschel & Procaccia 1983; Mandelbrot 1986), and are given by

$$D_q = \lim_{\epsilon \to 0} \left(\frac{1}{q-1} \frac{\log \Sigma\, p_i^q}{\log \epsilon} \right), \tag{5.1}$$

where p_i is the probability of finding points of the set in the ith box of length ϵ. For high values of q, D_q indicates the scaling behaviour of the more 'concentrated' regions; for low q, the character of the more 'sparse' regions is quantified. We have calculated these dimensions for several values of q, and these do display (as will be reported elsewhere) global characteristics similar to many strange sets discussed, for example, by Halsey *et al.* (1986).

5.5 *Fat fractals and turbulence*

At this stage, it is interesting to make some tentative connections between turbulence and what have been called fat fractals. In the literature, there is no apparent agreement on the precise meaning of fat fractals (contrast Umberger & Farmer 1985 with Grebogi *et al.* 1985), and this has to some extent dampened our own pursuit in this direction. At a basic level, however, the meaning of a fat-fractal set is that it occupies a finite volume (the box-counting algorithm applied to this set yields the dimension of the embedding space), but its boundary is a thin fractal. A possible example of a fat fractal is the set of all points in figure 3 where the smoke concentration is above a prescribed threshold; if the threshold properly sets apart the turbulent and non-turbulent regions, the 'skin' of the set is the interface whose dimension we have already measured in §2. Using a suitable integral of the measured intermittency factors in several standard turbulent flows, we have obtained rough estimates for the volume (say within the region $U < 0.99\, U_\infty$) occupied by the turbulent zone. The fraction of volume is about 0.5 for circular jets (with or without coflow), about 0.6 for plane wakes behind circular cylinders, and about 0.75 for the two-dimensional boundary layers in constant pressure. The somewhat larger value in the last case is consistent with the decreased intermittency near the wall.

The same argument can be extended to the set of points in space where a velocity component (see §3) is greater than a prescribed threshold u_1. The 'skin' of such a fat fractal is the u_1 iso-velocity surface.

6. Concluding remarks

We have shown that there are several facets of turbulent flows possessing fractal-like behaviour. We have measured fractal dimensions for some of them. The fractal dimension is only one measure of the properties of a fractal set, albeit the most important one, and higher-order dimensions (mentioned in §5.4) will help in specifying the fractal more completely.

It is necessary to remark that the present work falls far short of proving that 'turbulence is fractal' without need for qualifications and reservations. As discussed in various sections, the qualifications arise partly because of the limitations of the techniques employed; these can (and should) undoubtedly be bettered in the next generation of experiments. But it seems to us on the basis of the present measurements that turbulence (except perhaps for the dissipation field) genuinely loses its fractal-like behaviour when viewed on very long timescales. Thus, turbulence is perhaps a collection of a number of fractals each of which is slightly different. We think that this view can be reconciled roughly with the view of turbulence now in vogue as an ensemble of semi-organized motions.

While there is not much question that this work is interesting, its usefulness in better coming to grips with the hard issues of the 'turbulence problem' is less certain. In this context, we might interpret the 'turbulence problem' to mean the following: given the various fractal dimensions of several of its facets, how may one reconstruct the turbulent flow that generated them? We know of no serious enquiry of this sort being done in the context of turbulence, although some beginnings seem to have been made in a broader setting (Barnsley *et al.* 1986). Unless this issue is addressed, it is not clear how fractals will advance our understanding of turbulence dynamics. In fact, contrary arguments have often been advanced. A case in point is the description of the dissipation field. Its traditional description via either vortex lines, tubes or blobs, it is said, is physically more appealing than its new description as a thin fractal of dimension 2.7. Actually, this point of view is not quite correct because a satisfactory description via vortex elements that is in complete consonance with measurements has never been attained (Kuo & Corrsin 1972). At any rate, fractals may describe the geometry of turbulence (keep in mind all our disclaimers at different places!), but geometry and dynamics do not have a one-to-one correspondence.

It is appropriate to contrast the measurement difficulties in obtaining fractal dimensions in physical space with those in phase space. Even engineering flows (at low Reynolds numbers) possess attractors with fractal dimensions (Sreenivasan 1986), but their determination becomes extremely difficult and uncertain as the Reynolds number increases. In contrast, the determination of fractal dimensions in physical space becomes more definitive at higher Reynolds numbers.

As a final remark, we note that numerical work of the sort initiated by Chorin (1982), dedicated to questions on the dynamic evolution of vortex elements, will go some way in establishing possible connections between fractals and turbulence.

Our thanks must extend to David Aronstein who, as a summer student, laid the groundwork for part of the work reported in §2.1; to William van Altena for allowing us the use of his digitizer; to Paul Dimotakis for his permission to reproduce figure 4 and for his penetrating comments on an earlier draft; to Benoit Mandelbrot for commenting on the manuscript, and for providing the necessary impetus in the early stages of this work more than three years ago by refusing to believe KRS's negative conclusions of that time; to a number of colleagues (especially W. Van der Water, Celso Grebogi, Rick Jensen, and B. T. Chu) whose encouragement we received at various times; to Mark Lee and Paul Strykowski for carefully reading the manuscript and commenting on it; to Ted Lynn for cheerfully putting up with interruptions to his own boundary layer work; to Jim McMichael who encouraged its pursuit under an AFOSR grant. The last stages of this work were supported by the National Science Foundation.

Appendix: Growth of material lines in grid turbulence

A small water channel was used and lines of hydrogen bubbles were produced at $x/M = 18$ behind a turbulence-generating grid (solidity = 0.42, mesh size 3 mm). Downstream, a mirror was placed at an angle of 45° with the horizontal direction so that a camera placed directly over the flow could simultaneously take pictures of two (perpendicular) projections of the same hydrogen bubble line. By discretizing both lines and some simple trigonometric relations, it is then easy to determine the real length of the line in three dimensions.

Suppose we have two projections $\mathscr{L}_1$ and $\mathscr{L}_2$ (see figure 23) of a line in space, and

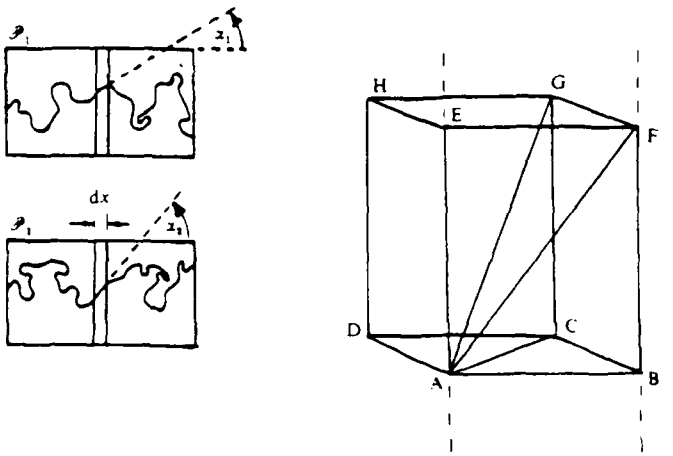

FIGURE 23. Orthogonal projections of a line segment and definition of angles and lines.

discretize them in equally spaced columns of width dx. From figure 23, the following relations can be inferred

$$dx = l_1 \cos\alpha_1 = l_2 \cos\alpha_2,$$

$$de\cos\beta = l_1,$$

$$de\sin\beta = l_2 \sin\alpha_2.$$

Thus,

$$\tan\beta = l_2 \sin\alpha_2 / l_1.$$

Finally, by expressing de as a function of dx and both angles, we get

$$de = \frac{dx}{\cos\alpha_1 \cos(\arctan(\cos\alpha_1 \sin\alpha_2/\cos\alpha_2))}$$

By measuring the angles α_1 and α_2 in each column of the discretized projections, and adding all the computed de, we get the real length (up to an accuracy of dx) of the line in three dimensions.

This was repeated for lines at several distances from the grid; resolution problems and fast diffusion of the hydrogen-bubble lines prevented us from analysing data at large distances.

REFERENCES

ANTONIA, R. A. & DASH, H. Q. 1977 *Phys. Fluids* **20**, 1050.

ANTONIA, R. A., PHAN-THIEN, N. & CHAMBERS, A. J. 1980 *J. Fluid Mech.* **100**, 193.

ANTONIA, R. A. & VAN ATTA, C. W. 1975 *J. Fluid Mech.* **67**, 273.

ANTONIA, R. A. & VAN ATTA, C. W. 1978 *J. Fluid Mech.* **84**, 561.

BARNSLEY, M. F., ERVIN, V., HARDIN, D. & LANCASTER, J. 1986 Solution of an inverse problem for fractals and other sets. *Proc. Natl. Acad. Sci. USA* **83**. (to appear)

BATCHELOR, G. K. 1959 *J. Fluid Mech.* **5**, 113.

BATCHELOR, G. K. & TOWNSEND, A. A. 1947 *Proc. R. Soc. Lond.* A **190**, 534.

BATCHELOR G K & TOWNSEND A A 1949 *Proc R Soc Lond* A **199** 239

CARTER P H CAWLEY R LICHT A L YORKE J A & MELNIK M S 1986 In *Dimensions and Entropies* (ed G Mayer-Kress) p 215 Springer

CHAMPAGNE F H 1978 *J Fluid Mech* **86** 67

CHORIN A 1982 *Commun Math Phys* **83** 517

CORRSIN S 1959 *J Geophy Res* **64** 2134

CORRSIN S & KARWEIT M 1969 *J Fluid Mech* **39** 87

CORRSIN S & KISTLER A L 1954 *NACA Tech Rep* 3133

CORRSIN S & PHILLIPS O M 1961 *J Soc Indust Appl Maths* **9** 395

DIMOTAKIS P LYE R C & PAPANTONIOU D Z 1981 In *15th Intl Symp Fluid Dyn Jachranka Poland*

FEIGENBAUM M J 1983 In *Nonlinear Dynamics and Turbulence* ed G I Barenblatt G Iooss & D D Joseph Pitman Advanced Publishing Program

FRIEHE C A VAN ATTA C W & GIBSON C H 1971 In *Proc of the AGARD Conf on Turbulent Shear Flows London AGARD Conf Proc* **93** 18-1

GIBSON C H & MANIELLO P 1972 In *Statistical Models and Turbulence* ed M Rosenblatt & C W Van Atta p 427 Springer

GIBSON C H STEGEN G R & WILLIAMS R B 1970 *J Fluid Mech* **41** 153

GREBOGI C McDONALD S W OTT E & YORKE J A 1985 *Phys Lett* **110A** 1

GURVICH A & YAGLOM M 1967 *Phys Fluids Suppl* **10** S59

HALSEY T C JENSEN M H KADANOFF L P PROCACCIA I & SHRAIMAN B I 1986 *Phys Rev* A**33** 1141

HENTSCHEL H G E & PROCACCIA I 1983 *Physica* **8D** 435

KIM H T KLINE S J & REYNOLDS W C 1971 *J Fluid Mech* **50** 133

KOLMOGOROV A N 1941 *C R Acad Sci URSS* **30** 299

KOLMOGOROV A N 1962 *J Fluid Mech* **13** 82

KOVASZNAY L S G KIBENS V & BLACKWELDER R F 1970 *J Fluid Mech* **41** 283

KUO A Y & CORRSIN S 1971 *J Fluid Mech* **50** 285

KUO A-Y & CORRSIN S 1972 *J Fluid Mech* **56** 477

LOVEJOY S 1982 *Science* **216** 185

LOVEJOY S & MANDELBROT B B 1985 *Tellus* **37A** 209

LOVEJOY S & SCHERTZER S 1986 Scale and dimension dependence in the detection and calibration of remotely sensed atmospheric phenomena In *2nd Conf on Satellite Meteorology and Remote Sensing Williamsburg Va* (submitted)

MANDELBROT B B 1974 *J Fluid Mech* **62** 331

MANDELBROT B B 1975 *J Fluid Mech* **72** 401

MANDELBROT B B 1982 *The Fractal Geometry of Nature* W H Freeman

MANDELBROT B B 1986 In *Dimensions and Entropies in Chaotic Systems* (ed G Mayer-Kress) p 19 Springer

McCONNELL S O 1976 The fine structure of velocity and temperature measured in the laboratory and the atmospheric marine boundary layer Ph D thesis University of California San Diego

MANWORTHY T 1986 *J Fluid Mech* **173** 95–114

OBUKHOV A M 1941 *C R Acad Sci URSS* **32** 22

OBUKHOV A M 1962 *J Fluid Mech* **13** 77

ONSAGER L 1945 *Phys Rev* **68** 286 (abstract only)

PARK J T 1976 Inertial subrange turbulence measurements in the marine boundary layer Ph D thesis University of California San Diego

POND S & STEWART R W 1965 *Izv Atmos Ocean Phys* **1** 530

RICHARDSON L F 1922 *Weather Prediction by Numerical Process* Cambridge University Press

SREENIVASAN K R 1986 In *Dimensions and Entropies in Chaotic Systems* (ed G Mayer-Kress) p 222 Springer

SREENIVASAN, K. R., ANTONIA, R. A. & BRITZ, D. 1979 *J. Fluid Mech.* **94**, 745.

SREENIVASAN, K. R., ANTONIA, R. A. & DANH, H. Q. 1977 *Phys. Fluids* **20**, 1238.

SREENIVASAN, K. R., PRABHU, A. & NARASIMHA, R. 1983 *J. Fluid Mech.* **137**, 251.

SUNYACH, M. & MATHIEU, J. 1969 *Intl J. Heat Mass Transfer* **12**, 1679.

TOWNSEND, A. A. 1956 *The Structure of Turbulent Shear Flows*. Cambridge University Press.

UMBERGER, D. & FARMER, J. D. 1985 *Phys. Rev. Lett.* **55**, 661.

VAN ATTA, C. W. & ANTONIA, R. A. 1980 *Phys. Fluids* **23**, 252.

WEIZSACKER, C. F. VON 1948 *Z. Phys.* **124**, 614.

WILLIAMS, R. M. & PAULSON, C. A. 1977 *J. Fluid Mech.* **83**, 547.

WYNGAARD, J. C. & TENNEKES, H. 1970 *Phys. Fluids* **13**, 1962.

YEH, T. T. 1971 Spectral transfer and higher-order correlations of velocity and temperature fluctuations in heated grid turbulence. Ph.D. thesis, University of California, San Diego.

Physica 23D (1986) 246–258
North-Holland, Amsterdam

TRANSITION INTERMITTENCY IN OPEN FLOWS, AND INTERMITTENCY ROUTES TO CHAOS

K.R. SREENIVASAN and R. RAMSHANKAR
Center for Applied Mechanics, Yale University, New Haven, CT 06520, USA

The intermittent transition to turbulence in open flows (mainly pipe flows) is examined in the context of intermittency routes to chaos. Preliminary conclusions are that some quantitative connections can be discerned, but that they are incomplete. In a similar manner, connections with phase transition and other critical phenomena are also imperfect. Some measurements which we hope will be helpful in developing alternative models describing the essentials of the phenomenon are described. Some difficulties are highlighted.

1. Introduction

This paper is a part of an overall effort related to the exploration of quantitative connections between chaos in dissipative dynamical systems on the one hand, and transition and turbulence in the so-called open flow systems on the other. Open flows by definition possess a preferred direction, and there is a flux of mass across its boundaries. At least in some circumstances this elementary feature of open flows renders the nature of flow instability convective, as opposed to being absolute, which is the case observed in closed flow systems. This can have profound consequences on the origin of turbulence in open flow systems, which may in turn render our task quite difficult.

It has been known for over a hundred years now [1] that transition to turbulence in pipe flows occurs intermittently. For example, the velocity measured on the centerline at a fixed axial location in the pipe is typically as shown in fig. 1. It is this intermittent transition to turbulence that is our concern here. With increase in Reynolds number, the fraction of time that the flow is in the turbulent state increases, until eventually the flow is continuously turbulent. One observes qualitatively similar intermittency in the advanced stages of transition to turbulence in boundary layers (fig. 2), and channel (i.e., plane Poiseuille) flows, to which also we shall make a brief reference here.

Equally well known now is that many low-dimensional dynamical systems approach a chaotic state in an intermittent fashion, qualitatively similar to the intermittent transition to turbulence just

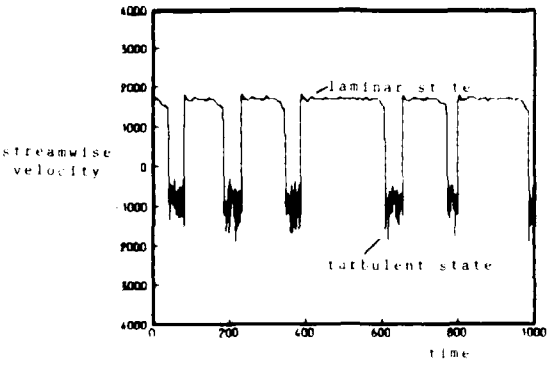

Fig. 1. The streamwise (or axial) velocity measured as a function of time on the centerline of a pipe flow. The measuring tool is a standard hot wire operated on a constant temperature mode. The signal oscillates apparently randomly between an essentially steady laminar state and a turbulent state. For a given axial position, a velocity trace obtained simultaneously at another radial position will show a coincident alternation between the two states, but the amplitude difference between the two states is a function of radial position. Both the ordinate and the abscissa are drawn to arbitrary scales.

0167-2789/86/$03.50 © Elsevier Science Publishers B.V.
(North-Holland Physics Publishing Division)

Fig. 2. Oscillograms of velocity fluctuations in the advanced stages of transition to turbulence in a constant pressure boundary layer. Time interval between markers is [illegible] s. Source: ref. [illegible]

discussed. Fig. 3 is an example. The Lorenz equations [2], the Logistic map [3], and the RCL oscillator [4] are some of the other simple examples. Pomeau and Manneville [5] identified three generic intermittency routes which they called Type I, Type II and Type III each differing from the other in terms of how the eigenvalues of the Floquet matrix, describing the return map linearized around a closed trajectory, cross the unit circle. Type I intermittency occurs when the linear stability of the limit cycle is lost by an eigenvalue of the Floquet matrix leaving the unit circle at +1, Type III when the crossing occurs at −1, and Type II when two complex conjugate eigenvalues simultaneously cross the unit circle. That these intermittent routes to chaos are relevant to fluid flow phenomena governed by partial differential equations has been demonstrated, for example, by Bergé et al. [6] and Dubois et al. [7] in the Rayleigh Benard experiment, and by Pomeau et al. [8] in the Belousov–Zhabotinsky reaction.

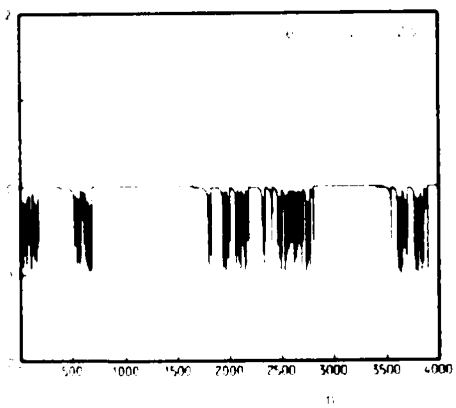

Fig. 3. Iterations of the one dimensional map [illegible] mod 1, [illegible] 0.00025 for this plot. The map is the result of a reduction [24] from the so-called Type II intermittency [5]. The relevant aspects of this type of intermittency route to chaos are mentioned in the text. The qualitative analogy with fig. 1 is quite obvious.

It may be argued on the basis of these interesting findings that intermittent transition in open flows may belong to some kind of universality class: Even though as already mentioned open flows are different in several non-trivial ways from the highly confined flows (see also [9]), it looks reasonable to ask whether there are any connections between the intermittency routes to chaos mentioned above and the intermittency routes to turbulence in open flows. As we shall see, the process involved in the latter are more complex; it is to their partial characterization that this paper is devoted.

2. The physical phenomenon

It is useful to recapitulate briefly the physical mechanism responsible for the temporal intermittency observed in fig. 1. Evidence from our own work – at least in pipes whose length is of the order of a few hundred diameters – as well as that of others (chiefly Wygnanski and Champagne, [10]), suggests that 'disturbances', whose developed state corresponds to the turbulent regions in the intermittent signal, arise locally (in radial, azimuthal as well as axial directions) in the entrance region of the pipe where the flow is laminar and steady, and is not fully developed (see fig. 4a). Once created in the boundary layer region, the disturbance quickly spreads over the entire cross-section of the pipe, and moves like an independent entity within the pipe; laminar regions are present both upstream and downstream of this entity – which now goes by the name 'slug'. (They have

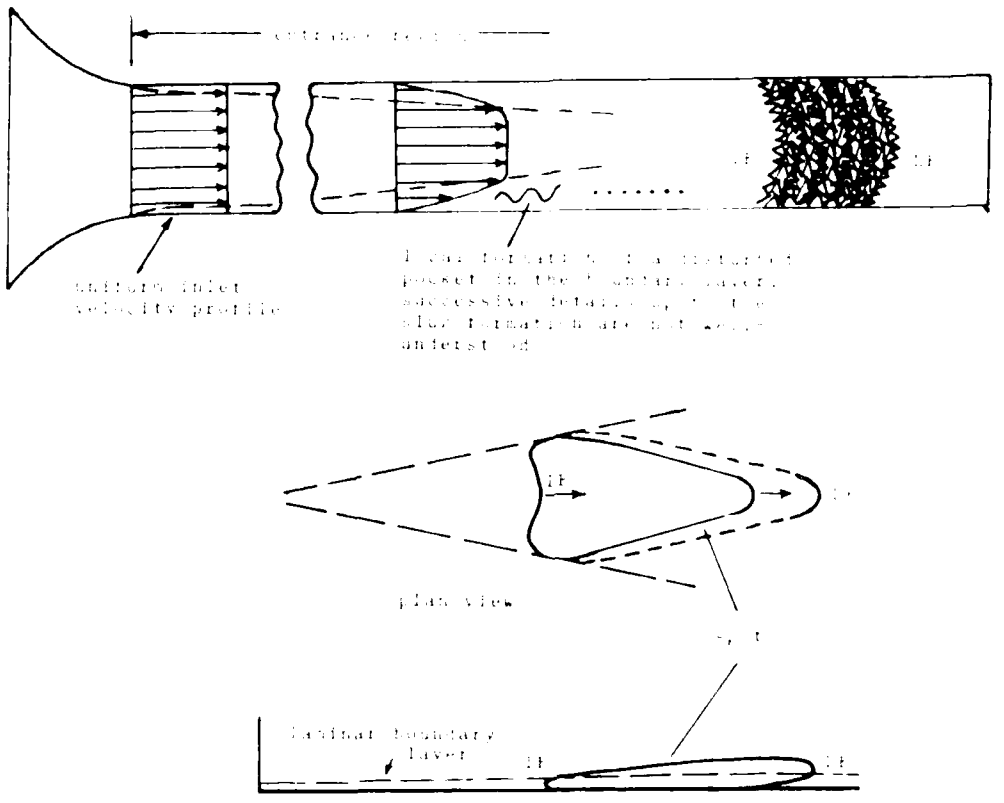

been called "flashes of turbulence" by Reynolds [1] and "plugs" by several workers, for example, Lindgren [11]). A probe fixed at any point in the flow alternately sees the procession of slugs with laminar regions interspersed between them; the output signal consists of intermittent excursions from the laminar to the turbulent state, followed by the return (in the Eulerian frame of reference) in some stochastic manner to the former. The physical reasons for the return to the laminar state are the following. Usually in most pipe flows, it is the pressure difference between the inlet and the exit that is held constant. A given pressure difference can support a larger mass flow when the flow is laminar than when it is turbulent. As the slugs form and grow, the increased friction due to the turbulent flow in them produces a reduction in mass flux, thus inhibiting the instabilities at the inlet. New slugs are most likely to be born only after the first slug completely passes out of the pipe. It is not hard to argue similarly that intermittent transition can occur also when the mass flux is fixed but momentum variations occur, but it is possible that the two types of intermittencies do not share the same detailed properties.

Corresponding to slugs in pipe flows, the transitional structure in boundary layers and in channel flows is the so-called turbulent spot (fig. 4b). Unlike the slugs which are constrained except in the axial direction, the boundary layer spots can grow in all directions. (There are some non-trivial differences between spots in channel flows and boundary layers, but these details are not relevant here.)

It turns out that the speed of propagation U_{tip} of the leading edge of the slug or a spot is different

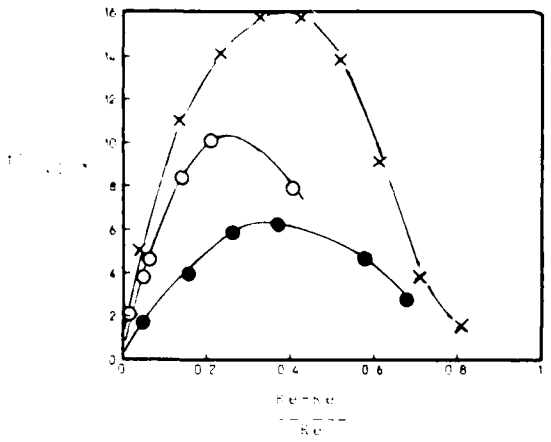

Fig. 5. Typical variation of the frequency of slugs as a function of Re for three streamwise locations. The topmost and the bottommost curves are from Wygnanski and Champagne [10] and pertain to (Re, x/D) of (21 × 10³, 220) and (19 × 10³, 95), respectively. The middle curve: Re = 30000 and x/D = 67 in present measurements. U_c is the so-called bulk velocity, or flow rate/cross sectional area of the pipe. Re = $U_c D/\nu$.

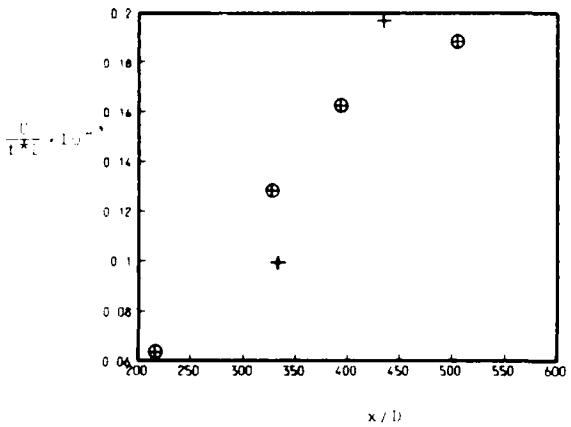

Fig. 6. Inverse of the peak slug frequency ($1/D$, U_c) as a function of the streamwise distance. Noting that all measurements were made at the exit of pipes of different lengths, the streamwise distance must really be understood to mean the pipe length. The circled points are from Wygnanski and Champagne [10].

from the trailing edge speed U_{te}. Clearly, slugs (or spots) grow with distance if $U_{le} > U_{te}$. In the following we concentrate on the slugs. If the slugs are generated at some mean frequency, and if more than one slug resides in the pipe at the same time, the leading edge of a slug could catch up with the trailing edge of the preceding one, resulting in merger and a consequent reduction in their passage frequency with axial distance. These two factors could then provide a plausible mechanism for the streamwise dependence, at any given Reynolds number, of all measured temporal quantities. The two most important parameters in the problem are thus the Reynolds number Re and the (normalized) axial distance x/D, where D is the pipe diameter. The frequency of the slugs, for example, depends on both of these parameters, as shown in fig. 5. A characteristic value of this frequency (say, the peak value) varies inversely with x/D (fig. 6), and seems to be independent of the Reynolds number. (Strictly, one must plot on the abscissa the quantity $x - x_0$, where x_0 is a virtual origin for the slugs; it is possible that the scatter in the plot partly originates from this source. However, since x is relatively large compared to x_0, this is believed to be of small consequence.)

Several points must be made explicit. Both in figs. 5 and 6 (and in the others to follow), x/D is really L/D, where L is the pipe length. That is, measurements were actually made at the exit of pipes of different lengths. Although we have retained the notation x/D above in conformity with previous practice, it is not clear to us that measurements made at different axial locations of the same long pipe will show the behaviors of figs. 5 and 6. A look at fig. 5 shows that the mean length of slugs ($\sim U_c/f$) is greater than the pipe length, suggesting that more than one fully developed slug is unlikely to reside in a pipe at any given instant of time. Thus, the probability of merger is quite small. The reason for the observed reduction in the characteristic frequency with pipe length (fig. 6) must then be attributed largely to the reduction of the formation frequency of slugs with pipe length. This makes sense if we remember that longer pipes mean longer slugs which take longer to pass the entire pipe. We conclude that detailed and careful measurements at several stations in

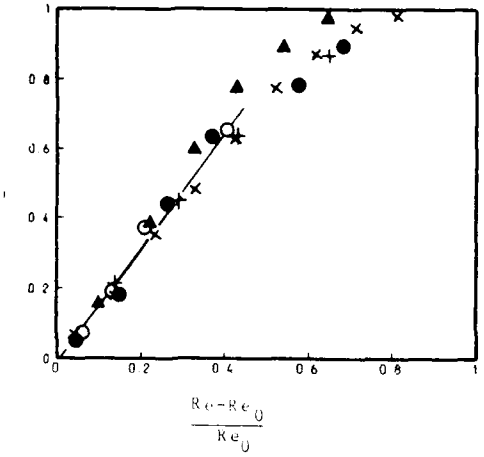

Fig. 7. Typical data on the intermittency factor γ as a function of $(Re - Re_0)/Re_0$. ▲: $L/D = 505$ [10]; ×: $L/D = 435$ (present). Other symbols as in fig. 5.

extremely long pipes (say, length to diameter ratio $> 10^4$) is overdue.

As one varies the flow Reynolds number, the appearance of the intermittent state is quite abrupt. The intermittency factor γ, defined as the fraction of time the flow is turbulent, appears to vary approximately linearly with the Reynolds number. By a backward extrapolation to zero of the measured intermittency factor, one can define a unique value of the onset Reynolds number Re_0. Fig. 7 shows that γ is a unique linear function of $Re - Re_0$ in a certain non-trivial neighborhood of Re_0; x/D or L/D is thus an inconsequential parameter for this quantity.

A reasonable goal now is to describe in phase space the main features of these processes. Returning now to fig. 1, it appears plausible to think that the steady laminar state is essentially zero-dimensional – that is, a proper orthogonal decomposition of the temporal signal contains no time dependent function. (Unfortunately, estimates of statistical properties such as the entropy and dimension from the velocity signal obtained entirely in the laminar state, for example just before the onset of intermittency, is dominated by the high-dimensional, low-amplitude noise overriding the laminar motion. The noise here does not arise merely from instrumentation or other 'purely random' fluctuations in the background; as mentioned elsewhere [9], the background 'noise' in most open flow systems is usually dominated by large-scale pressure fluctuations which are far from being structureless.) From this fixed point, the motion escapes to an attractor representing the turbulent state, and gets reinjected near the fixed point at apparently random intervals. Two relevant questions can be asked: 1) Can one quantitatively capture by a low-dimensional map the essential dynamics of this intermittent motion from the fixed point? 2) What are the characteristics of the chaotic attractor? Answers to these questions are attempted below.

3. The route to chaos

Fig. 8 shows a close-up of the vicinity of the velocity signal near the leading edge of a typical slug. Corresponding to the laminar as well as this interface regions, we have constructed by discretization a return map of u_{n+1} vs u_n (fig. 9). A close look in the vicinity of the fixed point shows that the map is much like that from which fig. 3 was constructed. Secondly, the slope of the return map near the fixed point is close to but greater than unity. This shows that the fixed point is unstable once the onset of intermittency occurs; the laminar and interface regions are thus merely a reflection of the duration spent in the narrow channel in the vicinity of the fixed point. There is some hope, then, that the dynamics of the leading edge interface can be described (approximately) by a one dimensional map of some kind, for example that used in fig. 3 (for small x_n). This observation lends some emphasis to our original question of possible connections to the generic intermittency routes to chaos. We must right away note a simple fact: Pipe flows strictly belong to neither type of intermittency mentioned in section 1, an obvious reason being that, unlike in the Pomeau–Manneville formulation, intermittent transition in open flows (see especially fig. 2) occurs from a *steady state* and not from a limit cycle. (For a

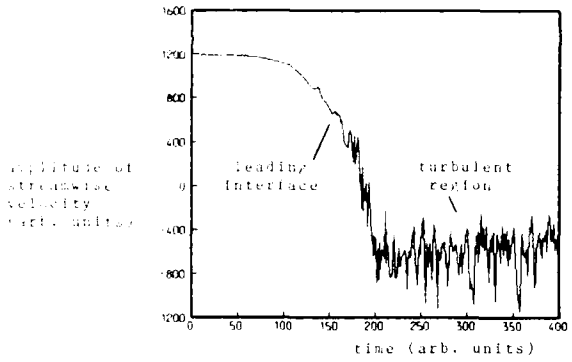

Fig. 8. A close-up of the velocity signal near the leading edge of a typical slug.

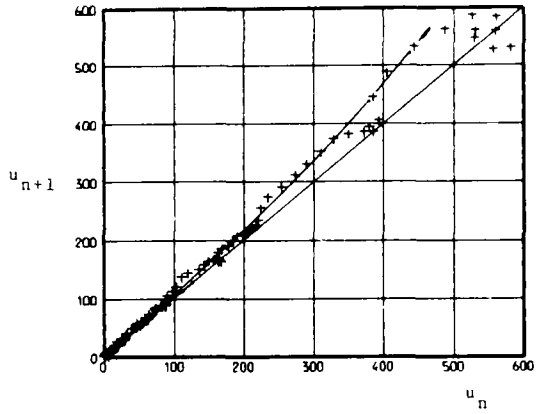

Fig. 9. The return map of u_{n+1} vs u_n for the interface region shown in fig. 8, obtained by the discretization of the signal. The origin is the fixed point representing the laminar state.

brief reexamination of this point see section 6.) This may be interpreted to mean that Poincaré sections of the Pomeau–Manneville intermittencies have a direct bearing on pipe flow transition, but it will unfold that this is not the entire story. As we shall show soon, this is related to the non-uniform manner in which the motion in phase space gets reinjected to the vicinity of the unstable fixed point. (We take the view that to label reinjection by 'relaminarization' – as is often done – is to miss the point altogether. While in the Eulerian frame of reference one sees an alternation between laminar and turbulent states, this does not imply relaminarization of fluid that was once turbulent. As must be clear from section 2, in the Lagrangian frame of reference, there is no relaminarization of fluid entrained by a slug: one is talking merely about the slug/no-slug situation.)

All three types of intermittencies mentioned in section 1 make definite predictions for certain statistical quantities of the intermittent signals, against which the outcomes of experiments can be tested. Apart from the nature of the return maps themselves, the important predictions concern the probability distribution for the duration of the laminar regions; from this distribution one can in particular calculate their mean duration as a function of the departure from the critical value of the control parameter, $\mathrm{Re} - \mathrm{Re}_0$ here. At any rate, it is useful to measure these quantities in the hope that they will help us build alternative models.

Fig. 10 shows a plot of the average length L_l of the laminar regions as a function of $\mathrm{Re} - \mathrm{Re}_0$. The data for several experimental conditions all tend to show that $L_l \sim (\mathrm{Re} - \mathrm{Re}_0)^{-1}$. This behavior is common to both Type II and Type III intermittencies. The measured inverse cumulative distributions for the length of the laminar intervals (fig. 11) follows the expression

$$P(l > l_0) \sim \left[e/\exp(4el_0 - 1)\right]^{1/2}, \qquad (1)$$

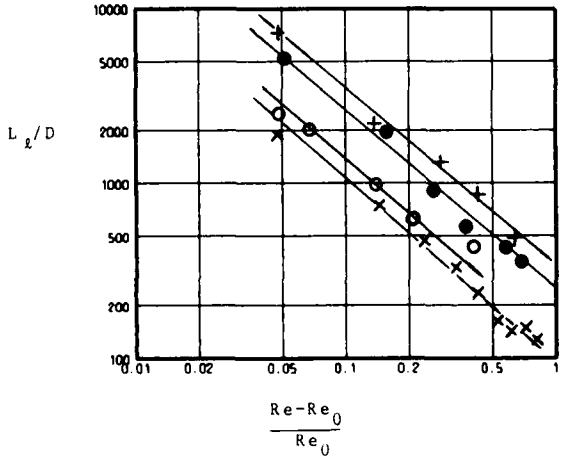

Fig. 10. The mean length of the laminar regions in the measured velocity signals, plotted as a function of the distance from the critical Reynolds number. Lines correspond to the -1 power predicted for Type II and Type III intermittencies. ○, $L/D = 435$, $\mathrm{Re}_0 = 4480$. Other symbols as in fig. 5.

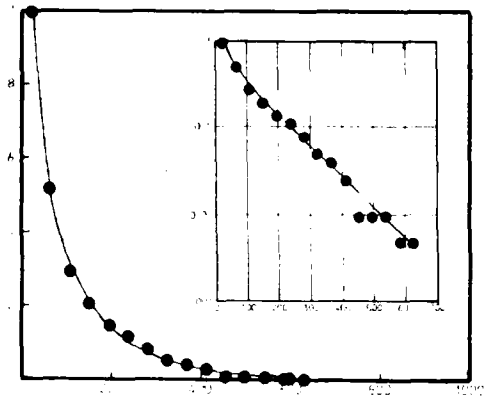

Fig. 11. The cumulative distribution of the laminar intervals. Re = 4725, $\gamma = 0.379$, $e = 0.004$. Note that, except for a small l, the behaviour of P is very nearly exponential.

which is a result known to hold for Type III intermittency. Here, the parameter e should be identified as being proportional to $(\mathrm{Re} - \mathrm{Re}_0)/\mathrm{Re}_0$. The inset, which is an expanded log linear plot shows that the fit is very good even towards the tail region.

In spite of these concurrences, one cannot identify the pipe flow with Type III intermittency for two reasons. Firstly, the hallmark of Type III intermittency is the subcritical period-doubling [7], with the primary effect of nonlinearity being a dramatic enhancement of the subharmonic component just before the flip to the chaotic state occurs. The system, instead of subsequently following the period doubling route to chaos, somehow decides to go the intermittency route. As already mentioned, the nonturbulent state is not a limit cycle. Secondly, and more importantly, in arriving at expression (1), the assumption has been made that whenever reinjection occurs from the chaotic attractor to the vicinity of the limit cycle, the distance from the fixed point of a Poincaré map where this reinjection occurs is uniformly distributed [12]. We have measured (see Appendix) the distribution of the reinjection distance from the unstable fixed point (in this case), and obtained the result that it is approximately an inverse power law (fig. 12) over a certain range. The

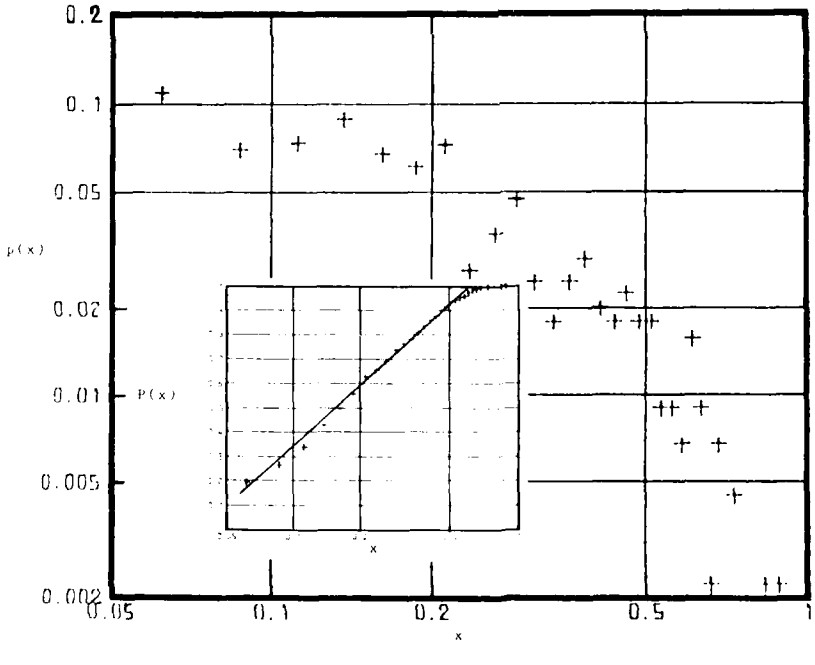

Fig. 12. The measured reinjection probability. For a discussion of how this was obtained, see Appendix. The inset which is a log linear plot shows that the cumulative probability for the reinjection distance increases logarithmically with the reinjection distance from the fixed point (laminar state).

log linear plot of the cumulative distribution shown in the inset is a less scattered comparison because of the averaging involved in the integrating process.

This nonlinearity associated with the reinjection probability adds an additional 'dimension' to the problem, and should be explicitly incorporated in any model of the problem. Using this empirically determined reinjection probability, it is easily shown that Type II intermittency also leads precisely to the expression (1) for the cumulative distribution of laminar lengths. This result, together with figs. 9 and 10, might be taken to indicate a closer connection with Type II. It is also worth recalling that the one-dimensional map from which fig. 3 was constructed was obtained after some simplification from Type II. Perhaps the connection is even closer if we realize that a suitably obtained Poincaré section of Type II intermittency is qualitatively similar to the measured velocity signals here (figs. 1 and 2).

Before closing this section, we note that, independent of the agreement between measurement in fig. 10 and the intermittency models, the almost exponential variation of the data (fig. 11) is pointing to some simple mechanism of slug generation (e.g., a Poisson process).

4. The chaotic state

From traces of the type shown in fig. 1, we have constructed a composite velocity signal by stringing together all the turbulent patches; that is, by removing the laminar as well as the parts corresponding to the interface between the two states. For this composite signal, we have calculated the correlation dimension using the Grassberger–Procaccia [13] algorithm. Calculations show the scaling exponent of the correlation function is about 18. To the extent that one can trust calculations resulting in such large numbers and their interpretation, the dimension of the attractor is about 18. This relatively high dimension does not come as a surprise to us, because it is consistent with our experience with most open flow systems [14]; for all Reynolds numbers except those very close to the onset of turbulence, low-dimensional attractors do not seem to exist. (The number of data points used in these calculations is not as large as is usually believed to be necessary for calculating dimensions of the order 18 reliably, but far fewer (~ 3000). We have however calculated the dimension from several independent patches of the composite signal each of which is about 3000 points long, and performed ensemble averaging over these segments. We have found on other occasions – to be described elsewhere – that this procedure gives stable numbers. In any case, the issue here is not whether the dimension is 18.1 or 18.2, but whether it is 2, 6 or 18. The safest conclusion to draw from here is that the dimension is *not* small, of the order of 5, say.)

We conclude that pipe flow transition exhibits partial similarities with known intermittency routes to chaos – especially with Type II – but it does not strictly belong to any of them, at least because of the preferential nonlinearity in the reinjection mechanism. Although the dynamics appears low-dimensional on the interface region, it is clearly not so elsewhere. For this reason, it is helpful to examine the problem from another point of view.

5. Analogy with phase transitions

As we already mentioned in section 2, the change of state from a laminar to a turbulent one occurs in pipe flows essentially discontinuously at an onset Reynolds number Re_0, and at any instant at a spatial location it is easy to say to which of the two states the fluid flow belongs. Above this onset Reynolds number the laminar and turbulent phases can be thought of as coexisting, with the fraction of time the flow is turbulent increasing monotonically with the Reynolds number; in the intermittent regime all the mean flow properties (such as the pressure drop in the pipe) change continuously from the laminar values to the fully turbulent values. Following the lead of Dhawan and

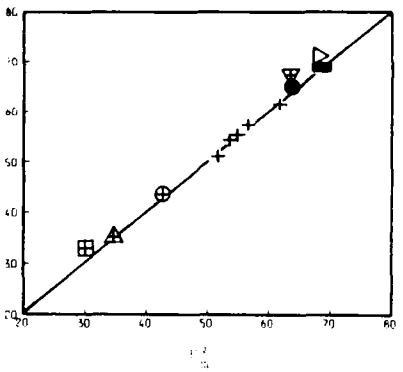

Fig. 13. The measured time-mean square of the streamwise velocity compared with the sum of γ times the turbulent value (for that Reynolds number) and $(1-\gamma)$ times the laminar value. ⊞, Re = 4214, γ = 0.87; ▲, 4006, 0.72; ⊕, 4110, 0.54; ▽, 4774, 0.32; ●, 4882, 0.43; ▶, 4451, 0.05; ■, 4559, 0.16. For calibration purposes, completely laminar values (+) have also been plotted. We suspect that this agreement will not hold so well if the critical Reynolds number is large.

Narasimha [15] in boundary layers, we show in fig. 13 that, at any given Reynolds number during the intermittent transition, one can express to a good approximation some measured time average flow properties (such as the dynamic head on the pipe axis) as a linear combination of the laminar and fully turbulent properties appropriate to that Reynolds number. Noting that the intermittency factor itself appears to vary linearly with $\mathrm{Re} - \mathrm{Re}_0$ (see fig. 6), it is clear that flow properties in the vicinity of Re_0 can be expressed as linear combination of the laminar and turbulent ones, with γ replaced by $(1 - \mathrm{Re}/\mathrm{Re}_0)$.

The above description tempts us to explore possible connections with phase transitions. Since all phase transitions can be described in similar terms, the crucial step is to identify an order parameter, which is such that it takes on different values in coexisting phases, and jumps discontinuously in the course of the phase transition; the magnitude of the jump is zero at the critical point. As an example, the order parameter in the gas liquid phase transition is the difference between the actual density and the density at the critical point.

While many details are not clear and the analogy has not yet been pushed to its logical conclusion, one can identify an order parameter with the (normalized) difference speed ΔU between U_{le}, the leading edge speed, and U_{te}, the trailing edge speed, of the slug or the spot. Fig. 14 shows that in all flows in which ΔU has been measured to-date, the relationship

$$\Delta U \approx \alpha(\mathrm{Re} - \mathrm{Re}_c)^{1/2} \qquad (2)$$

holds quite well in a nontrivial neighbourhood of Re_c, where Re_c is a 'critical' Reynolds number akin to the critical temperature in the gas-liquid phase transition. It is surprising that this should be so, considering that the four flows studied in fig. 14 are quite different in detail; they range, on one extreme, from spots which grow in all directions to slugs on the other extreme which are constrained in all but the axial direction.* We also find it very interesting that the 'critical exponent' must take on the classical value of 0.5.

For the boundary layer, $\mathrm{Re}_c = 200$ according to fig. 14. This suggests that attempts to create sustained spots below Re_c must necessarily fail because, interpreted literally, fig. 14 suggests that the trailing edge should then travel faster than the leading edge. If this does occur we would have on our hand a case of relaminarization but, in reality, spot-like structures below Re_c will break up and decay. To our knowledge, detailed tests relating to this issue have not been made. In the literature on spots, we have found no documentation of spots

*For all cases but that involving boundary layer spots, a linear fit between ΔU and $(\mathrm{Re} - \mathrm{Re}_c)$ is not unthinkable, but the fit (2) is a bit better when $\mathrm{Re} - \mathrm{Re}_c$ is not too large. Also, we believe that the departure from (2) in fig. 14d, for example, is largely due to the fact that the flows were generally set up in pipes which were not long enough for the fully developed parabolic state to emerge. This means that the leading edge speed of the slug, which is essentially equal to the largest speed anywhere in the flow field, cannot be as high as it would be if one had a parabolic distribution of velocity ahead of the slug. Data from Alavyoon et al. [31] in plane Poiseuille flow became available too late for inclusion here, but they follow the equation $\Delta U^2 = 0.727 \times 10^{-4}(\mathrm{Re} - 800)$; the fit appears as unambiguous as for the boundary layer data of fig. 14(a).

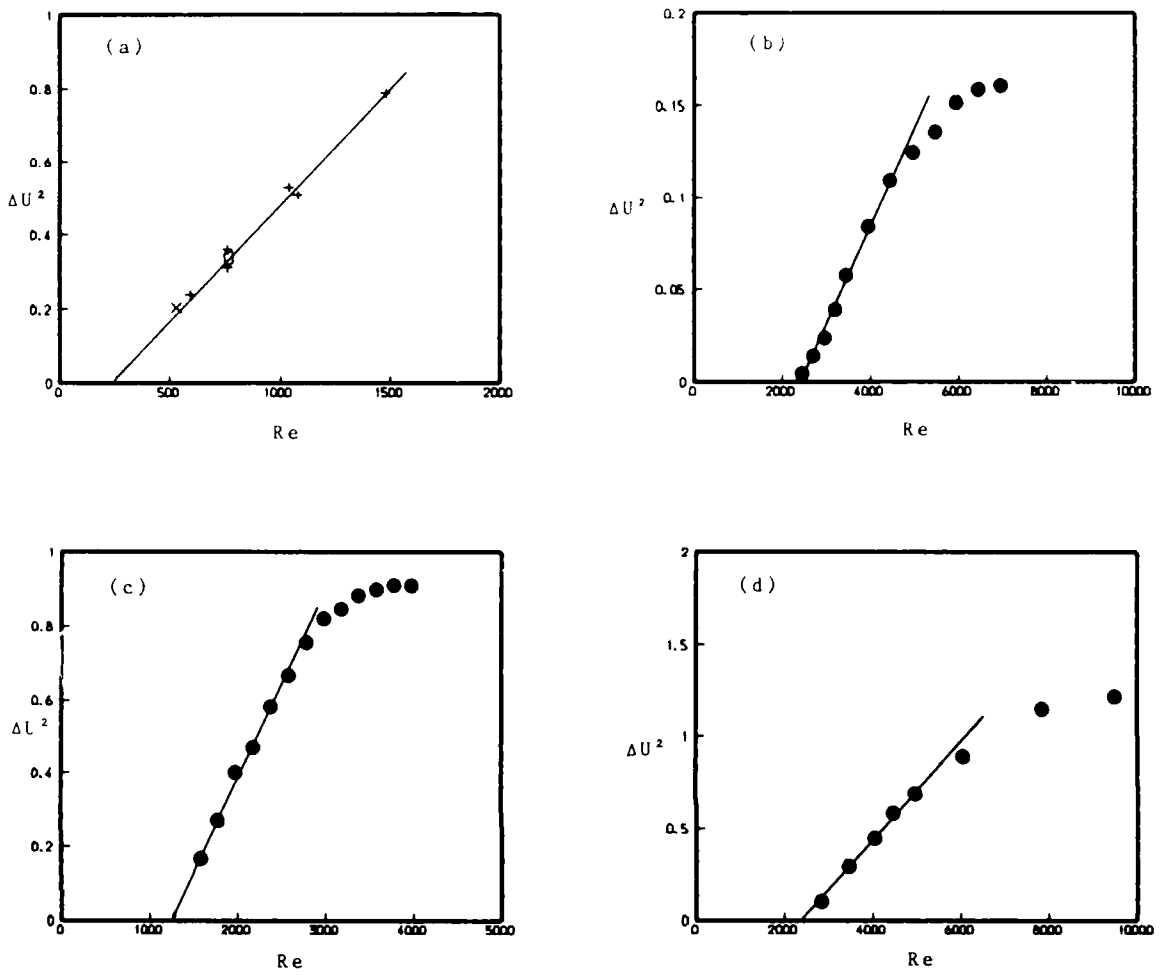

Fig. 14. The difference between the propagation speeds of the leading and trailing edges of the slug as a function of the flow Reynolds number. (a) Spots in a two-dimensional boundary layer: Re is based on the freestream speed U_∞ and the displacement thickness. The normalizing speed for ΔU is U_∞. ×, Cantwell et al. [24]; +, Wygnanski [18]; ○, Zilberman (see Wygnanski [18]). Since Reynolds number (no matter how defined) increases with streamwise distance in boundary layers those used here are the Reynolds numbers at which spots were created. ——, 3.65×10^{-4} (Re − 200). (b) Spots on an axisymmetric body. When the spots grow to sufficient sizes, they wrap around the body. Data from Rao [25]. – – –, 5.6×10^{-5} (Re − 2500); Reynolds numbers are based on the boundary layer thickness. (c) Transitional structure in a rectangular pipe, aspect ratio 4.0; Reynolds numbers are based on the hydraulic radius. Data from Sherlin [26]. – · –, 5.0×10^{-4} (Re − 1240); (d) Slugs in circular pipes. Data from one experimental run, present. – – –, 2.56×10^{-4} (Re − 2350). Similar data have been obtained by Lindgren [27], Pantulu [28], Coles [29] and Wygnanski & Champagne [10].

generated below Re_c, the lowest such Reynolds number being around 210 due to Elder [16]. Although Elder did not make specific claims that spot generation attempts below Re_c were unsuccessful, the absence of any documentation contrary to our conclusion must be deemed to be significant. Similarly for pipes attempts to generate slugs below a Reynolds number of about 2400 are known to be unsuccessful.

We draw attention to two minor matters. First, the constant α in each of the four flows is of the same order of magnitude when proper account is taken of the differences in the definitions of the Reynolds number and different normalizing speeds

used in ΔU. Second, the rate of spread of the spanwise extent of the spots (the 'width') in constant pressure boundary layers is only a weakly increasing function of the Reynolds number. (It goes up by about 20% in a Reynolds number differing by a factor of about 3 in the experiments of Schubauer and Klebanoff [17], and by about half as much in a similar Reynolds number range in Wygnanski's [18] experiments.) Not enough data exist on the Reynolds number dependence of the growth of the spot height normal to the plane.

We should remark on the likelihood that the expression (2) may signify nothing more than a characteristic shared by propagation fronts in diverse circumstances, where a power-law usually describes the relation between the propagation speed of the front and the distance from the critical value of the control parameter. Some examples are the speed of propagation of the turbulence front produced by an oscillating grid in a tank of still water [32], the speed with which the upper (lower) surface vortex propagates into the lower (upper) vortex in a short aspect ratio (= 1.25) Taylor–Couette apparatus housing only two vortex rolls [19, 20], the propagation speed of solidification fronts in dendritic growths [21] the speed of the so-called 'directed lattice animals' in percolation theory [22], etc. Even this is an interesting enough conclusion.

6. Discussion and conclusions

The behaviors described so far are not strictly applicable for large $\mathrm{Re} - \mathrm{Re}_0$. For example, as the intermittency factor approaches unity, increasingly larger departures occur between expression (1) and the measured probability distribution of laminar regions; similarly (2) is violated for large values of $\mathrm{Re} - \mathrm{Re}_c$. This in itself is no serious detraction, since all 'universality theories' aim to explain only the region immediately after the onset of intermittency. We want to emphasize one further point. For certain combinations of experimental conditions which are poorly understood,

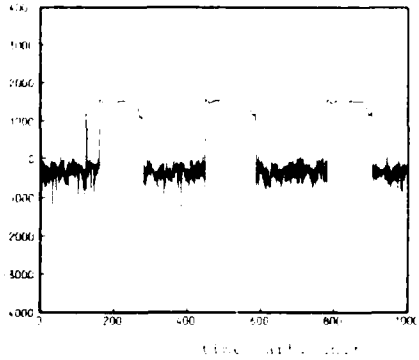

Fig. 15. A velocity signal measured on the pipe centerline for conditions different from those of fig. 1. Unfortunately, the differences are not documentable in detail.

the alternation between the two states occurs regularly (fig. 15); the distribution of the laminar intervals in this case obviously peaks sharply around some value. This last fact serves as a reminder of the complexity of the process involved. Further, even restricting to what one might call the generic features of this transition process, it should be clear from section 4 that the dynamics does not entirely reside on a low-dimensional attractor.

Nevertheless, several common features exist between pipe flow transition and purely mathematical models like one-dimensional maps; further work is needed to be completely certain of this, as well as about possible analogies to physical processes like phase transitions. In any case, a more realistic model than the existing ones need to be invented to duplicate the observed facts in detail. We think that a suitable modification of the Rössler equations [23] may serve this end to some extent.

One of our contentions has been that transition in the examples studied here occurs intermittently between a *steady state* and a chaotic one. In particular, the laminar regions do not correspond to any periodic states, as is especially clear from fig. 2. It may, however, be of interest to recall that in the experiments of Schubauer and Klebanoff [17] the first-born spots are generally accompanied by an undulating (*not* steady) laminar state, but

once a newly born spot sweeps by the fluid, it produces a 'calming effect' that subsequently eliminates the undulations in the laminar state.

Finally, we must remark that the standing of the conclusions of this paper is only preliminary unless substantiated by measurements in extremely long pipes (length to diameter ratios well in excess of 10^4) in which the mass flux (instead of the usual pressure drop) is held constant. We believe that such an experimental effort is worthwhile. Pipe flows are fascinating also because they provide counter examples to the commonly observed bifurcations, as well to many beliefs usually held, in dynamical systems. For example, 'noise-free' pipe flows are strictly stable at all Reynolds numbers, which clearly requires the presence of *sustained* noise for initiating transition; it is therefore not clear to what extent the intermittency statistics reflect the statistical properties of the noise itself. In contrast to transition to turbulence in convection problems (for example), much less appears to be known about the type of 'metastable' transition observed in pipe flows. The purpose of this paper is more than adequately served if it brings these problems to the attention of a wider audience than that customarily involved in them.

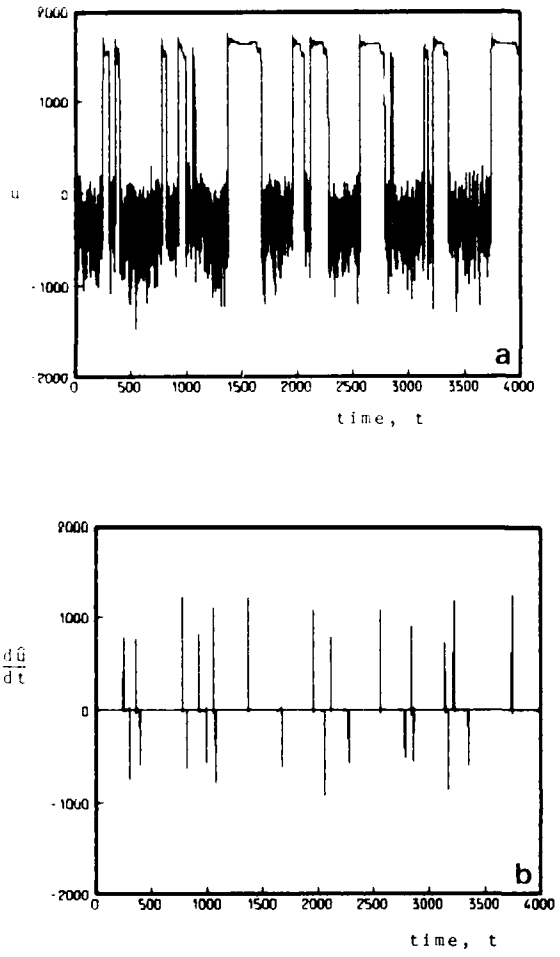

Fig. 16. The upper trace (a) is a velocity trace which, when modified as described in the text and differentiated, yields the lower trace (b).

Acknowledgements

We are indebted to Dr. G. Meyer-Kress for refusing to believe the earlier interpretation given by one of us (KRS). Our thanks are due also to Professors B.-T. Chu, J.F. de la Mora and R.V. Jensen for helpful comments, and Dr. J. McMichael and AFOSR for the financial support. Some preliminary work was done by Julia Usher during the summer of 1983.

Appendix

Transition from the turbulent to laminar state is very sharp as can be seen in fig. 1. (It is in fact sharper than the transition from the laminar to turbulent one.) It thus seems reasonable to associate reinjection with sharp velocity gradients. Hence a numerical differentiation was performed on the time trace, after substituting the turbulent state by a constant, say, 500 on the ordinate of fig. 16a. This modified signal u, when differentiated, looks as in fig. 16b. The reinjection point is then identified as the distance from the reference laminar state where the largest velocity gradient occurs. (Other plausible definitions yield much the same result.) Fig. 12 was obtained after rescaling the distance.

References

[1] O. Reynolds, An experimental investigation of the circumstances which determine whether the motion of water shall be direct or sinuous, and of the law of resistance in parallel channels, Phil. Trans. Roy. Soc. 44 (1883) 51.

[2] P. Manneville and Y. Pomeau, Different ways to turbulence in dissipative dynamical systems, Physica 1D (1980) 219.

[3] I.E. Hirsch, B.A. Hubermann and D.J. Scalapino, Theory of intermittency, Phys. Rev. A25 (1982) 519.

[4] C. Jeffries and J. Perez, Observation of a Pomeau–Manneville intermittent route to chaos in nonlinear oscillator, Phys. Rev. A26 (1982) 2117.

[5] Y. Pomeau and P. Manneville, Intermittent transition to turbulence in dissipative dynamical systems, Comm. Math. Phys. 74 (1980) 189.

[6] P. Bergé, M. Dubois, P. Manneville and Y. Pomeau, Intermittency in Rayleigh–Benard convection, J. de Physique (lettres) 41 (1980) L-341.

[7] M. Dubois, M.A. Rubio and P. Bergé, Experimental evidence of intermittencies associated with a subharmonic bifurcation, Phys. Rev. Lett. 51 (1980) 1446.

[8] Y. Pomeau, J.C. Roux, A. Rossi, S. Bachelart and C. Vidal, Intermittent behavior in the Belousov–Zhabotinsky reaction, J. de Physique (lettres), 42 (1981) L-271.

[9] K.R. Sreenivasan, Transition and turbulence in fluid flows, and low-dimensional chaos, in: Frontiers of Fluid Mechanics, S.H. Davis and J.L. Lumley, eds. (Springer, Berlin, 1985), p. 41.

[10] I. Wygnanski and F.H. Champagne, On transition in a pipe, Part I: The origin of puffs and slugs, and the flow in a turbulent slug, J. Fluid Mech. 59 (1973) 281.

[11] D.J. Tritton, Physical Fluid Dynamics (Van Nostrand, New York, 1977).

[12] H.G. Schuster, Deterministic Chaos, Physik-Verlag, (1984).

[13] P. Grassberger and I. Procaccia, Characterization of strange attractors, Phys. Rev. Lett. 50 (1983) 346.

[14] K.R. Sreenivasan, Chaos in open flow systems, in: Dimensions and Entropies in Chaotic Systems, G. Mayer-Kress, ed. (Springer, Berlin, 1986) p. 222.

[15] S. Dhawan and R. Narasimha, Some properties of boundary layer flow during the transition from laminar to turbulent motion, J. Fluid Mech. 3 (1958) 418.

[16] J.W. Elder, An experimental investigation of turbulent spots and breakdown to turbulence, J. Fluid Mech. 9 (1960) 235.

[17] G.B. Schubauer and P.S. Klebanoff, Contributions on the mechanics of boundary layer transition, NACA Tech. Note 3489 (1955).

[18] I. Wygnanski, The effects of Reynolds number and pressure gradient on the transitional spot in a laminar boundary layer, in: The Role of Coherent Structures in Modelling Turbulence and Mixing, Lecture Notes in Physics, 136 (Springer, Berlin, 1980) p. 304.

[19] M. Lucke, M. Mihelcic, K. Wingerath and G. Pfister, Flow in small annulus between concentric cylinders, J. Fluid Mech. 140 (1984) 343.

[20] A. Aitta, G. Ahlers and D.S. Cannell, Tricritical phenomena in rotating Couette–Taylor flow, Phys. Rev. Lett. 54 (1985) 673.

[21] J.S. Langer, Instabilities and pattern formation in crystal growth, Rev. of Mod. Phys. 52 (1980) 1.

[22] J.P. Nadal, B. Derrida and J. Vannimenus, Directed lattice animals in two dimensions: numerical and exact results, J. de Physique 43 (1982) 1561.

[23] O. Rössler, C. Kahlert and B. Uehleke, Tori and chaos in a simple e^1 system, in: Nonlinear Dynamics of Transcritical Flows, H.L. Jordan, H. Oertel and K. Robert, eds. (Springer, Berlin, 1985), p. 51.

[24] B. Cantwell, D. Coles and P. Dimotakis, Structure and entrainment in the plane of symmetry of a turbulent spot, J. Fluid Mech. 87 (1978) 641.

[25] G.N.V. Rao, Mechanics of transition in an axisymmetric laminar boundary layer on a circular cylinder, Z. f. Angew. Math. & Phys. 25 (1974) 63.

[26] G.C. Sherlin, Behavior of isolated disturbances superimposed on laminar flow in a rectangular pipe, J. Research of the National Bureau of Standards 64A (1960) 281.

[27] E.R. Lindgren, Propagation velocity of turbulent slugs and streaks in transition pipe flow, Phys. Fluids 12 (1969) 418.

[28] P.V. Pantulu, Studies on the transition from laminar to turbulent flow in a pipe, M. Sc. Thesis, Dept. Aero. Engg. Ind. Inst. Sci., Bangalore (1962).

[29] D. Coles, Interfaces and intermittency in turbulent shear flow, in: Mécanique de la Turbulence, A. Favre, ed., Paris: C.N.R.S. (1962) p. 229.

[30] P. Manneville, Intermittency, self-similarity and $1/f$ spectrum in dissipative dynamical systems, J. de Physique 41 (1980) 1235.

[31] F. Alavyoon, D.S. Henningson and P.H. Alfredson, Turbulent spots in plane Poiseuille flow–flow visualization, Phys. Fluids 29 (1986) 1328.

[32] S.C. Dickenson and R.R. Long, Laboratory study of the growth of a turbulent layer in a fluid, Phys. Fluids 21 (1978) 1698.

[9]H. S. Husain, Ph.D. thesis, University of Houston (in preparation).
[10]A. Krothapalli, D. Baganoff, and K. Karamcheti, J. Fluid Mech. 107, 201 (1981).
[11]K. B. M. Q. Zaman and A. K. M. F. Hussain, J. Fluid Mech. 103, 133 (1981).
[12]A. Michalke, J. Fluid Mech. 22, 351 (1965).
[13]M. J. Lee and W. C. Reynolds, Bull. Am. Phys. Soc. 27, 1185 (1982).
[14]M. A. Z. Hasan and A. K. M. F. Hussain, J. Fluid Mech. 115, 59 (1982).

An instability associated with a sudden expansion in a pipe flow

K. R. Sreenivasan[a] and P. J. Strykowski
Mason Laboratory, Yale University, New Haven, Connecticut 06520

(Received 21 June 1983; accepted 27 July 1983)

An instability characteristic of a fully developed laminar flow encountering a sudden expansion in a circular pipe is briefly described.

Consider a sudden expansion in a circular pipe shown in Fig. 1. A hot wire located on the centerline some distance downstream of the sudden expansion will register, beyond a threshold value of the Reynolds number, oscillations of the type shown in Fig. 2. The regularity of these oscillations is so remarkable, and their general repeatability so good, that a brief exploration of the phenomenon seemed worthwhile. This letter is a short report of a preliminary effort.

In our initial setup, oscillations which would appear at a threshold Reynolds number R_1 (based on the upstream section average velocity $\langle U \rangle$ and the upstream pipe diameter d_1) of about 1500 would disappear completely when R_1 exceeded a value of about 1700. Also a 0.24 mm diam needle inserted along a diameter through a hole slightly upstream of the expansion would destroy the oscillations everywhere in the pipe; removing the wire and resealing the hole with scotch tape (for example) would restore them exactly. On the other hand, a slightly thinner wire (0.17 mm diam) would not at all affect the occurrence of the oscillations.

It is soon realized that the 0.24 mm needle was of sufficiently large diameter (Reynolds number based on the maximum velocity in the upstream pipe and the wire diameter ~ 48) to shed Kármán–Bénard vortices which could indeed be observed. These vortices were probably of sufficiently large magnitude to prevent the oscillations (for reasons to be explained below) from occurring. The 0.17 mm wire shed no vortices—the wire Reynolds number of 35 being lower than the critical value of about 40 (Ref. 1)—and would leave the oscillations quite intact. In fact, we found that fairly low levels of turbulence created at the expansion would disrupt the oscillations totally. This immediately suggested to us that the disappearance at $R_1 = 1700$ of these oscillations had to do with the upstream disturbances whose residue at the expansion remained sufficiently strong for destroying the oscillations mentioned earlier. We then built a new pipe of the same nominal dimensions but with more carefully designed inlet conditions having a significantly lower disturbance level. For this setup, the oscillations at a certain axial location appeared at around $R_1 = 1500$ as before, but persisted in varying forms up to at least twice that value.

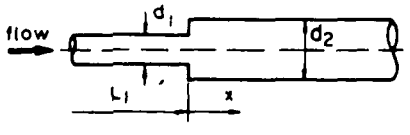

FIG. 1. The experimental configuration.

FIG. 2. Oscillations seen by a hot wire located on the pipe axis at $x/d_2 = 11$. Corresponding experimental conditions are $R_1 = \langle U \rangle d_1/\nu = 1500$, $d_1 = 0.635$ cm, $d_2 = 1.27$ cm, and $L_1 = 425\, d_1$. The uppermost trace is the unfiltered signal, the midtrace is low-pass filtered below 10 Hz, the lowermost trace being high-pass filtered above 10 Hz. Most of the fluctuations seen in the last trace are below about 500 Hz. Time scale: from left to right of figure, 4.8 sec.

 0031-9171/83/102766-03$01.90 © 1983 American Institute of Physics

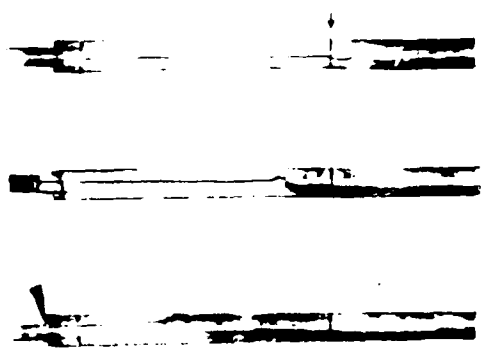

FIG. 5. Flow visualization results for $R_{d_1} = 1900$. In (a), the breakdown of the oncoming dye streak occurs downstream of the mark indicated by the arrow, while in (b), this breakdown occurs upstream of the mark. In (c) it is seen that a needle placed just upstream of the expansion anchors the breakdown point.

lation along the pipe. Thus, if one concentrated at a fixed observation station along the pipe axis (such as the mark in Fig. 5), one would alternately see an unruffled dye streak or a situation in which the broken-up dye streak filled the entire cross section. An unruffled dye streak at the observation station implies a velocity there that is characteristic of the jet-like oncoming flow from the upstream smaller pipe whereas, once the reattachment occurred, the flow would fill up the entire pipe thus reducing the average velocity. This is essentially what makes a hot wire record (as in Fig. 2) two different levels of velocity with periodic alternation between them. In fact, we noticed that the upper level of velocity in the oscillations of Fig. 2 corresponded roughly to the centerline velocity in the smaller upstream pipe, while the lower one corresponded approximately to the average velocity that would result if the flow coming out of the smaller pipe filled the entire downstream pipe uniformly. Further, it may be seen (cf. the uppermost trace of Fig. 2) that the upper velocity level is essentially laminar-like, while the lower one is somewhat turbulent-looking, reflecting the fact that the lower level in the velocity oscillation of Fig. 2 represents a turbulent situation downstream of reattachment.

Why does the reattachment point oscillate back and forth so regularly? The answer probably lies in the complex interaction between the velocity field downstream of the expansion and the oscillatory pressure field further downstream. Presumably, the velocity distribution downstream of the expansion would be nearly parabolic in the core, but would be surrounded by a region of reverse flow. The resulting complex velocity distribution has several inflection points, and is obviously prone to instabilities which are quite possibly excited in phase by the downstream pressure field, thus providing the mechanism for the regularity of the oscillations. These instabilities grow and eventually lead to the breakdown of the flow at some point downstream. When this occurs, the turbulence that develops and the consequently increased pressure drop would shift the reattachment point upstream. One may surmise that this upstream shift of the reattachment point would restore the stability of the flow by altering its velocity distribution just enough, so that the reattachment point would move downstream to its original position; this self-perpetuating act repeats itself.

Inserting a small wire slightly upstream of the expansion [see Fig. 5(c), where the head of the needle can be seen], which in the air experiments had the effect of destroying the oscillations, always resulted in a premature breakdown and reattachment of the flow at around $x/d_2 = 4$. Disturbances because of the wire upstream, or any other artificially created disturbance, would hasten the breakdown by bypassing the normal oscillatory growth stage, and anchor so well the reattachment point at around $x/d_2 = 4$ that, upstream of this point, the flow would simply be a laminar "jet" of fluid coming from the upstream pipe. Here, a hot wire located along the pipe axis would continuously record very nearly the peak velocity $2(\bar{U})$ in the upstream parabolic distribution, whereas downstream of this point, it would simply record continuously the lower velocity corresponding approximately to $(d_1/d_2)^2(\bar{U})$.

Now we may note a few vagrancies of this flow. Under nominally identical circumstances, the velocity trace would sometimes deviate in shape from that shown in Fig. 2. For example, the time spent in any cycle in each of the two states discussed above could be unequal (i.e., the duty cycle of the signal of Fig. 2 would be different from 0.5); or, the velocity would not be constant in the upper and lower states but very gradually (see, for example, the lowest trace in Fig. 3). Sometimes, the small-scale oscillations superposed on the upper state (see the lowest trace of Fig. 3) would not be easily discerned. We found that small levels of turbulence or some asymmetric constraints imposed at the expansion would destroy the phenomenon or alter it to varying degrees. The extraordinary sensitivity of the phenomenon to these various details, and the narrow range of Reynolds number within which it seems to occur unless special care is taken, may well explain why it has not been noticed before. However, we believe that it is not an uncommon phenomenon altogether; for example, something similar could be occurring downstream of a sharp orifice in enclosed flow measuring devices.

Finally, we might mention the practical relevance of the sudden expansion configuration in the context of ram jets and dump combustors.

ACKNOWLEDGMENTS

We would like to thank Professor B. T. Chu and Professor M. V. Morkovin for their many useful comments. If all their many critical questions have not been answered here, it is because this study was a byproduct of another investigation on turbulence control.

We also acknowledge the financial support of the Air Force Office of Scientific Research.

* Present address: DFVLR, Institute for Theoretical Fluid Mechanics, Bunsenstrasse 10, 3400 Gottingen, West Germany

[1] L. S. G. Kovasznay, Proc. R. Soc. London Ser. A **198**, 174 (1949).
[2] O. Reynolds, Phil. Trans. R. Soc. **174**, 935 (1883).

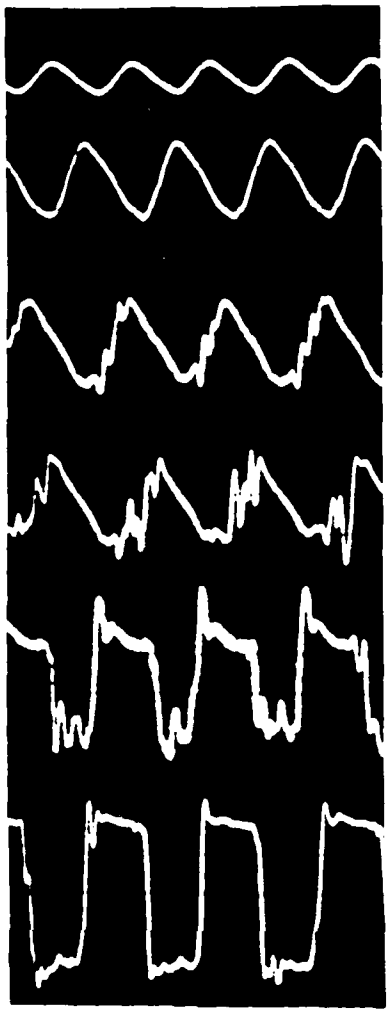

FIG. 3. Development and growth of the oscillations along the pipe axis downstream of expansion. From top to bottom, the oscillograms correspond to x/d_2 = 5.8, 7, 8, 9, 10, and 22, respectively. Signals low-pass filtered to 10 Hz. Unfiltered signals at x/d_2 of 5.8 and 7 are no different from the filtered ones; at other x/d_2, however, the signals do develop an increasingly higher frequency content. Time scale: from left to right of figure, 4 sec.

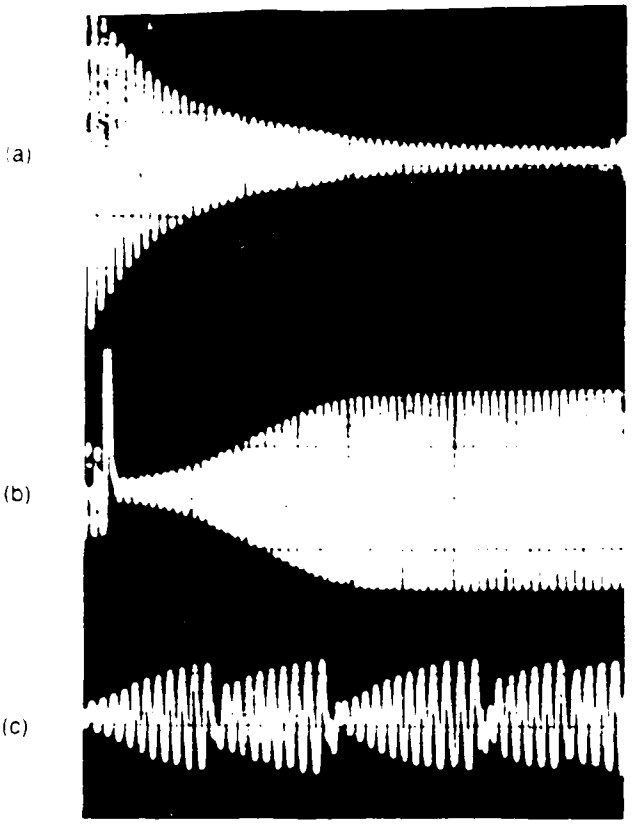

FIG. 4. Artificially triggered oscillations at $x/d_2 = 4.5$. In (a) the oscillations eventually decay, while in (b), they build up to a self-sustained state. In (c), they grow initially to a saturation amplitude and then decay abruptly before growing again. The cycle repeats indefinitely. Time scale: from left to right of figure, 50 sec.

Figure 3 is a record of the development and growth of the oscillations along the pipe axis. It is immediately clear that they are not the result of oscillations in mass flux (for, if they were, they should be seen with nearly the same amplitude everywhere axially), but must be characteristic of an instability of the oncoming flow. For $x/d_2 \lesssim 4$, no natural oscillations are seen; they can however be excited artificially by giving, for example, an impulsive but small motion to the hot-wire probe. This is sufficient to trigger oscillations (arising probably from probe–flow interactions) which may either decay with time [Fig. 4(a)], or grow into self-sustained state [Fig. 4(b)] depending probably on the initial amplitude of the impulse and the precise location of the probe in the flow. In certain cases, the oscillations grow to a saturation amplitude, decay abruptly to smaller amplitude, and build up again [Fig. 4(c)].

To better determine the nature of these oscillations, we set up a simple flow visualization experiment in water. To eliminate the possibility that the dye-introducing device placed upstream of the expansion would produce enough disturbances to destroy the flow oscillations, we introduced the dye at the inlet to the smaller pipe itself upstream of the contraction (as in the original experiments of Reynolds[2]). The contraction (area ratio ≈ 150) would damp out the disturbances produced by the dye-injecting needle to sufficiently small magnitude so as not to be disruptive to the process that resulted in the oscillations in the first place.

The dye streak downstream of the expansion would remain straight and smooth for x/d_2 of the order of about 5, apparently unaffected by the expansion. Thereafter, it would develop rapidly growing oscillations [see Fig. 5(a) and compare with Fig. 3], and would abruptly break down at some point depending on the Reynolds number; when this breakdown occurred, the dye filled the entire pipe crosssection downstream, suggesting that the breakdown and the reattachment of the oncoming flow occur essentially simultaneously. Just as abruptly, however, the reattachment "point" would move back, only to return to its original location, resulting in an essentially periodic back and forth oscil-

Some Studies of Non-Simple Pipe Flows

K R SREENIVASAN

SUMMARY A variety of phenomena occurs in pipe flows, especially if we stray away from straight circular pipes of uniform crosssection. This paper illustrates a few of the complexities arising from two relatively simple changes in geometry, namely, the sudden expansion and the coiling of a circular pipe.

1 INTRODUCTION

Pipe flows, far from being well-understood and dull, are very complex and highly interesting, and often show unexpected behaviours. Consider as an example a low speed, constant temperature, adiabatic flow in a long round pipe. The flow may be laminar or turbulent. Most books assert that, in a region sufficiently far away from the entrance, the static pressure varies linearly with the axial distance. Measurements, on the other hand, show that for air flow in a long, straight and thin tube (say, 6 mm diameter, 4000 diameters long), manometers located at equal intervals along the pipe length do not show equal readings; they increase with increasing downstream distance. (For the specific example chosen, and for a turbulent flow at a Reynolds number of the order of 10,000, the manometer reading over the last 100 diameters may be nearly twice as high as that, say, between 300 and 400 diameters.) Further, the wall shear stress is not simply proportional to the pressure drop.

This seemingly puzzling observation is not hard to understand, however. Without going into details (which can be worked out rather simply), we may note that, when the pipe is long and the axial pressure drop is substantial, the absolute pressure at the pipe entrance will have to be significantly higher than at the exit. In the present example, the pressure difference between the entrance and the exit will be of the order of one atmosphere. This gives rise to a substantial change in air density. With density a decreasing function of the axial distance, the flow will have to accelerate continuously, thus accounting for the observed behaviours. Thus, the classical notion of a linear pressure drop in a long pipe is exact (for gases) only in the limit of negligible pressure drop!

This is but one example of unsuspected behaviour. In the remainder of this paper, we shall discuss some intriguing phenomena arising from two simple changes in pipe geometry, namely, the sudden expansion and the coiling of a circular pipe. We shall not dwell at all on the complexities associated with flow of non-Newtonian fluids.

2 SUDDENLY EXPANDING PIPES

Consider a sudden expansion in a circular pipe shown in figure 1. Different phenomena occur in different ranges of parameter space, where the chief governing parameters are the Reynolds number Re, the axial distance x and the conditions upstream of the expansion. Here, all Reynolds numbers, unless specified otherwise, will be based on the diameter D of the downstream section and the bulk average velocity there. The origin for the downstream distance will be at the expansion itself. All results in this section refer to a diameter ratio of 2. Exceptions will be noted.

2.1 The Oscillatory Flow Regime

2.1a The Phenomenon: A hot wire located on the centreline of the pipe some distance downstream of the expansion will register, in a certain range of Re and for sufficiently smooth upstream conditions, oscillations of the type shown in figure 2, with amplitudes typically comparable to the average velocity in the downstream section. These oscillations are remarkable for their regularity and general repeatability (provided some care is taken, see below).

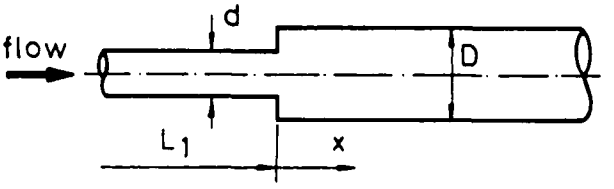

Figure 1 Schematic experimental configuration

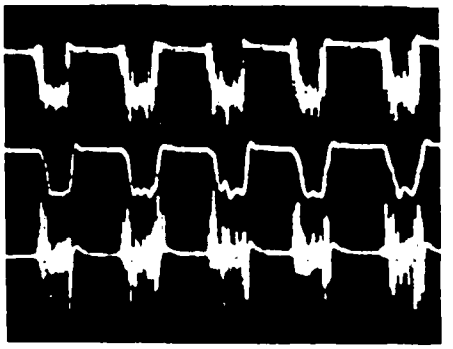

Figure 2 Oscillations seen by a hot-wire located on the pipe axis at x/D = 11. Re = 750, d = 0.635 cm, L_1 = 425 d. The uppermost trace is the unfiltered signal, the mid-trace is low-pass filtered below 10 Hz, the lowermost trace being high-pass filtered above 10 Hz. Most of the fluctuations seen in the last trace are below 500 Hz. Time scale: from left to right of figure, 5 sec.

K R Sreenivasan is with the Mason Laboratory, Yale University, New Haven, Ct. 06520, U.S.A.
This paper was originally presented as one of nine keynote addresses at the Eighth Australasian Fluid Mechanics Conference held at the University of Newcastle, NSW 2308, 28 November - 2 December 1983. (Paper M1227 received 8 November 1983).

DISCUSSION ON THIS PAPER WILL BE ACCEPTED FOR PUBLICATION UNTIL 14 MARCH 1984

These oscillations have several interesting properties. First, they appear when Re reaches a value of the order of 750, with the upper Reynolds number limit depending strongly on the degree of smoothness of the flow upstream of the expansion. If the entrance conditions to the upstream pipe are sufficiently smooth - say, in a qualitative way, smooth enough for the laminar-turbulent transition there to be delayed until an upstream pipe Reynolds number of the order of 7500 is reached - the oscillatory phenomenon seen in figure 2 persists until an Re of around 1500. For less smooth conditions, the Reynolds number window shrinks, and the oscillations may disappear altogether for certain conditions. In fact, if small levels of disturbance are artificially created just upstream of the expansion, or if the tube is squeezed hard asymmetrically at the expansion, the oscillations are disturbed rather strongly. They can even be controlled at will: for the conditions of figure 2, inserting a 0.24 mm diameter needle along a diameter through a hole carefully drilled just upstream of the expansion destroys the oscillations completely; removing the needle and resealing the hole restores them exactly. (The Reynolds number based on the maximum velocity in the upstream section and the needle diameter is approximately 50. The vortex shedding behind this needle, which we did indeed observe, perhaps creates enough asymmetry in the flow to prevent the oscillations from being formed. A slightly thinner needle, say, of 0.17 mm diameter, does not affect the oscillations, presumably because,its Reynolds number of 35 being lower than the critical value of about 40 (Kovasznay 1949), no vortex shedding appears.) Some further observations on this flow can be found in Sreenivasan & Strykowsky (1983a).

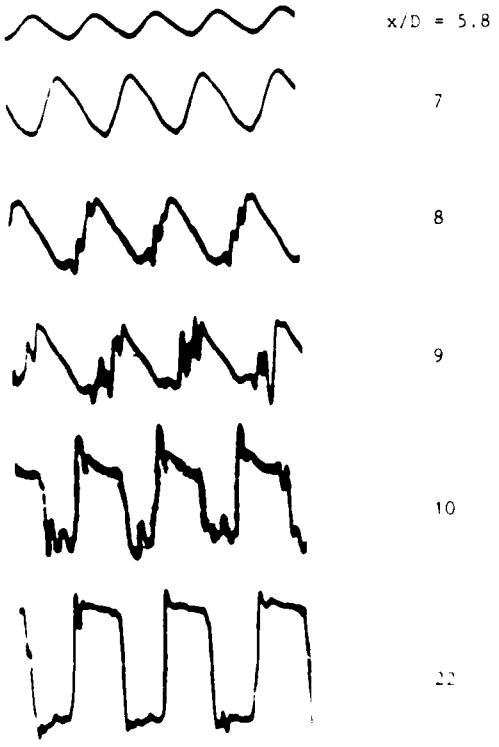

Figure 3 Development and growth of [illegible] pipe axis downstream of the expansion [illegible] pass filtered to 10 Hz. Unfiltered signals at [illegible] 5.8 and 7 are no different from the [illegible] other x/D, signals do develop [illegible] frequency content. Time scale [illegible] figure, 4 sec.

2.1b In search of an explanation: How do these oscillations arise and what physical phenomenon do they represent? A partial answer can be seen from figure 3 which records the development and growth of oscillations along the pipe axis. It is immediately clear that they do not represent oscillations in mass flux (for, if they did, oscillations should have been seen with nearly equal intensity at all x/D) but, rather, may be representative of the instability developing downstream of the expansion.

For further clarification, we set up a simple flow visualization experiment in water. An initial problem was that any dye-introducing device placed upstream of the expansion would produce enough disturbance to destroy the flow oscillations. However, a dye streak introduced at the inlet to the upstream pipe itself (much as in the original experiments of Reynolds,1883) served our purpose quite well. The large area ratio of the contraction (≈150) damped out the disturbances produced by the dye-injecting needle to sufficiently small values so as not to be disruptive to the process that resulted in the oscillations in the first place.

We may summarize our flow visualization results as follows. The dye streak downstream of the expansion would remain straight and smooth for x/D of the order of 5, apparently unaffected by the expansion. Thereafter, depending on the precise value of the Reynolds number (as long as it exceeded a 'critical' value of about 750) it would develop rapidly growing oscillations (see figure 4a and compare it with figure 3), and would abruptly break down at some point; when this break-down occurred, the dye filled the entire pipe crosssection downstream, suggesting that the break-down and reattachment of the oncoming flow occur essentially simultaneously. Just as abruptly, however,

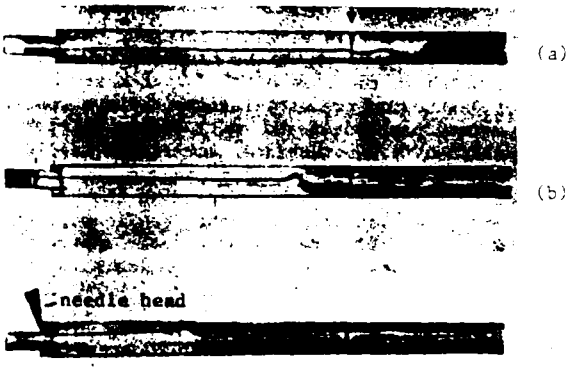

Figure 4 Flow visualization results for Re = [illegible] (a), the break-down of the oncoming dye-streak [illegible] downstream of the mark indicated by the arrow. [illegible] in (b), this break-down occurs upstream of the [illegible] In (c), it is seen that the needle placed [illegible] the expansion anchors the break-down [illegible]

the reattachment would move [illegible] along the pipe, only to move [illegible] position later. This [illegible] essentially periodic [illegible] at a fixed observation [illegible] (such as the mark [illegible] see an oscillation [illegible] the time [illegible] oscillation [illegible]

AD-A185 643 TURBULENCE TURBULENCE CONTROL AND DRAG REDUCTION(U) 2/2
YALE UNIV NEW HAVEN CT MASON LAB K R SREENIVASAN
01 AUG 87 AFOSR-TR-87-0984 $AFOSR-82-0299

UNCLASSIFIED F/G 20/4 NL

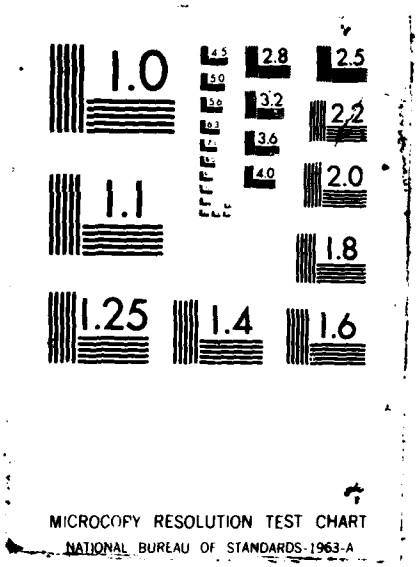
1.0
1.1
1.25
1.4
1.6
2.8
3.2
3.6
4.0
2.5
2.2
2.0
1.8
MICROCOPY RESOLUTION TEST CHART
NATIONAL BUREAU OF STANDARDS-1963-A

centre-line velocity in the smaller pipe, while the lower level approximately to the average velocity that would result if the flow coming out of the smaller pipe filled the entire downstream pipe uniformly. Further, it may be seen that (cf. the uppermost trace of figure 2) the upper velocity level is essentially laminar-like, while the lower one is turbulent-looking, reflecting the fact that the lower level in the oscillations of figure 2 represents a turbulent situation downstream of reattachment.

Why does the reattachment point move back and forth so regularly? The answer lies probably in the complex interaction between the stability of the velocity field downstream of the expansion and the oscillatory pressure field further downstream. At this point, our knowledge of the process is meagre, but a possible (necessarily speculative) explanation follows.

The velocity distribution downstream of the expansion would be nearly parabolic in the core, but surrounded by a region of reverse flow. The resulting complex velocity distribution has several inflexion points, and is obviously prone to instabilities which are quite possibly excited in phase by the downstream pressure field, thus providing the mechanism for the regularity of the oscillations. These instabilities grow and eventually lead to the break-down of the flow at some point downstream. When this occurs, the turbulence that develops and the consequently increased pressure drop would shift the reattachment point upstream. One may surmise that this upstream shift of the reattachment point would restore the stability of the flow by altering the velocity distribution just enough, so that the reattachment point would now move downstream to its original position. This self-perpetuating act repeats itsef indefinitely.

Inserting a small needle slightly upstream of the expansion (see figure 4c where the head of the needle can be seen), which in the case of air experiments had the effect of destroying the oscillations, always resulted in a premature break-down and reattachment of the flow at around x/D of 4. Disturbances due to the needle upstream, or any other artificially created disturbance, would hasten the break-down by bypassing the normal oscillatory growth stage, and anchor the so well the reattachment point at around x/D =4 that, upstream of this point, the flow would simply be a laminar 'jet' of fluid coming from the upstream pipe – here, a hot-wire on the pipe axis would continuously record very nearly the peak velocity in the upstream pipe – whereas downstream of this point, it would simply record continuously the lower velocity corresponding approximately to that after reattachment. This is essentially why no oscillations were seen by the hot-wire.

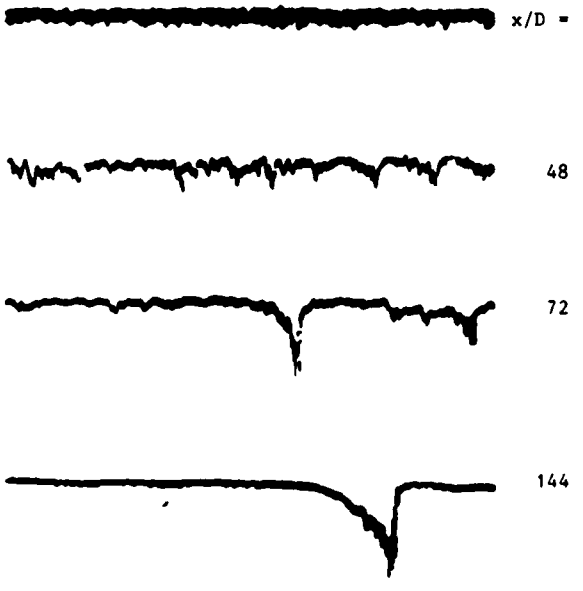

Figure 5 Oscillograms along the centre-line downstream of the expansion. Re = 2200.

2.2 The Puff Region

Further downstream of the expansion, the smoothness or otherwise of the flow in the upstream pipe becomes irrelevant, and the Reynolds number and the downstream distance become the only relevant parameters. The downstream evolution of the flow for a fixed Reynolds number of 2200 is shown in figure 5. The flow is fully turbulent at x/D of 24, where the uppermost trace was obtained. With increasing distance, the signal is seen to build up in isolated regions while, at the same time, the general level of turbulence slowly diminishes elsewhere (see the middle two traces). Eventually, one has (as in the lowest trace of figure 5) nearly perfect laminar regions interspersed with characteristic signatures of structures known as puffs (Wygnanski & Champagne, 1973). Figure 6 presents the complementary information, namely, the flow evolution with increasing Reynolds number at a fixed x/D of 144. Below an Re of

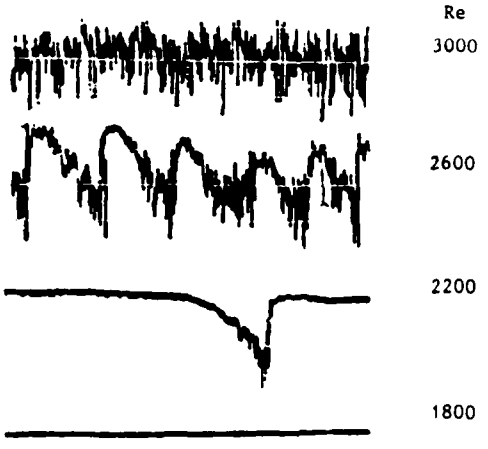

Figure 6 Oscillograms on pipe center-line. x/D = 144

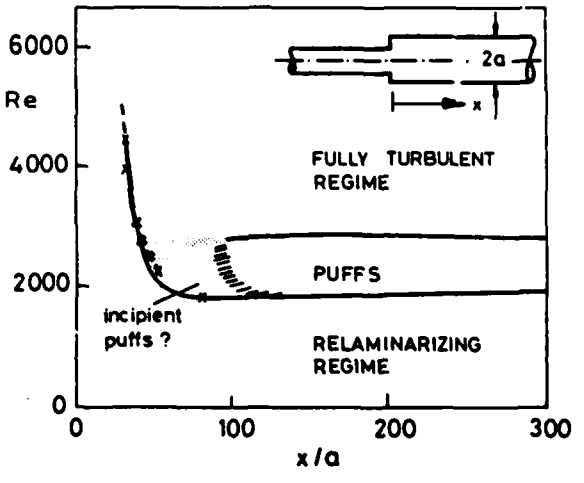

Figure 7 Boundaries between the turbulent, puff and relaminarizing regimes downstream of a sudden expansion.

DISCUSSION ON THIS PAPER WILL BE ACCEPTED
FOR PUBLICATION UNTIL 14 MARCH 1984

about 2000, the flow is entirely laminar; considering that the expansion renders the flow downstream of it turbulent irrespective of whether the oncoming flow is turbulent or not, the above observation simply means that the flow is completely relaminarized for Re ≤2000 (see section 2.3). With increasing Reynolds numbers, puffs begin to appear more and more frequently, until eventually (for all practical purposes, beyond an Re of 2700) a fully turbulent flow results from the interaction and conglomeration of puffs.

By obtaining similar traces at different x/D, one can construct a map marking boundaries between the turbulent, puff and relaminarizing regimes (see figure 7). Similar maps have been constructed before for other cases by Wygnanski & Champagne (1973) and Champagne & Helland (1978). The map is self-explanatory in the region x/D ≥ 100. In the region marked 'incipient puffs?' one cannot see a distinct puff-like structure, but can recognise something similar (see the second trace from above in figure 5) which will evolve into puffs further downstream. Turbulence level downstream of the expansion seems always to decrease for a certain initial distance; whether it continues to decay or not depends on the Reynolds number. Crosses in the figure indicate the x/D positions where the minimum in the mean-square level of turbulence occurs for a given Re. The line joining the crosses thus demarcates the region of decaying turbulence to its left from that of increasing and stable levels of turbulence to its right.

It is known that puffs once formed may either merge with each other or split to form more than one (Wygnanski et al., 1975), depending on the Reynolds number. An equilibrium puff is one that does neither, and sustains itself indefinitely; it occurs around an Re of 2200. In structure, an equilibrium puff consists probably of several toroidal vortices (Rubin et al., 1980), and its occurrence follows a Poisson distribution rather well. Recently, Bandyopadhyay & Hussain (1983) seem to have identified the regeneration mechanism that allows the equilibrium puff to survive indefinitely in spite of the continually occurring turbulent energy dissipation. It appears that when the laminar flow from upstream of a puff enters it — figures 5 and 6 show that the puffs are relatively slow moving and have sharp upstream interface — rather well-organized vorticity is generated (much as in an axisymmetric jet) which breaks up into small-scale turbulence subsequently. In the incipient stage, one surmises that this same process of regeneration must gradually start to occur after being initiated via statistical fluctuations.

2.3 Relaminarizing Regime

For Re ≤ 2000, the measured mean velocity profiles acquire increasingly laminar-like shape with increasing downstream distance. One expects that for large x/D, the theoretical Poiseuille flow will be established asymptotically. At any station downstream of the expansion where the measured velocity distribution u(x,r) — r being the radial distance from the centre-line — has not quite reached its asymptotic shape, one can write:

$$u(x,r) = u_0(r) + \varepsilon u_1(x,r) + O(\varepsilon^2),$$
$$v(x,r) = \varepsilon v_1(x,r) + O(\varepsilon^2),$$
$$p(x,r) = p_0(x) + \varepsilon p_1(x,r) + O(\varepsilon^2), \qquad (1)$$

where $u_0(r)$ and $p_0(x)$ are the asymptotic velocity and pressure distributions, and u_1, v_1 and p_1 are the departures of the axial and normal velocity components, respectively, and of the pressure, from the asymptotic distributions. (Note: $v_0 \equiv 0$.) We have retained only ε-order terms, which implies that (1) can be expected to hold only sufficiently far from the pipe expansion where departures from the asymptotic state are small. The parameter ε is the inverse of the characteristic Reynolds number based on the thickness of the inner laminar layer developing (in some asymptotic sense) from the expansion itself, and the average velocity in the pipe. It is these layers that grow and eventually merge to form the asymptotic shape of the velocity profile (Narasimha & Sreenivasan, 1979), the process being much like that in the entrance region of a straight pipe (Goldstein, 1938).

For the fluctuations too, we may write:

$$u' = \varepsilon u_1' + O(\varepsilon^2); \quad v' = \varepsilon v_1' + O(\varepsilon^2), \qquad (2)$$

the expectation being that in the asymptotic state the fluctuations are zero. We may now write the Reynolds shear stress τ as

$$\tau = -\overline{u'v'} = c_\tau(\tilde{u}\tilde{v}) = c_\tau[O(\varepsilon^2)], \qquad (3)$$

where c_τ is the correlation coefficient, the tilde denote root-mean-square values, and the last step in (3) follows from (2). Measurements show that during relaminarization of this type, not only do the fluctuations decay with distance but also become decorrelated (see, for example, Badrinarayanan, 1968); that is, c_τ tends to zero as $x/D \to \infty$ or $\varepsilon \to 0$. It is thus reasonable to take $c_\tau = o(1)$, so that, from (3), we may write

$$\tau = o(\varepsilon^2), \qquad (4)$$

or, that τ is higher order in smallness than ε^2. Using (1),(2) and (4) in the Reynolds averaged continuity and momentum equations, we obtain, to O(1):

$$\mu\left[\frac{d^2u_o}{dr^2} + \frac{1}{r}\frac{du_o}{dr}\right] = \frac{dp_o}{dx}, \quad u_o(a) = 0$$

whose solution, as expected, is the classical parabolic distribution. To order ε, we get:

$$\frac{1-\eta}{\eta}\frac{\partial}{\partial\xi}\left(\eta\frac{\partial u_1}{\partial\eta}\right) = 2\frac{\partial^2}{\partial\eta^2}\left(\eta\frac{\partial u_1}{\partial\eta}\right), \qquad (5)$$

where $\eta = r^2/a^2$, and $\xi = xa/Re$; $\int_0^1 u_1 d\eta = 0$. Putting $\eta(\partial u_1/\partial\eta) = C\exp(-2\lambda\xi)\,\phi(\eta)$, we can write (5) as:

$$\phi'' + \lambda(1-\eta/\eta)\phi = 0, \qquad (6)$$

with $\phi(0) = 0$ and $\int^1 \phi\, d\eta = 0$. Our interest is in the first odd eigenfunction and the corresponding eigenvalue for (6).

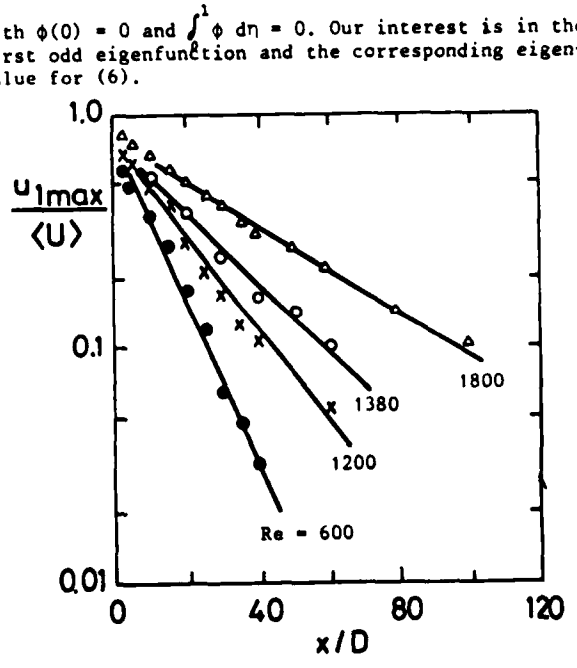

Figure 8 Exponential approach to the asymptotic state. ●,×,Δ: sudden expansion data from Sibulkin (1962); D/d = 4.5. O, gradual expansion, Laufer (1962).

DISCUSSION ON THIS PAPER WILL BE ACCEPTED FOR PUBLICATION UNTIL 14 MARCH 1984

There are some nice consequences of this analysis. First, a characteristic value of u_1, say u_{1max} which is the centre-line value of u_1, should decay exponentially with x. Figure 8 shows this to be true to a good approximation. Interestingly, the exponential decay which, by virtue of having retained only two terms in (1), could a priori have been expected to hold only for large x/D, holds true quite close to the expansion, especially for low Reynolds numbers. Second, the rate at which u_{1max} decays is inversely proportional to the Reynolds number. (That is, if $u_{1max} \sim \exp(-mx/a)$, the product mRe should be a constant independent of Re.) Figure 9 shows that this is true not only for the sudden expansion case but also for gradual expansions and bifurcating pipes. Finally, figure 10 shows that the experimentally determined distribution of u_1/u_{1max} agrees quite closely with the approximate eigenfunction for (6). Again, the theory holds for x/D as low as 8.

3 FLOW IN HELICALLY COILED PIPES

Flow in curved pipes — which encompasses the topic under discussion— has been a subject of numerous investigations, but it appears that even some of the gross phenomena have not been understood. Our intention here is not to discuss curved pipe flows exhaustively — a recent survey by Berger et al.(1983) does this very well — but to point out a few interesting results.

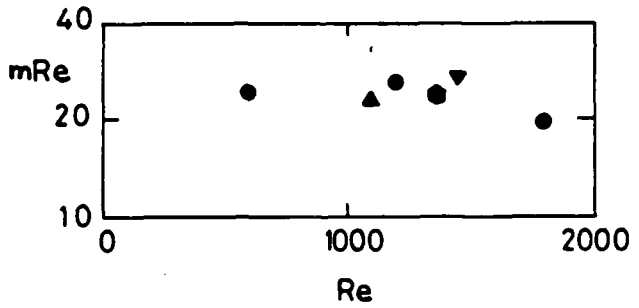

Figure 9 The product mRe in relaminarizing pipe flows. Sudden expansion: ●, Sibulkin, ▲, present. ⬤, gradual expansion, Laufer. ▼, branching pipe, Lynn & Sreenivasan (1982).

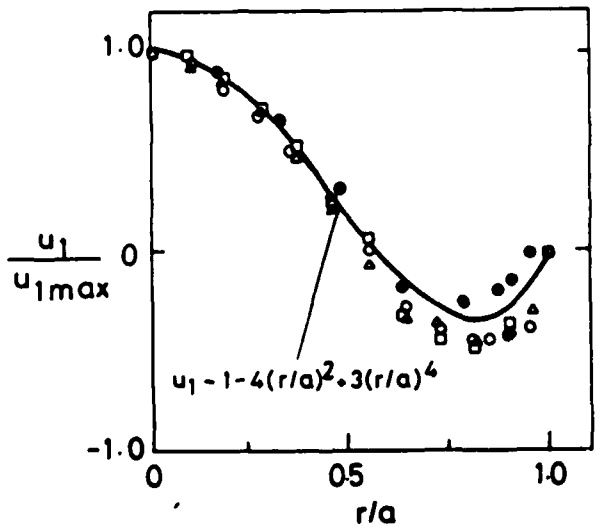

Figure 10 A comparison with theory of the departure of the measured distribution from the asymptotic parabolic profile. Sibulkin: O, x/D = 8; Δ,17; □,35. Present: ●, x/D = 17.5.

Consider a long straight section of a smooth pipe followed by a coiled section; following the coil is another long straight section (see figure 11). Several phenomena we want to discuss are related to the question of transitional Reynolds numbers in this set-up, and we shall mention this first.

Since we made no special attempt to keep the flow in upstream straight section unusually disturbance-free, the onset of transition occurred there at a Reynolds number of about 2300. Typically, this manifests itself in the form of puffs, and transition proceeds with increasing Reynolds numbers much as in figure 6. As determined from intermittency measurements, transition to turbulence is complete around an Re of 3200. This holds up to the entrance to the coil. Once inside the coil, the nature of transition depends, even at a fixed axial distance and for a given radius ratio (that is, the ratio of the radius of the pipe to the radius of curvature of the coil), strongly on the precise location in the pipe. It is not easy to determine, or even define convincingly, the onset of transition to turbulence (although a preliminary attempt has been made by Sreenivasan & Strykowsky, 1983b), but two limiting situations can be defined relatively unambiguously: the upper Reynolds number limit for the existence of a steady laminar flow ('steady laminar limit') and the lower Reynolds number limit at which the flow is turbulent everywhere in a given crossection of the curved pipe ('turbulent limit'). Notice that in the special case of the straight pipe the steady laminar limit coincides with the onset of transition to turbulence; of course, the turbulent limit retains its meaning throughout of the completion of transition to turbulence.

Figure 12 shows both steady laminar and turbulent limits for the set-up shown in figure 11. (The data correspond to a pipe which was 173 diameters long upstream of the coil, had 20 $^1/_2$ turns in the coil and was 937 diameters long in the downstream straight section. The diameter 2a was 0.635 cm, and the radius ratio a/R was 0.058. The fluid was air. All transitional Reynolds number data were determined with a hot-wire.) One effect of the coil is to increase both the steady laminar and turbulent limits up to the end of about three turns or

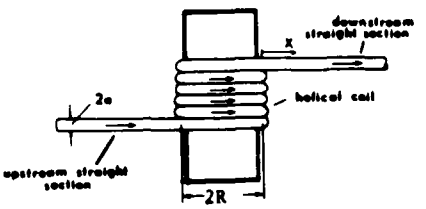

Figure 11 Schematic of the experimental set-up.

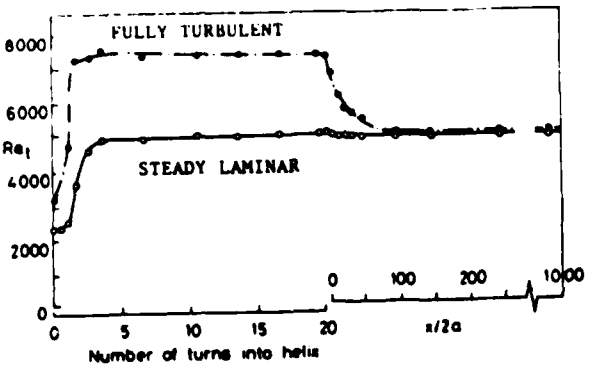

Figure 12 The steady laminar and turbulent Reynolds number limits for the set-up shown in figure 11.

DISCUSSION ON THIS PAPER WILL BE ACCEPTED FOR PUBLICATION UNTIL 14 MARCH 1984

so; thereafter, some asymptotic state seems to have been reached. In this asymptotic state, the flow remains laminar and steady for Reynolds numbers up to about 4800, and does not become fully turbulent until an Re of 7900 or so is reached; clearly, the gap between the two curves is larger inside the coil than that at the entrance to the coil. Perhaps surprizing is the behaviour downstream of the coil: while the turbulent limit drops as expected, the steady laminar limit does not, but stays approximately at the same elevated level as in the coiled section. In other words, the onset of turbulence has been permanently raised to an Re of 4800 in contrast to about 2300 in the upstream section!

Why does the flow remain steady and laminar for higher Reynolds numbers in the coiled section than it usually does in the upstream straight section? Can the asymptotic values of the two limiting Reynolds numbers be increased indefinitely? What makes the flow remain steady and laminar for Reynolds numbers as high as it does in the downstream straight section? Can that too be increased indefinitely? These are some of the obvious questions that come to our mind. In what follows, we shall attempt at least partial answers to these questions drawing largely from our continuing study of this flow.

3.1 Stabilization Effects and Relaminarization

Within the coil, the flow near the inside wall sees a convex curvature whose effect has long been known to be stabilizing. However, the concave curvature associated with the outside wall is known to be destabilizing, and so, the explanation for the net stabilization effect observed in the present circumstances is a bit subtle. The clue lies in the behaviour of the mean velocity distribution. Essentially because of the centrifugal forces, the peak of the velocity in the plane of the helix moves to the outside; typically for a radius ratio of about 0.058, the peak occurs at a distance from the outer wall of a tenth of the pipe diameter. Over the bulk of the profile from the inside to the peak, the sense of the mean flow vorticity is the same as the 'angular velocity' in the pipe, so that, by Rayleigh's criterion – for a statement of the criterion most appropriate in the present context, see Coles (1965) – the flow is stable. There is however a small region near the outside wall where the mean vorticity and the 'angular velocity' vectors are oppositely aligned. But this region is quite thin for fairly large curvatures, and the governing instability there is of the boundary layer type. This 'boundary layer' too will be stable unless the Reynolds number based on its thickness is above the appropriate critical value; then and only then will the onset of instability and possible transition to turbulence occur. This explanation, in spirit due essentially to Lighthill (1970), cannot be complete because of the three-dimensionality of the velocity field but appears very reasonable.

One consequence of these stabilization effects is that, in a certain Reynolds number range (for the conditions of figure 12, 2300 ≤ Re ≤ 4800), a turbulent flow entering the coil can be expected to become laminar at some point in the coil. That does indeed happen, as can be seen from the oscillograms of figure 13. The flow, which begins its journey in a fully turbulent state at the inlet to the coil, has become completely laminar by about two turns in the coil. In fact, near the inside surface, the flow has lost most of its turbulent characteristics only half a turn into the coil!

3.2 Radius Ratio and Other Effects

We set up several coiled pipe flows in order to determine the effect of radius ratio on the asymptotic values of the steady laminar and turbulent limits discussed with respect to figure 12. Since the parameter governing the dynamic similarity in curved pipes is the so-called Dean number (White, 1929),

$$De = Re(a/R)^{0.5}, \qquad (7)$$

the data obtained were plotted (see figure 14) as the limiting Dean numbers against the radius ratio a/R. It is seen that the limiting Dean numbers (whose meaning is the same as that of the asymptotic limiting Reynolds numbers of figure 12) increase with increasing tightness of the coil until an a/R of 0.04. Thereafter, we note that steady laminar flow cannot be found for Dean numbers above about 1100, however large the radius ratio. (This constancy in the steady laminar limit for the Dean number actually implies a decrease in the corresponding Reynolds number for increasingly larger a/R; see equation (7).) On the other hand, the turbulent limit appears to increase monotonically (in terms of both the Dean and Reynolds numbers) with the radius ratio.

If we replot the data of figure 14 in terms of Reynolds numbers instead of Dean numbers (Srecnivasan & Strykowski, 1983b), it can be seen that the lower curve of figure 14 shows a peak for a/R of 0.039 and Re of 5400. This simply means that the most stable conditions

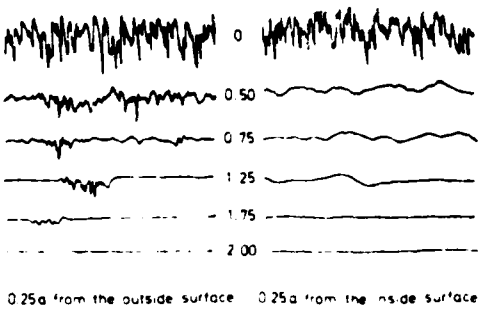

Figure 13 Typical oscillograms of hot-wire traces during relaminarization. Re = 3450, a/R = 0.058. The numbers marked in the middle of the figure correspond to the number of turns into the coil.

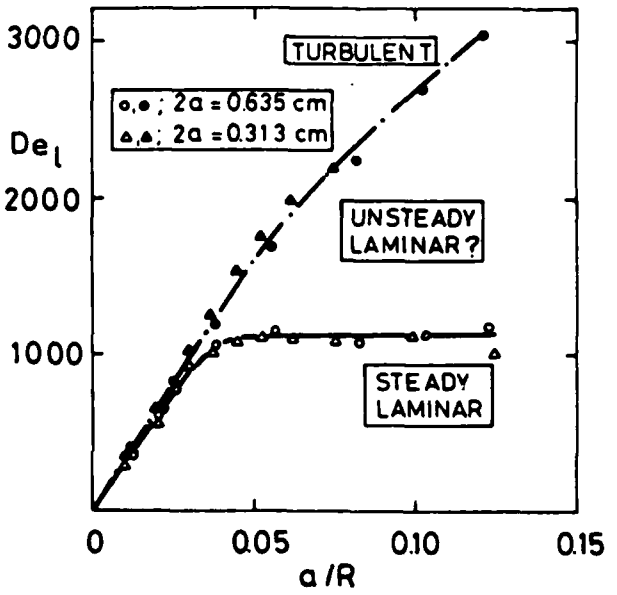

Figure 14 Asymptotic values of the limiting Dean numbers in the coiled section, measured at the end of 20 turns for all radius ratios.

DISCUSSION ON THIS PAPER WILL BE ACCEPTED FOR PUBLICATION UNTIL 14 MARCH 1984

obtain for a radius ratio of 0.039 and the highest Reynolds number for which a steady laminar flow is possible in the asymptotic state in the coiled pipes is 5400. This appears to be so independent of how large the critical Reynolds number is upstream of the coil (or, how smooth the inlet is to the upstream straight pipe); our data at this point are not extensive but seem enough to hold this view. We therefore conclude that, if we can maintain the flow upstream of the coil steady and laminar for Re ≥ 5400, it actually loses its stability upon entering the coil — a notion that seems to have been ruled out in the long history of curved pipe flows! Curvature in this case is not always stabilizing!

3.3 Unsteady Laminar Flow in Tightly Coiled Pipes?

For convenience, we shall call coiled pipes with a/R higher than about 0.04 (corresponding to the flat lower curve in figure 14) as tightly coiled pipes. We shall now qualitatively examine the nature of the flow with increasing Dean number for a typical tightly coiled pipe. Figure 15 shows several oscillograms, all obtained at the end of 10 turns of a coiled pipe with radius ratio 0.1. It is useful to note that the traces look much the same over most of the crossection of the pipe, except perhaps in the vicinity of the outside wall in the plane of the coil. It is clear that, while the flow loses its steady characteristics in the neighbourhood of a De of 1100, it is still laminar-looking up to a much higher Dean number (see the second, third and the fourth traces in figure 15). We therefore make a hypothesis that the stable laminar state yields to another laminar state, with transition to turbulence

If an intermediate unsteady laminar state does indeed occur, it is clear that theoretical analyses of the laminar motion must somehow incorporate this at large Dean numbers. This failing may well be the chief reason why, Van Dyke's (1978) extension to De → ∞ of Dean's(1927) analysis of laminar motion in curved pipes, while being technically sound, yeilds results with qualitatively incorrect dependence of friction factor on the Dean number. We may also note that Van Dyke's friction factors are lower than the experimentally measured ones, as should indeed be expected if the present discussion is correct.

3.4 The Downstream Straight Section

We may now return briefly to the flow in the straight section downstream of the coil. We recall from figure 12 that the Reynolds number corresponding to the steady laminar limit stays essentially at the same elevated level as in the coiled section. We have found this to be true (Sreenivasan & Strykowsky 1983b) for coils with several other radius ratios too. This seemed surprizing at first, but is natural upon recollecting that the critical Reynolds number for a pipe flow (i.e., the Poiseuille flow), as determined theoretically from linear disturbance theory, is strictly infinite. In practice, the flow undergoes transition at finite and variable Reynolds numbers depending on the level of disturbances. Because of the continual dissipation of turbulence and other disturbances in the thin boundary layer-like regions, it is possible that the coiled section acts like a very successful filter that removes the most critical disturbances, or at least diminishes their amplitude, alters their frequency content, or both, in such a way that the remainder of the disturbances does not become critical until after a fairly high Reynolds number (depending on the radius ratio of the coil, number of turns, etc.) is attained. The picture is made more complicated by the fact that there is a strong swirl at the inlet to the downstream straight section, and the boundary layers that get established in the developing region may in fact set the upper limit to the transitional Reynolds number there. These and other questions cannot be settled

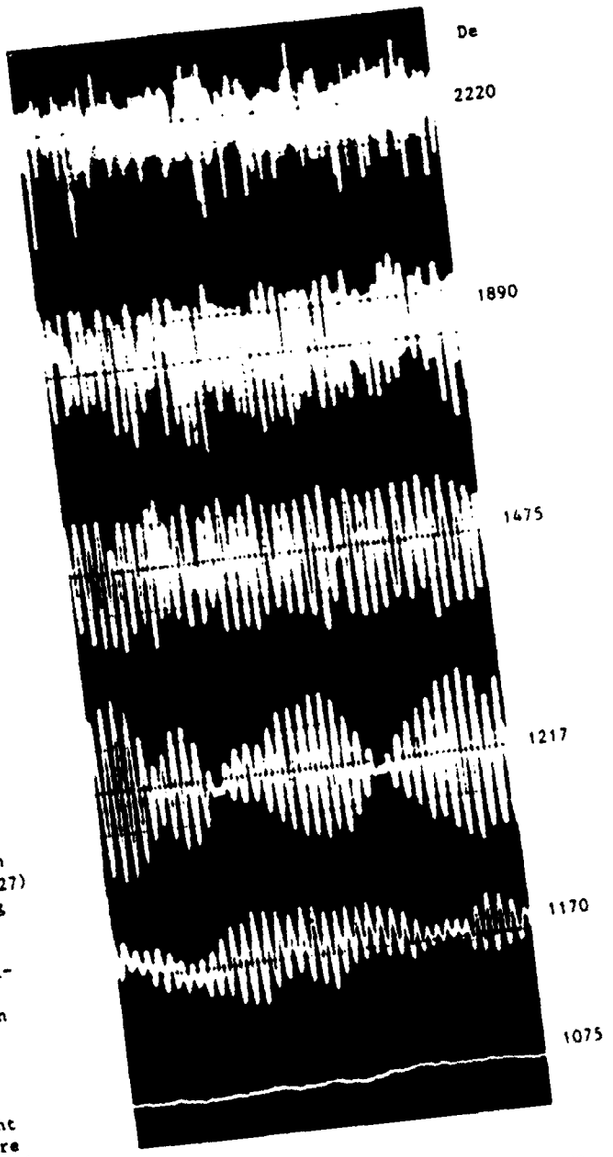

Figure 15 Oscillograms of hot-wire signals, a/R = 0.1. The gain for the top four traces is the same, but it increases by 2 each time for the following two traces. The time scale is the same for all traces.

without careful and quantitative studies, but it may be relevant to point out that an artificial disturbance, created immediately after the flow exits from the coil by inserting a fine needle across the pipe diameter (recall the arrangement in section 2.1), does not affect the transitional Reynolds number in the downstream straight section. On the other hand, the same needle, when inserted further downstream (say, x/D of 100), results in a precipitous drop in the steady laminar limit to around 2200.

Finally, we may note that the gap between the loss of steady laminar motion and the completion of transition to turbulence is relatively quite small (of the order of 0.5% of the steady laminar limit) in the downstream straight section. This catastrophic transition, not uncommon in pipes with relatively smooth inlets — the coil seems to serve much the same purpose indirectly — is quite different from that characteristic of the

DISCUSSION ON THIS PAPER WILL BE ACCEPTED
FOR PUBLICATION UNTIL 14 MARCH 1984

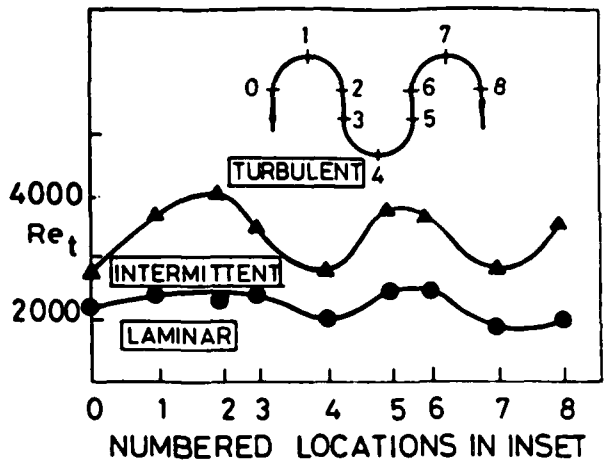

Figure 16 Transitional Reynolds numbers in a 'heat-exchanger-type' pipe configuration shown in the inset.

process in the upstream straight section with no specially smooth inlet, and is marked by the appearance of the so-called slugs (in contrast to puffs upstream) which are regions of turbulence filling the entire pipe section comparable in length to the pipe length itself, characterized by relatively sharp laminar-turbulent interfaces at both the front and back ends. (For a discussion of slugs, see, for example, Pantulu(1962), Lindgren (1969), Wygnanski & Champagne (1973), etc.)

4 SOME OTHER EXAMPLES

In addition to the two non-simple pipe flows discussed in the previous sections, we have also examined in varying degrees of detail:

(a) pipe flow with a right angle bend,
(b) pipe flows which bifurcate into two equal or unequal branches, and
(c) typical heat exchanger pipes in which the flow reverses direction every half a turn; see inset to figure 16.

In engineering practice, these and other configurations are widely used. Several important gross parameters have been measured for a long time, and a number of working engineering correlations relating to their performance have been in existence also for a long time. But a more detailed look at any of these configurations reveals many interesting and unexplored facets. (See, for example, Tunstall & Harvey (1969) for a very curious phenomenon associated with sharp bends in fully developed pipe flows.) Perhaps, we are saying nothing but attesting to the obvious reality of the fascinating science of fluids!

We close our discussion of non-simple pipe flows with some data on the transitional Reynolds numbers measured in an example of (c) above. Again, we have plotted in figure 16 the two limiting Reynolds numbers (recall our discussion with respect to figure 12) as a function of position. It is seen that the two limiting Reynolds numbers first increase for the first half a turn or so, just as they do in the coiled pipes, but thereafter, follow the geometry of the pipe in some rough sense. The important point to note is that the onset and completion of transition occur around the same values common in straight pipes with disturbed inlet conditions. Clearly, this fact is important in heat exchangers and the like where it is no surprise to find this configuration, rather than a helically coiled pipe, in common use.

5. ACKNOWLEDGEMENTS

It is a pleasure to acknowledge contributions of Professor B.-T. Chu, Mr. T.B. Lynn, Professor M.V. Morkovin, Professor R. Narasimha, Mr. P.J. Strykowsky and Professor P.P. Wegener. I owe them all, especially Mr. Strykowsky, a debt of gratitude. Some of these studies were an outgrowth of a project on Turbulence Control sponsored by the Air Force Office of Scientific Research.

6. REFERENCES

BADRINARAYANAN, M.A. (1968) An Experimental Study of Reverse Transition in Two-Dimensional Channel flow, J. Fluid Mech., 31, 609-623.

BANDYOPADHYAY, P & HUSSAIN, A.K.M.F. (1983) The Organised Motion in 'Puffs' in Transitional Pipe Flow, Third Int. Symp. on Flow Vis. Univ. Michigan, Ann Arbor, Sept 1983.

BERGER, S.A., TALBOT, L. & YAO, L.-S. (1983) Flow in Curved Pipes. Ann. Rev. Fluid Mech. 15 , 461-512.

CHAMPAGNE, F.H. & HELLAND, K.N. (1978) Pipe Flow Relaminarization, Bull. Amer. Phy. Soc. 23 , Nov. 20.

COLES, D. (1965) Transition in a Circular Couette Flow, J. Fluid Mech. 21 , 385-425.

DEAN, W.R. (1927) Note on the Motion of Fluid in a Curved Pipe, Phil. Mag. J. Sci. 4 , 208-223.

GOLDSTEIN, S. (Editor) (1938) Modern Developments in Fluid Dynamics. Vol 1. Oxford: Clarendon Press.

KOVASZNAY, L.S.G. (1949) Hot-Wire Investigations of the Wake Behind Cylinders at Low Reynolds Numbers, Proc. Roy. Soc. Ser. A, 198 , 174-185.

LAUFER; J. (1962) Decay of Non-Isotropic Turbulent Field, In 'Miszellaneende Angewandte Mechanik, Festschrift Walter Tollmien,' Akademie-Verlag, Berlin.

LIGHTHILL, M.J. (1970) Turbulence. In 'Osborne Reynolds and Engineering Science Today' (D.M.McDowell & J.D. Jackson, Eds.), 83-146, Manchester Univ. Press.

LINDGREN, E.R. (1969) Propagation Velocity in Turbulent Slugs and Streaks in Transition Pipe Flow, Phys. Fluids, 12 , 418-425.

LYNN, T.B. & SREENIVASAN, K.R. (1982) The Flow in a Branching Pipe. Bull. Amer. Phys. Soc. 27, Paper EA3.

NARASIMHA, R. & SREENIVASAN, K.R. (1979) Relaminarization of Fluid Flows, Adv. Appl. Mech. 19, 221-309.

PANTULU, P.V. (1962) M.Sc. Thesis, Aero.Engg.Dept., Indian Inst. Sci., Bangalore.

REYNOLDS, O. (1883) An Experimental Investigation of the Circumstances which Determine Whether the Motion of Water Shall be Direct or Sinuous, and of the Law of Resistance in Parallel Channel, Phil. Trans. Roy. Soc. 174, 935-982.

RUBIN, Y., WYGNANSKI, I. & HARITONIDIS, J.H. (1980) Further Observations on Transition in a Pipe. In 'Laminar-Turbulent Transition' (Eppler, R. & Fasel, H., Eds) Springer-Verlag, Berlin.

SIBULKIN, M. (1962) Transition from Turbulent to Laminar Pipe Flow, Phys. Fluids. 5, 280-284.

SREENIVASAN, K.R. & STRYKOWSKY, P.J. (1983a) An Instability Associated With a Sudden Expansion in a Pipe Flow, Preprint.

DISCUSSION ON THIS PAPER WILL BE ACCEPTED FOR PUBLICATION UNTIL 14 MARCH 1984.

SREENIVASAN, K.R. & STRYKOWSKY, P.J. (1983b) Stabilization Effects in Flow Through Helically Coiled Pipes, Experiments in Fluids, 1, 31-36.

TUNSTALL, M.J. & HARVEY, J.K. (1969) On the Effect of a Sharp Bend in a Fully Turbulent Flow, J. Fluid Mech. 34, 585-609.

VAN DYKE, M. (1978) Extended Stokes Series: Laminar Flow Through a Loosely Coiled Pipe. J. Fluid Mech. 86, 129-145.

WHITE, C.M. (1929) Streamline Flow Through Curved Pipes, Proc. Roy. Soc. Ser. A 123, 645-663.

WYGNANSKY, I. & CHAMPAGNE, F.H. (1973) On Transition in a Pipe. Part I: The Origin of Puffs and Slugs and the Flow in a Turbulent Slug, J. Fluid. Mech. 59, 281-335.

WYGNANSKY, I., SOKOLOV, M. & FRIEDMAN, D. (1975) On Transition in a Pipe, Part II: The Equilibrium Puff J. Fluid Mech. 69, 283-304.

DISCUSSION ON THIS PAPER WILL BE ACCEPTED FOR PUBLICATION UNTIL 14 MARCH 1984

The Institution of Engineers, Australia

On the scaling of the turbulence energy dissipation rate

K. R. Sreenivasan
Mason Laboratory, Yale University, New Haven, Connecticut 06520

(Received 29 November 1983; accepted 23 February 1984)

From an examination of all data to date on the dissipation of turbulent energy in grid turbulence, it is concluded that, for square-mesh configuration, the ratio of the time scale characteristic of dissipation rate to that characteristic of energy-containing eddies is a constant independent of Reynolds number, for microscale Reynolds numbers in excess of about 50. Insufficient data available for other grid configurations suggest a possibility that the ratio could assume different numerical values for different configurations. This persistent effect of initial conditions on the time scale ratio is further illustrated by reference to the jet-grid data of Gad-el-Hak and Corrsin.

It has long been believed, essentially on dimensional grounds, that the time scale of the energy dissipation rate ϵ in fully turbulent flows is of the same order of magnitude as the characteristic time scale of the energy containing eddies (except where the effects of viscosity are directly felt, such as near a smooth wall). Probably the only *direct* attempt to test this notion against experiments has been that due to Batchelor,[1] who plotted the quantity $\epsilon L_f/u^3$ (where L_f is the longi-

 0031-9171/84/051048-04$01.90 © 1984 American Institute of Physics

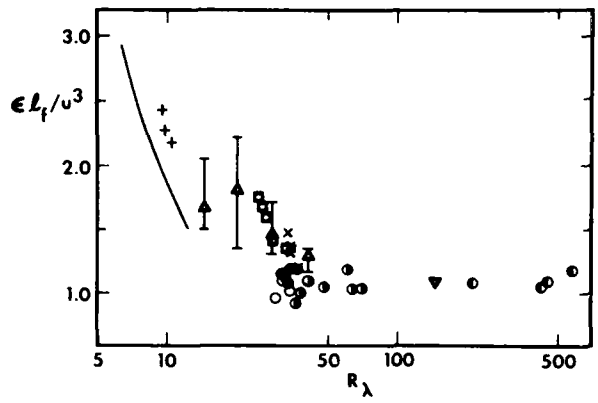

FIG. 1. The quantity $\epsilon L_f/u^3$ for biplane square-mesh grids. All data except + are for the initial period of delay, and are explained in Table I. + indicate typical data[11] in the final period of decay. — corresponds to Eq. (1).

tudinal integral scale, and u is the root-mean-square longitudinal velocity fluctuation) against the distance from the grid. He concluded that, in the so-called initial period of decay, the data are not generally inconsistent with the above expectation. (Here, u^2/ϵ can be regarded as the time scale of dissipation, and L_f/u as that characteristic of large eddies. While this latter quantity is not directly related to the time scale of the energy-containing eddies, the difference is not sufficiently significant to mask a real trend if it exists.) However, the relatively large scatter in the data collected by Batchelor permits one to speculate a weak Reynolds number dependence at least in the relatively narrow range covered ($14.4 < R_\lambda < 41$, where R_λ is the microscale Reynolds number based on u, the Taylor microscale λ, and kinematic viscosity ν). For example, Saffman[2] has pointed out that a logarithmic or $-\frac{1}{4}$ power dependence of $\epsilon L_f/u^3$ on R_λ is not necessarily inconsistent with the data. The point at issue is important, and is indeed one of the few key elements of a "semirational turbulence theory," and so, it seems desirable to examine the question in the light of much more recent data that have become available, extending over a wide Reynolds number range and a variety of conditions. This is the main purpose of this letter. We confine ourselves to data in grid turbulence (although we have examined shear flows also) (see Table I). With one exception (which will be noted), only those experiments in which L_f was either explicitly supplied by the authors,[1-12] or could be evaluated by us via their measured correlation function of spectral density, have been considered.

For consistency, we define $\epsilon = -\frac{1}{2} U_0(du^2/dx)$, with U_0 as the mean velocity in the test-section, even when, occasionally, one or both of the remaining two fluctuation components were measured; du^2/dx was evaluated from the best power fit possible for the u^2 data in the initial period of decay. (On those occasions where the authors gave a ready number for ϵ, we have always cross-checked it with the original data.)

Figure 1 shows all the data for biplane, square-mesh grids. It is clear that $\epsilon L_f/u^3$ is sensibly independent of R_λ for $R_\lambda \gtrsim 50$ although, for lower R_λ, there seems to be a recognizable trend.

That $\epsilon L_f/u^3$ could depend on R_λ for small R_λ is not surprising, considering that the constancy of $\epsilon L_f/u^3$ is only an asymptotic expectation. In particular, at very low Reynolds numbers where the inertia forces are weak, such as in the final period of decay, it is easily shown that

$$\epsilon L_f/u^3 = (\pi/2)^{1/2}(15/R_\lambda), \tag{1}$$

if we recall the relation $\epsilon = 15\nu u^2/\lambda^2$ and the result[1] that $L_f/\lambda \simeq (\pi/2)^{1/2}$. Typical experimental data from Bennett and Corrsin,[13] shown in Fig. 1, deviate from Eq. (1) because the measured values of L_f/λ are higher than $(\pi/2)^{1/2}$ and increase weakly as the Reynolds number decreases.

It is pertinent here to make reference to Rotta's[14] work. Rotta assumed that the spectral energy transfer occurs according to Heisenberg's theory,[15] and further that the so-called Loitsianskii invariant (see, for example, Ref. 1, p. 92) exists and is numerically equal to 4. With these assumptions he calculated that $\epsilon L_f/u^3 \to 0.76$ as $R_\lambda \to \infty$. (The corresponding value from Fig. 1 is around 1.) He also smoothly interpolated between this high Reynolds number solution and the low Reynolds number solution given by Eq. (1). The interpolated curve shows a behavior qualitatively not unlike that of the data in Fig. 1. However, because of the various dubious assumptions involved in the calculations, and also because of the numerical disparity in the high Reynolds number limit mentioned earlier, it was thought unnecessary to reproduce Rotta's interpolation curve.

While the situation appears quite satisfactory with respect to square-mesh grids, it is not so clear for other types of grids. For example, the quantity $\epsilon L_f/u^3$ for the flow behind an array of parallel rods,[16,17] plotted in Fig. 2, shows a considerable scatter and, more importantly, is higher on the average (assuming that the average is meaningful) than the corresponding square-mesh value. (It may be argued that the turbulence behind an array of parallel rods may not have attained homogeneity and isotropy to the same degree of approximation as in the case of square-mesh grids. We may,

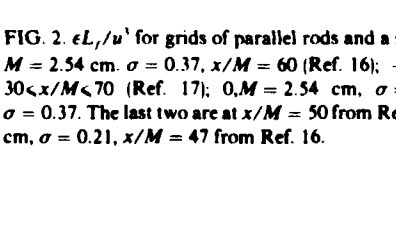

FIG. 2. $\epsilon L_f/u^3$ for grids of parallel rods and a slats grid. Parallel rods: △, $M = 2.54$ cm, $\sigma = 0.37$, $x/M = 60$ (Ref. 16); +, $M = 10.2$ cm, $\sigma = 0.37$, $30 < x/M < 70$ (Ref. 17); ○, $M = 2.54$ cm, $\sigma = 0.31$; ●, $M = 2.54$ cm; $\sigma = 0.37$. The last two are at $x/M = 50$ from Ref. 18. □, slats grid, $M = 1.9$ cm, $\sigma = 0.21$, $x/M = 47$ from Ref. 16.

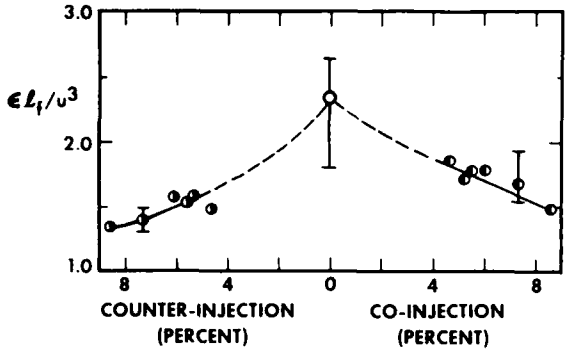

FIG. 3. $\epsilon L_f/u^3$ for jet-grids of Ref. 17. 0 at zero injection rate is an average of 10 data points ($99 < R_\lambda < 130$). Both ◐ and ◑ at injection rates of 7.32% are averages of six points each. $R_\lambda \simeq 110$ for ◐ and 150 for ◑.

however, note that in the region of measurement in Ref. 17, simple measures of homogeneity, such as the uniformity of mean velocity distribution in the "core region" of the wind tunnel and of isotropy such as the ratios of the root-mean-square intensities in different directions, were found to be rather typical.) Also plotted in Fig. 2 is a point for a slats grid (looking like an open Venetian blind) from Ref. 16. In Fig. 2, the length scale L_f for Gad-el-Hak and Corrsin's[17] measurements was obtained from the authors' tables, while for the Stewart and Townsend data[16] it was computed by the area L_g under transverse correlation curves and the assumption that $L_f = 2L_g$. (The vertical bar corresponds to the extremes on L_f depending upon which of the transverse correlation functions was used for integration.) Harris[18] did not measure L_f, and this is the exception mentioned earlier. For the typical data of Harris we have used, L_f/M was taken from Ref. 17 with the hope that the essentially similar configuration, grid solidity, and experimental conditions justify this step.

TABLE I. Guide to the biplane grid data of Fig. 1.

Source	Grid type	x/M	Symbol
Corrsin[1]	Biplane, round rods $M = 1.27$ cm, 2.54 cm $\sigma = 0.44$	34–230	□
Batchelor and Townsend[4]	Biplane, round rods $\sigma = 0.34$, $M = 0.635$, 1.27 and 2.54 cm	20–180	△[a]
Baines and Peterson[5]	Biplane, square rods $M = 3.38$ cm, $\sigma = 0.44$[b]	27–64	—
Mills *et al.*[7]	Biplane, round rods $M = 2.54$ cm, $\sigma = 0.44$	17–65	○
Kistler and Vrebalovich[8]	Biplane, square rods, $M = 17.15$ cm, $\sigma = 0.34$	45	◐
Comte-Bellot and Corrsin[9]	Biplane, square rods $M = 2.54$ and 5.08 cm $\sigma = 0.34$	42–385	◑
Lin and Lin[10]		55	▽[c]
Yeh and Van Atta[11]	Biplane, round rods $M = 4$ cm, $\sigma = 0.36$	23–48	×
Sreenivasan *et al.*[12] (only typical data presented)	Biplane, round rods $M = 2.54$ cm, $\sigma = 0.44$	12–102	●

[a] The symbol △ actually represents the mean of several sets of data whose range is indicated in Fig. 1 by a vertical bar in each case. At $R_\lambda = 14.4$ there are 9 sets of data, 15 at $R_\lambda = 20.3$, 9 at $R_\lambda = 28.4$, and 3 at $R_\lambda = 41$.

[b] Baines and Peterson's data cover seven biplane grids. Three grids have solidity of 0.61, 0.75, and 0.89, and are likely to have produced unstable flow downstream.[6] In two other cases ($M = 30.5$ cm and 20.3 cm), measurements did not proceed beyond x/M of about 12.5. In the seventh case, which alone could be considered here, $\epsilon L_f/u^3$ ranges from 1.29 to 1.86; unfortunately, the corresponding Reynolds numbers are unknown, preventing us from plotting the data in Fig. 1.

[c] Lin and Lin's grid is unconventional in that it is a complex structure of heated elements repeatedly folded into compact flow channels, which themselves are arranged in a square-mesh fasion. Its exclusion from Fig. 1 does not at all affect the conclusions.

Figure 3 shows that $\epsilon L_f/u^3$ in the downstream region correlates reasonably well with the injection rate of the jets. It is worth noting that for large injection rates, $\epsilon L_f/u^3$ seems to approach a value appropriate to square-mesh grid. This seems quite reasonable physically because the grid is essentially a parallel-rod type for small jet speeds, but becomes more square-mesh type at high jet speeds.

The data of Figs. 1 and 2 allow us to speculate that $\epsilon L_f/u^3$ may take on different values for different grid configurations. (Unfortunately, the perforated disc data of neither Ref. 5 nor Ref. 19 could be included because L_f is not available.) Investigators who compare theories of isotropic turbulence with grid turbulence data often implicitly assume that the turbulence sufficiently far behind a grid attains a character independent of the configuration of the grid. It does not quite appear justified, presumably because the scales of turbulence strongly affected by grid geometry contain a significant fraction of energy. This dependence on initial conditions can be seen more directly by examining the data of Gad-el-Hak and Corrsin,[17] who used an array of parallel rods, in combination with several jets of fluid (coflowing as well as counterflowing) evenly distributed along each rod, to produce nearly homogeneous and isotropic turbulence. Figure 3 shows that $\epsilon L_f/u^3$ in the downstream region correlates reasonably well with the injection rate of the jets. It is worth noting that for large injection rates, $\epsilon L_f/u^3$ seems to approach a value appropriate to square-mesh grid. This seems quite reasonable physically because the grid is essentially a parallel-rod type for small jet speeds, but becomes more square-mesh type at high jet speeds.

If it is true that the effects of grid geometry do persist, it is legitimate to ask why there does not seem to be any noticeable difference (see Fig. 1 and Table I) between square-mesh grids of round rods and square-mesh grids of square rods. One would also like to know, for instance, whether there are noticeable differences in $\epsilon L_f/u^3$ between single plane grids of square rods and single plane grids of round rods. We suspect that the asymptotic character of two grid flows will not be "noticeably" different if the grid configurations are "sufficiently" close, and that, even in square-mesh grids, if one changes the grid solidity σ by a large amount, the flow characteristics will change significantly. We note (with some surprise) that a large body of literature on turbulence behind square-mesh grids is confined to grids of solidity not very different from 0.4 (see Table I).

ACKNOWLEDGMENT

During the preparation of this letter the author held a Humboldt fellowship. Thanks are due to Dr. H. Oertel for the hospitality extended at his institute in DFVLR, Göttin-

gen, and Dr. L. Kleiser for bringing Rotta's work to his attention.

This work forms a part of inquiry into the effects of initial conditions on the development of turbulent flows, supported by the Air Force Office of Scientific Research.

[1]G. K. Batchelor, *The Theory of Homogeneous Turbulence* (Cambridge U. P., Cambridge, 1953), Chap. 6.
[2]P. G. Saffman, in *Topics in Nonlinear Physics*, edited by N. Zabusky (Springer, Berlin, 1968).
[3]S Corrsin, Ae.E. thesis, California Institute of Technology, 1942.
[4]G. K. Batchelor and A. A. Townsend, Proc. R. Soc. London Ser. A **193**, 539 (1948).
[5]W. D. Baines and E. G. Peterson, Trans. Am. Soc. Mech. Eng. **73**, 477 (1951).
[6]S. Corrsin, in *Hanbuch der Physik*, edited by S. Flugge and C. Truesdell (Springer, Berlin, 1963), Vol. 8, Part 2, p. 524.
[7]R. R. Mills, A. L. Kistler, V. O'Brien, and S. Corrsin, N.A.C.A. Technical Note No. 4288, 1958.
[8]A. L. Kistler and T. Vrebalovich, J. Fluid Mech. **26**, 37 (1966).
[9]G. Comte-Bellot and S. Corrsin, J. Fluid Mech. **48**, 273 (1971).
[10]S. C. Lin and S. C. Lin, Phys. Fluids **16**, 1587 (1973).
[11]T. T. Yeh and C. W. Van Atta, J. Fluid Mech. **58**, 233 (1973).
[12]K. R. Sreenivasan, S. Tavoularis, R. Henry, and S. Corrsin, J. Fluid Mech. **100**, 597 (1980).
[13]J. C. Bennet and S. Corrsin, Phys. Fluids **21**, 2129 (1978).
[14]J. C. Rotta, *Turbulente Strömungen* (Teubner, Stuttgart, 1972), p. 116.
[15]W. Heisenberg, Z. Phys. **124**, 628 (1948).
[16]R. W. Stewart and A. A. Townsend, Philos. Trans. R. Soc. London Ser. A **243**, 359 (1951).
[17]M. Gad-el-Hak and S. Corrsin, J. Fluid Mech. **62**, 115 (1974).
[18]V. G. Harris, M. S. thesis, Johns Hopkins University, 1965.
[19]G. Comte-Bellot and S. Corrsin, J. Fluid Mech. **25** 657 (1966).

Approved for public release;
distribution unlimited.

 0031-9171/84/051051-04$01.90 © 1984 American Institute of Physics

END

12-87

DTIC